



Long-term CO₂ injection into basalt at Nesjavellir, Iceland

Semester Thesis
on behalf of Orkuveita Reykjavíkur, Reykjavík Energy, Iceland

Mischa Werner
Lasse Wallquist

Zurich, February 29th, 2008

Distribution:

Dr. Marco Mazzotti, ETH Zurich

Dr. Nicolas Gruber, ETH Zurich

Dr. Einar Gunnlaugsson, Orkuveita Reykjavíkur

Dr. Grímur Björnsson, Orkuveita Reykjavíkur

February 29th 2008, Digital-Version

Authors: Mischa Werner
Limmatstrasse 52
CH-8049 Zurich
miswerne@student.ethz.ch


Lasse Wallquist
Mutschellenstrasse 17
CH-8002 Zurich
lassew@student.ethz.ch

Supervision ETH: Prof Dr Marco Mazzotti
Institute of Process Engineering
Separation Processes Laboratory
ETH-Zurich, Switzerland
marco.mazzotti@ipe.mavt.ethz.ch

Prof Dr Nicolas Gruber
Inst. of Biogeochemistry & Pollutant Dynamics
Professorship for Environmental Physics
ETH Zurich, Switzerland
nicolas.gruber@env.ethz.ch

Supervision OR: Dr Einar Gunnlaugsson
Manager of Geothermal Research
Orkuveita Reykjavíkur
Reykjavík, Iceland
einar.gunnlaugsson@or.is

Front page illustration: Nesjavellir geothermal power plant on a clear winter day; 15.11.2006. Photo by M. Werner, taken during a first internship at Orkuveita Reykjavíkur from Nov. 05 – Apr. 06

Skráningarblað skýrslna	
Útgáfustaður	

Skýrsla nr. 2008-	Dags., mán., ár 29.02.2008	Dreifing OR, ETH Zurich
-----------------------------	--------------------------------------	-----------------------------------

Heiti skýrslu, aðal- og undirtitill Long-term CO₂ injection into basalt at Nesjavellir, Iceland Company report & Term paper at the ETH Zurich	Upplag 1 + PDF
	Fjöldi síðna 49 + Appendices

Höfundar Mischa Werner & Lasse Wallquist	Verknúmer
--	-----------

Unnið fyrir

Samvinnuaðilar

Útdráttur

At Nesjavellir geothermal power plant, SW-Iceland, CO₂ enriched condensate has been injected via a shallow well between 1990 and 1998. This could be understood as a long-term injection experiment, and its evaluation a contribution to Iceland's current research efforts in the field of geological CO₂ sequestration in basaltic formations. After an initial seepage phase, the condensate mixed with groundwater and was further transported to the outflow of the aquifer at the adjacent Lake Thingvallavatn. The objectives of the present study are to find out how much CO₂ has been injected and to investigate its fate in the containment area.

A mass balance scheme was proposed, framing the containment area from the plant to the adjacent Lake Thingvallavatn. Degassing and mineral trapping were considered as possible sinks and a nearby pond as an additional source of the species of concern. The gas exchange, pH developing and silicate dissolution were modeled for the initial seepage phase through the vadose zone. The further transport in the local aquifer was investigated using the data from the water chemistry monitoring of the groundwater outflow at the lake. Main drawback was the fact, that the containment area is to date poorly described. This led to numerous but well-founded assumptions, though in some cases also to uncertainties that were not completely to eliminate.

Total CO₂ input was found to be 4'500 tons. None of the calculated seepage scenarios revealed carbonate precipitation to be possible as the conditions were constantly far from solubility equilibrium of calcite and magnesite. The same applied for the conditions in the aquifer upon mixing. Hence, it was shown that the fate of the entire CO₂ input was, sooner or later, the disadvantageous release into the atmosphere.

To conclude, the unintended CO₂ injection at Nesjavellir does not allow for the investigation of mineral sequestration in basalt. No further research on the event was recommended.

Efnisorð CO₂, Carbon dioxide Capture and Storage, Mineral Trapping, Old injection field at Nesjavellir, Sequestration in Basalt	Yfirfarið
--	-----------

Abstract

At Nesjavellir geothermal power plant, SW-Iceland, CO₂ enriched condensate has been injected via a shallow well between 1990 and 1998. This could be understood as a long-term injection experiment, and its evaluation a contribution to Iceland's current research efforts in the field of geological CO₂ sequestration in basaltic formations. After an initial seepage phase, the condensate mixed with groundwater and was further transported to the outflow of the aquifer at the adjacent Lake Thingvallavatn. The objectives of the present study are to find out how much CO₂ has been injected and to investigate its fate in the containment area.

A mass balance scheme was proposed, framing the containment area from the plant to the adjacent Lake Thingvallavatn. Degassing and mineral trapping were considered as possible sinks and a nearby pond as an additional source of the species of concern. The gas exchange, pH developing and silicate dissolution were modeled for the initial seepage phase through the vadose zone. The further transport in the local aquifer was investigated using the data from the water chemistry monitoring of the groundwater outflow at the lake. Main drawback was the fact, that the containment area is to date poorly described. This led to numerous but well-founded assumptions, though in some cases also to uncertainties that were not completely to eliminate.

Total CO₂ input was found to be 4'500 tons. None of the calculated seepage scenarios revealed carbonate precipitation to be possible as the conditions were constantly far from solubility equilibrium of calcite and magnesite. The same applied for the conditions in the aquifer upon mixing. Hence, it was shown that the fate of the entire CO₂ input was, sooner or later, the disadvantageous release into the atmosphere.

To conclude, the unintended CO₂ injection at Nesjavellir does not allow for the investigation of mineral sequestration in basalt. No further research on the event was recommended.

Summary

Carbon dioxide capture and storage is believed to contribute significantly to the fight against the observed climate change with its associated predominantly negative effects on humans and the natural environment. Amongst other CCS options, geological sequestration stands out, owing to the worldwide abundance of suitable storage formations and the proven technological feasibility. Injecting CO₂ into basalt in order to enhance mineral trapping mechanisms did poorly attract attention so far. The neo-volcanic geology of Iceland predestines the country to play a key role in this field of research. At the same time when the world's first large scale Basalt-injection experiment in SW-Iceland was being planned, Orkuveita Reykjavíkur, the main stakeholder of the current Carb-Fix geo-sequestration project and Iceland's biggest provider of geothermal energy remembered an old injection event at Nesjavellir geothermal power plant, which is owned by the company. At Nesjavellir, CO₂ enriched condensate was disposed into the local post-glacial lava over a period of almost 8 years. The idea came up, that such a quasi injection experiment could contribute to the fundamental research of CO₂ sequestration in Basalt, and any finding and cognition from its evaluation could be of good use for the pioneer project at Hellisheidi, which is located only a few kilometers southwest of Nesjavellir. The present study was assigned to reveal the fate of this unintentional CO₂ input.

A mass balance scheme in accordance to a substance flow analysis was proposed, framing the unconfined aquifer and the overlying vadose zone from the power station to the groundwater outflow at Lake Thingvallavatn, 5.5 km northeast of the power plant. Degassing and mineral trapping were identified to denote the possible sinks of the CO₂ load in the injected fluid. An additional groundwater charge from a seeping pond halfway to the lake could account for a possible source, which was to consider at the outflow. The pond's water chemistry was under influenced by the superficial disposal of geothermal brine, which was conveyed but not used in the production line of the power plant at that time.

The quasi injection experiment started with the commissioning of the power plant in September 1990 and came to end when it was extended to a co-generating plant for both thermal and electrical power output in May 1998. By then, a total amount of 4500 tCO₂ had been injected via a shallow well just in front of the power station. The fact that the injection took place a decade ago and that the containment area is to date poorly described with respect to the parameters of concern made it necessary to propose numerous but well-founded assumptions and simplifications. For the seepage phase from the well bottom to the groundwater table, a model for the gas exchange in rivers was adapted to a simplified geometry of the pore space in the vadose zone. Keeping the pore geometry parameters variable allowed for the simultaneous calculation of different model scenarios. The same geometrical assumptions and dissolution rates from literature were used for the estimation of basalt dissolution, in order to quantify the calcium and magnesium release. Comparing the resulting concentrations with the solubility equilibrium for the carbonates of concern revealed mineral trapping to be inexistent during the seepage

phase. The impact of the plant's discharge was qualitatively investigated by interpreting the time series of the water chemistry at the outflow and at the pond, which has been monitored throughout the plant's production history. It followed a better understanding of the mixing conditions and background processes between the plant and the lake and it was found, that also during the groundwater transport saturation conditions for carbonate precipitation were never reached. Instead, the discharge from the power plant exhibited a diluting effect, which could have even led to the dissolution of already present carbonates. The model validity was proven by comparing a calculated estimation of the outflow concentrations with the actually monitored averages.

In conclusion, this study showed that sooner or later during the seepage phase and groundwater transport, all of the injected CO₂ had degassed and the fate of the entire input was the disadvantageous release into the atmosphere.

The Nesjavellir injection event does not allow for the investigation of CO₂ fixation in basalt, hence does not render a benefit to Iceland's efforts in this upcoming field of research. Consequently, no further investigation of the event was recommended, which could have been, for instance, by means of shallow core drillings at specific locations with expected mineral trapping, induced by the 8 years of steady CO₂ injection.

Acknowledgment

First and foremost, we are indebted to Einar Gunnlaugsson, Manager of Geothermal Research, Orkuveita Reykjavíkur (Reykjavík Energy), for rendering the internship possible, which was the starting point of the present study. His supervision and support was of great value.

Major thanks go to our supervisors at the ETH Zurich, Prof Marco Mazzotti and Prof Nicolas Gruber, for their guidance and support throughout the work progress. Their agreement on the two-fold character of the present study, being both company report and semester thesis, eliminated the administrative barriers and made it possible to undertake the assigned task in Iceland.

We also like to thank our colleagues from Orkuveita Reykjavíkur's research department, namely Edda Sif Aradóttir, Gestur Gíslason, Grétar Ivarsson and Gunnar Hjartansson for their help and guidance. A special thank goes to Grímur Björnsson, whose appreciation for the project gave the basis for its realization.

Furthermore, we owe our thank to Bjarni Reyr Kristjánsson from ISOR – Iceland GeoSurvey, Eric Meyer from Vatnaskil – Consulting Engineers, Rolf Kipfer from EAWAG – Aquatic Research and Manuel Koller from the D-MAVT – ETH Zurich for spending time on providing valuable documentations and answering our questions.

Amongst many other new fellows from Iceland, our dear friends Asgeir Jónsson and Birgir Örn deserve a special thank for making our time in and off Reykjavík unforgettable.

Table of contents	page
Abstract	I
Summary	II
Acknowledgment	IV
Table of contents	V
List of figures	VI
List of tables	VII
List of acronyms	VIII
1. Introduction	1
1.1. Carbon dioxide Capture and Storage	1
1.2. Area under investigation	6
1.3. Objectives	7
2. Methods	8
2.1. Input evaluation	9
2.2. Sources and sinks: Containment area specifications	11
2.3. Sinks: Modeling the seepage phase	17
2.3.1 Geometrical approach	17
2.3.2 Degassing model	20
2.3.3 pH developing	23
2.3.4 Mineral trapping	27
2.4. Sources, sinks and outflow: Groundwater transport	29
2.4.1 Groundwater charge at Lækjarhvarf	29
2.4.2 Qualitative considerations	29
2.4.3 Quantitative estimations	30
3. Results and discussion	34
3.1. Input	34
3.2. Sinks during seepage phase	34
3.3. Sources and sinks during groundwater transport	40
3.3.1 Qualitative interpretations	40
3.3.2 Quantitative calculations	42
3.4. Mass balance summary	44
4. Conclusions	45
References	46
Appendices	49

List of figures	page
Figure 1-1: Contributions of main emission reduction measures.	2
Figure 1-2: Schematic plant design 1990-1998.	7
Figure 2-1: Mass balance scheme for the containment area.	8
Figure 2-2: Ratio of injected condensate and produced hot water.	9
Figure 2-3: Dissolved CO ₂ and H ₂ S in the condensate.	10
Figure 2-4: A ₁₁ surface vs. number of pores n at 100% saturation.	19
Figure 2-5: A ₁₁ surface vs. pore radius at 100% pore water saturation.	19
Figure 2-6: Total reactive surface area vs. pore saturation.	20
Figure 2-7: Pore geometry and adapted depth.	22
Figure 2-8: Adapted and unadapted exchange distance.	23
Figure 2-9: Dissolution rates of Icelandic basaltic glass.	26
Figure 2-10: Background concentration scheme.	30
Figure 2-11: Concentration developing scheme during injection.	32
Figure 3-1: Daily input of CO ₂ from condensate injection.	34
Figure 3-2: Developing of CO ₂ concentration during seepage phase.	36
Figure 3-3: Developing of the pH during seepage phase.	37
Figure 3-4: Developing of the formation of SO ₄ ²⁻ during seepage.	38
Figure 3-5: Developing of the Ca ²⁺ concentration during seepage.	39

List of tables	page
Table 2-1: Temperature of the condensate.	10
Table 2-2: Theoretical and actual gas composition in heat exchangers.	11
Table 2-3: CIPW norm for a post-glacial lava flow in SW-Iceland	12
Table 2-4: The composition of Icelandic basaltic glass and MORB.	13
Table 2-5: Background water chemistry from plant to lake.	16
Table 2-6: Background concentration developing.	31
Table 3-1: Input statistics.	34
Table 3-2: Solubility equilibrium calculations.	40
Table 3-3: Concentration developing for maximum impact.	42
Table 3-4: Concentration developing for minimum impact.	43
Table 3-5: Differences btw. measured and calculated outflow conc.	43
Table 3-6: Final destination and corresponding quantities.	44

List of acronyms

A	Background groundwater conditions
A_{il}	Surface area wetted by 1 liter of water
A_c	Cross section area of 1 pore
A_{tot}	Reactive surface area for 1 sec of total flow
A_w	Reactive surface area for 1 pore in 1 sec
a_w	Angle of the water filled segment
B	Monitored conditions in outflow at Lake Thingvallavatn
c	Chord of the air filled segment
C°	Standard concentration
$C_{o,i}$	Concentration of species i at t=0
C_a	Concentration of acid a
$C_{A,i}$	Background conc. in groundwater
$C_{aM,i}$	Measured conc. of species i after mixing at Lækjarhvarf before 1990
$C_{MaM2,i}$	Calculated conc. of species i after mixing at Lækjarhvarf during injection
$C_{B,i}^\circ$	Measured conc. of species i in the outflow at Varmagjá before 1990
$C_{B,i}$	Measured conc. of species i in the outflow at Varmagjá during injection
$C_{bM,i}^\circ$	Calculated conc. of species i before mixing at Lækjarhvarf before 1990
$C_{bM2,i}$	Calculated conc. of species i before mixing at Lækjarhvarf during injection
C_{Ca}	Concentration of Ca,
$C_{co,i}$	Modeled conc. of species i in condensate
C_{CO_2}	Concentration of CO ₂
$C_{CO_2,eq}$	Equilibrium concentration of CO ₂
C_{CO_3}	Concentration of CO ₃ ²⁻
$C_{eq,i}$	Equilibrium concentration of species i
$C_{H,g}$	H ⁺ conc., influenced by CO ₂ degassing
$C_{H+,ox}$	H ⁺ conc., influenced by oxidation
$C_{H+,Si}$	H ⁺ conc., influenced by silicate dissolution
$C_{H_2CO_3}$	Concentration of H ₂ CO ₃
C_{H_2S}	Concentration of H ₂ S
$C_{HCO_3^-}$	Concentration of HCO ₃ ⁻
C_i	Concentration of species i
$C_{Mi,i}$	Calculated conc. after mixing with condensate
C_{Mg}	Concentration of Mg ²⁺ ,
C_{O_2}	Concentration of O ₂
$C_{O_2,eq}$	Equilibrium concentration of O ₂
C_{tot}	Concentration of total DIC
CCS	Carbon Capture and Storage
CIPW	Normative mineralogy calc. after Cross, Iddings, Pirsson & Washington
d	Adapted depth (gas exchange distance)
δ_{u10}	Boundary layer thickness at given u10
D	Difference between calculated and monitored conc. in the outflow
D_p	Pore diameter
Dg	Degassing
D_i	Molecular diffusion coefficient of species i
DIC	Dissolved Inorganic Carbon
EOR	Enhanced Oil Recovery
ETH	Swiss Federal Institute of Technology
ε	Additional correction factor for river depth adaptation btw. 0.7-0.9
f	Flow of condensate
GERM	Geochemical Earth Reference Model

h	River depth in gas exchange model for rivers
H	Height of the air filled segment
η	Additional correction term for river depth adaptation btw. 0.6-1.0
IPCC	Intergovernmental Panel on Climate Change
k	Intrinsic permeability
$K_{\text{H}_2\text{CO}_3}$	1- dissociation constant, $K_{\text{H}_2\text{CO}_3} = 10^{6.40}$
K_{HCO_3}	2- dissociation constant, $K_{\text{HCO}_3} = 10^{10.47}$
$k_{\text{diss,Si}}$	Dissolution rate of Si
$k_{\text{g,CO}_2}$	Gas exchange rate of CO ₂
$k_{\text{g,H}_2\text{S}}$	Gas exchange rate of H ₂ S
$k_{\text{g,i}}$	Gas exchange rate of species i
$k_{\text{g,O}_2}$	Gas exchange rate of O ₂
k_{ox}	pseudo first order oxidation rate
K_s	Solubility equilibrium constants
K	Hydraulic conductivity
l	Specific weight of water
Lh	Groundwater charge at Lækjarhvarf
m	Dynamic viscosity of water
M	Mixing at Lækjarhvarf before 1990
M1	Mixing with condensate
M2	Mixing at Lækjarhvarf during injection period
MORB	Mid Ocean Ridge Basalt
MT	Mineral Trapping
n	Number of pores
n_{100}	Number of pores at saturation = 100%
OR	Orkuveita Reykjavíkur (Reykjavik Energy)
pK_a	Acidic strength of acid a
$\text{pK}_{\text{H}_2\text{CO}_3}$	Acidic strength of H ₂ CO ₃
$\text{pK}_{\text{H}_2\text{S}}$	Acidic strength of H ₂ S
$\text{pK}_{\text{H}_2\text{SO}_4}$	Acidic strength of H ₂ SO ₄
pK_{HSO_4}	Acidic strength of HSO ₄ ⁻
ppm	Parts per million
Q	Flow rate
Q_A	Background groundwater discharge
Q_{brine}	Flow rate of disposed geothermal brine
Q_{co}	Flow rate of condensate
Q_{Lh}	Flow rate of natural runoff in the brook Nesjavallalækur
Q_M°	Discharge in aquifer after mixing at Lækjarhvarf before 1990
Q_{M1}	Discharge in aquifer after mixing with the condensate
Q_{M2}	Discharge in aquifer after mixing at Lækjarhvarf
r	Pore radius
SRCCS	Special Report on Carbon Capture and Storage
T	Temperature
u_{10}	Wind speed in 10 m elevation
v_f	Flow velocity
VI_1	Various Influences on conc. of species I btw. the plant and Lækjarhvarf
VI_2	Various Influences on conc. of species I btw. Lækjarhvarf and lake
V_p	Volume of 1 pore for 1 sec of flow
V_w	Water volume in 1 pore in 1 sec
$v_{w,i}$	Transfer velocity of gas i
WA	State of Washington
WG	Working Group

1. Introduction

Motivation

Humans are responsible for the climate change we are observing. Last year's fourth assessment report of the Intergovernmental Panel on Climate Change (IPCC) brought widely accepted certainty to this question. Hence, we are challenged to prevent harm to both other humans and the natural environment. Currently, 80% of the global energy use relies on the combustion of fossil fuels (IPCC, 2005). Two centuries of economical development have generated gigatons of carbon dioxide (CO₂) emissions, which are the principle cause of climate change. Consequently, atmospheric CO₂ concentration rose from 280ppm in the 19th century to a value as high as 379 ppm by the year 2005 (IPCC WGI, 2007). Fighting the rise in atmospheric CO₂ concentration has become the world's crucial task in order to prevent global warming higher than 2°C relative to pre-industrial times. A temperature increase in this order of magnitude is believed to border major changes in ecosystems with predominantly negative consequences (IPCC WGII, 2007). In fact, this stands for a hardly predictable economical and ecological loss. The quest for counter strategies is urgent, as global average temperature near the earth's surface has already increased by 0.74 °C during the last 100 years (IPCC WGI, 2007).

Realistically, this task needs a broad portfolio of mitigation options. Emission reduction programs are currently driven by national and international politics, more or less successfully. In science, efforts are made to reduce the use of fossil fuels either by efficiency improvements or by promoting feasible substitutes such as hydrogen (produced with alternative energy sources: solar, geothermal, wind and others). All three approaches are in good agreement with the modern conception of pollution control, i.e. to minimize end-of-pipe interventions and to implement cleaner production.

1.1. Carbon dioxide Capture and Storage

From EOR to CCS

In the early 1970s, a novel idea emerged. The US oil industry gave birth to a concept later named Carbon Dioxide Capture and Storage (CCS). CO₂, a side product of the oil production process, was collected and injected in the vicinity of production wells. This should establish the desired extra pressure for a complete exploitation of the depleting oil field, a process now known as enhanced oil recovery (EOR). Thus, CO₂ is captured and stored, i.e. sequestered, outside the atmosphere. Having the considerations pollution control in mind, sequestration of CO₂ signifies traditional end-of-pipe thinking, labeled the wrong approach by critics. Indeed, it was not before 1996, that CCS gained credibility and worldwide attention. It was the year when Norway's Statoil initiated the world's first large-scale storage project at the Sleipner gas field in the North Sea.

In 2003, IPCC agreed on the elaboration of a special report on carbon dioxide capture and storage. Two years later it was published. Today, CCS is widely regarded as a potentially important mitigation option, as illustrated below.

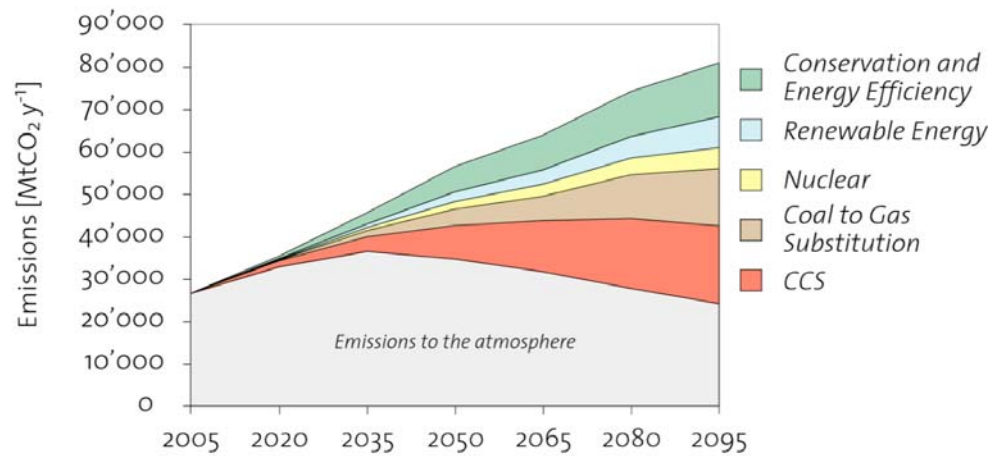


Figure 1-1: The global CO₂ emissions and corresponding contributions of main emission reduction measures in the current mitigation portfolio (IPCC, 2005).

The special report from 2005 defines CCS as the collection of CO₂ from large point sources (or ambient air) and its storage in suitable reservoirs, including the logistical challenge of transport, site selection and site management.

Technological options for CCS

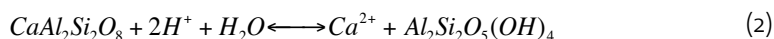
Several technologies exist to capture CO₂ from large point sources. The state of the art method conventionally involves the scrubbing of a CO₂ enriched gas stream with a chemical solvent. Also the storage problem allows for more than one technological solution. Comparing global storage capacities and current CO₂ emissions reveals only two natural reservoirs with the potential for a safe disposal over centuries. This is on the one hand the deep ocean, where high pressure and the slow water circulation is believed to guarantee long enough retention, though this may have harmful side-effects to the maritime biosphere. Moreover, CO₂ will unavoidably dissolve and equilibrate with the atmosphere. On the other hand, geological formations are predestined to fulfill capacity, accessibility and safety requirements in order to sequester CO₂ permanently on a historical time scale (IPCC, 2005).

Geological storage and trapping mechanisms

Different geological media are thinkable for CO₂ storage. Spent oil or gas fields, deep saline aquifers, unminable coal beds and basalt formations have been suggested (IPCC, 2005). Prerequisite for each of them is the existence of a thick enough cap rock with adequate sealing qualities, depicting the stratigraphic trap. Other physical and chemical mechanisms determine the effectiveness of the storage. Structural traps such as faults or fractures can act as permeability barriers or backup capacities in case of leakage from the containment formation. The latter occurs when density differences between compressed CO₂ and formation fluids express buoyancy. Residual trapping occurs when CO₂ is retained in the pore space by capillary forces. Concerning the storage in aquifers over time, most of the physically trapped CO₂ dissolves into the formation fluid, a process often referred to as solubility trapping. In case of water, this lowers the pH by forming carbonic acid (H₂CO₃), which dissociates to bicarbonate (HCO₃⁻) and carbonate (CO₃²⁻) after the following reaction:



The liberated protons cause dissolution of the rock matrix, as exemplified by the dissolution of feldspar anorthite (CaAl₂Si₂O₈):



The detached ionic species can react with the deprotonated carbonic acid to form solid carbonate minerals such as calcite and magnesite, denoting the so-called mineral trapping:



The overall reaction (reactions 1-3) is slightly exothermic and thus a spontaneously occurring natural process. On a geological time scale, it plays a key role in silicate weathering and the formation of secondary minerals. Solidifying magma causes a steady CO₂ flux into overlying formations, where it comes to silicate weathering and carbonate precipitation, as part of the global carbon cycle. (e.g. Lasaga, 1981; Berner and Lasaga, 1989). This process is slow, but ever lasting. In terms of CCS, it is referred to as mineral trapping. Using it to sequester CO₂ was first proposed by Seifritz (1990) and initially investigated by Dunsmore (1992), Gunter et al. (1993), Bachu et al. (1994) and Lackner et al. (1995), to name a few amongst others.

Mineral Carbonation and
Mineral Sequestration

Two different approaches are currently being developed, even though not attracting the same degree of attention.

The first approach, the so-called mineral carbonation, can be described as the engineered form of ex-situ mineral trapping. Silicates are mined, ground and the carbonation reaction takes place in a chemical processing plant, where temperature and pressure conditions are optimized towards maximum efficiency. The reaction products are stored suitably, for example in depleted mines. In an ideal mineral carbonation scheme, the reactor is located next to the power plant with a nearby silicate quarry, in order to avoid over all transportation costs.

The second approach, instead, aims to optimize the aforementioned final stage of geological storage, i.e. the in-situ dissolution of the rock matrix and filling of the pore-space with precipitation products. In this case, optimizing means to evaluate the best suitable geology concerning silicate composition, pore space and hydrodynamic properties, but also which injection strategy should be chosen in order to match the underground chemical and physical conditions. It would be best describable using the term enhanced mineral trapping, but is later referred to as mineral sequestration, consistent with literature. Compared to the ex situ mineral carbonation, the main benefit of an in situ approach are the significantly lower costs per ton CO₂ sequestered. IPCC (2005) concludes in situ storage costs being up to 30 times lower for onshore formations and 4 times lower for those offshore (Newall et al., 2000 and Allinson et al., 2003).

Lack of long-term field
experience

Mineral Sequestration, however, is still an immature field of research. Striking is the lack of long-term field experiments, which could fill the gaps in knowledge concerning, for instance, the suitability of the geological formation or the in situ kinetics of

water-rock interaction. Gíslason and Oelkers (2003) state as a concluding remark their laboratory findings could be readily used to describe natural systems, as long as surface area conditions can be accurately characterized. According to Marini (2007), results from both laboratory investigation and field tests are unsatisfactory without coherent geochemical modeling, owing to the long lapses of time that are predicted for the progress of the involved reactions. Nevertheless, temporal and spatial requirements as well as safety issues and public acceptance are, strongly bound to experience made in the field over years and decades.

Current projects

Currently, only two large-scale projects have been initiated, where the injection site was evaluated with regard to the enhancement of mineral trapping¹. One project is run in the US near Richland, WA, with the Columbia River basalt group serving as the target formation for supercritical gas injection (Spane et al., 2007).

Information on the other project, the Carb-Fix project in SW-Iceland, was very recently published. It is a collaboration between the national university, international institutes and Iceland's biggest geothermal energy provider Orkuveita Reykjavíkur (OR), which holds the project management and is the main sponsor (Gíslason et al., 2007; OR press release, 2007). All further specifications concerning the project are company-internal information and may be confidential. See also box insertion on page 5).

The Carb-Fix project at Hellisheidi

The injection site is located 30km east of the capital, at the slopes of the volcanic ridge Mount Hengill, where OR runs the recently commissioned geothermal power plant Hellisheidi (see photo documentation in appendix 1). Unused exploration wells and reservoir control wells downstream the target aquifer will serve as injection and monitoring wells. CO₂ will be collected directly from the plant, where CO₂ is inevitably conveyed together with geothermal steam. Besides these infrastructural benefits, the main reason for a project in Iceland is its geology. The biggest part of the island consists of mid ocean ridge basalt (MORB), a silicate that is chemically favorable for mineral sequestration, due to the high content of basic cations (Matter et al, 2007). Additionally, the young rock age is advantageous, since porosity is still high. Secondary minerals due to rock alteration do not clog the pore space, which is the case in many older formations at other places in the world (Gustavson, 2006).

Injection start is planned by summer 2008 at an average rate of 90-170 tCO₂ per day. The gas will be dissolved under pressure into groundwater prior to injection, unlike in many other sites where a pure gas stream is first compressed and then injected as a supercritical fluid. Thus, neither buoyancy forces nor residual trapping nor the time it takes the CO₂ to dissolve into the formation water delay or even inhibit the actually intended mineral trapping.

It is scheduled to inject a total amount of 50 ktCO₂ by the year 2010.

The Nesjavellir event

While planning the Carb-Fix project, another CO₂ relevant event attracted attention: The "old" injection field at Nesjavellir power plant, just 10 kilometers northeast of Hellisheidi.

¹ Not to be confused with forced mineral trapping as proposed by McGrail et al. (2001).

This plant is also run by OR, which explains the sudden interest (Björnsson, G., 15.06.2006, stakeholder meeting at OR).

During the 1990ies, over a period of almost 8 years, CO₂ enriched condensate was disposed into the post-glacial lava underneath the power station, at a rate up to 2 tCO₂ per day. The analogy to Hellisheidi is palpable. This wastewater disposal could be understood as an unintentional long-term injection experiment, and its evaluation a contribution to OR's engagement at Hellisheidi, i.e. to Iceland's current research efforts in the field of geological CO₂ sequestration in basaltic formations.

Company profile of Orkuveita Reykjavíkur

Insertion:

Orkuveita Reykjavíkur (Reykjavík Energy) is an independent service company owned for the most part by the City of Reykjavík. Within its service area, OR distributes electricity and district heat from geothermal resources as well as cold water for consumption and fire fighting.

More than four decades of experience in reservoir engineering and drilling in basaltic rocks have made OR for a leading stakeholder of Iceland's upcoming research in the field of mineral sequestration. For the current Hellisheidi project, partnerships exist with local and foreign institutions such as the University of Iceland, the Lamont-Doherty Earth Observatory at Columbia University in New York and the Lawrence Berkeley National Laboratory at the University of California.

Assignment

Early 2007, OR considered to evaluate the feasibility of a profound investigation of the Nesjavellir event, i.e. to find out, whether and to what extent sequestration research should be supported, additionally to the Hellisheidi project. Two trainees were employed and assigned to do the evaluation amongst other tasks.

Instead of a regular company report, the authors intended to elaborate a term paper in accordance with the guidelines of the Swiss Federal Institute of Technology (ETH) in Zurich, Switzerland. Two resident experts were addressed to supervise the writing in Zurich, namely Prof. Dr. Marco Mazzotti, coordinating leading author for the IPCC special report on mineral carbonation (2005) and head of the Separation Process Laboratory at the Institute of Process Engineering and Dr. Nicolas Gruber, professor for environmental physics at the Institute of Biogeochemistry and Pollutant Dynamics.

Author's connection to OR

The author's affiliation to OR stems from an internship at the research department in spring 2007, when firstly professional work experience was achieved in the field of geothermal energy production and secondly data, documents and contacts were acquired in order to elaborate this study. The internship was successfully completed under the supervision of Einar Gunnlaugsson, the company's manager of geothermal research. During 3 months, company-internal data and documents were visible and oral information available to the authors. Any company-internal information will, if expedient, later be referred to as *OR, 2007*.

1.2. Area under investigation

Iceland	Geologically, Iceland's history of origins is rather simple. Situated between the Eurasian and North American plate, in the middle of the Atlantic, the island is primarily composed of mid-ocean ridge basalts (MORB), as mentioned above. A neovolcanic zone crosses the country from North East to South West in an Y-shaped form, depicting the plate boundary.
Local geography	Mount Hengill volcanic system developed on the western branch of the active rift zone in SW-Iceland, 30km east of the capital Reykjavik. The geothermal reservoir relates to one of the biggest high temperature areas in Iceland (Bodvarsson, 1951). It provides the energy for both Hellisheidi and Nesjavellir power plant. The latter is situated in a short valley adjacent to the southwestern shore of Lake Thingvallavatn at an elevation of 175 m a.s.l.. The region is highly fractured and faulted, owing to the geological history of the surroundings; just north of the Hengill area, each summer-day hundreds of visitors marvel at the clearly visible features of the formation of the Thigvellir graben, which emblemizes the tectonic spreading between Europe and North America. In appendix 2, a map of Southwest Iceland is attached, containing the geographic information of concern. It is accomplished by an overview of the whole country.
Nesjavellir geothermal power plant	<p>Geothermal research in the vicinity of the old farm Nesjavellir had been going on for decades, when the first stage of the power plant was commissioned in September 1990. Initially, only four boreholes were connected to the production line, exploiting the geothermal heat in 1000 to 2000 meters depth. The power generation of the plant at that time reached 100 MW thermal.</p> <p>Together with geothermal brine and steam, big amounts of non-condensable gases were conveyed to the surface. These consisted in particular of 75% CO₂, 21% hydrogen sulfide (H₂S) and 1-3% hydrogen (H₂) (Olafsson, 1992; Gíslason, 2000). Preliminary to the power production, the 198°C hot geothermal fluid was separated by gravity and expansion into its water and gas phase.</p>
Production line 1990-1998	<p>The water phase was cooled down to atmospheric pressure and disposed in the nearby brook Nesjavallalækur. Further downstream, this brook forms the pond Lækjarhvarf, where it disappears entirely into the lava (see photo documentation in appendix 1).</p> <p>The gas phase, instead, was conducted to the powerhouse, where control valves reduced the initial separation pressure from 15 to 2 bars. Condensate was injected to cool the steam from 198°C to saturation conditions at 120°C, a measure to protect the gaskets of the heat exchangers. These were located inside the powerhouse and harnessed the remaining enthalpy of the steam by heating 4°C cold groundwater up to 83°C (the fresh water is pumped from the pump station Grámelur near Lake Thingvallavatn). Thus, the non-condensable part got separated from the condensing water vapor, but residence time in the exchangers was long enough for a considerable part of the CO₂ and H₂S to dissolve into the condensate. The hot water was pumped to Reykjavík and fed into the municipal district heating system, to date the most sophisticated in the world. Figure 1-2 illustrates a schematic overview of the</p>

plant design at that time. The original draft of the powerhouse layout is attached in appendix 3.

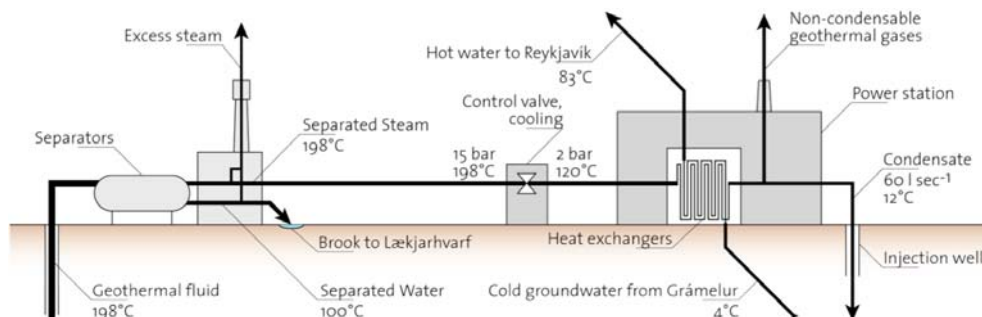


Figure 1-2: Schematic plant design 1990-1998.

Injection of the condensate

The CO₂ and H₂S enriched condensate was injected into a shallow well just a few meters in front of the power station. The well reached a depth of 15 m and was drilled with a well bottom diameter of 60 cm, hence suitable for disposal purposes. Appendix 3 contains the original technical draft of this well, which was called Nidurrennsliholá.

Extension of the plant

In summer 1998, Nesjavellir was extended and redesigned to a co-generation plant for both hot water and electricity production. From then on, new heat exchangers harnessed the energy of the geothermal brine, while the steam was conducted to two turbine units. After the flush, condensers with vacuum pumps guaranteed maximum efficiency, leading to an output of 60 MW electric in addition to 150 MW thermal power. As a consequence, the CO₂ content of the condensate decreased substantially, due to the rapid evacuation of the non-condensable gases in the condensers by pumps. Thus, the quasi injection experiment had come to an end.

1.3. Objectives

Nobody ever intended to sequester CO₂ in Nesjavellir. Having this in mind was vitally important, when setting the objectives of the present study. The injection event was basically a disposal of wastewater, accordingly data logging and management was perfunctory for the plant operators at that time. The fate and transport of the co-injected CO₂ was, understandably, of no concern.

The aim of the present study is, firstly to reconstruct and evaluate to CO₂ input over the injection period from September 1990 until May 1998, and secondly to investigate the fate of the CO₂ in the containment area, which spans the unconfined aquifer and the overlying vadose zone from the power station to the groundwater outflow at Lake Thingvallavatn, 5.5 km northeast of Nesjavellir. The according research questions were posed as follows:

Research questions

1. How much CO₂ was injected in total at Nesjavellir from 1990 until 1998 by the disposal of condensate?
2. What was the final destination of the injected CO₂ in the containment area and how much of it did end up there?

2. Methods

General

Following the objectives, a mass balance scheme on the basis of a substance flow analysis was proposed (Baccini and Brunner, 1991) in order to determine input and fate coevally.

The system boundary was chosen to frame the containment area from the well bottom to the shoreline of Lake Thingvallavatn. Literally, this frame is depicting a black box with computable input, but unknown sources and sinks. The outflow on the other hand, was well documented by the monitoring of the water chemistry at several station on the shores of Lake Thingvallavatn.

As the system was assumed to be in equilibrium with regard to background concentrations of atmospheric and lithospheric CO₂, the only possible source for additional CO₂ was found to be the groundwater charge at Lækjarhvarf, which was affected by the disposal of geothermal brine.

Instead, two possible sinks have been identified, namely degassing and mineral trapping.

Mass balance in equation form

In equation form, the mass balance can be summed up to:

$$Input = Outflow + Dg + MT - Lh , \quad (4)$$

where

Dg = degassing [tCO₂],

MT = mineral trapping [tCO₂],

Lh = groundwater charge at Lækjarhvarf [tCO₂].

Mass balance scheme

Soon upon injection, the condensate reached the groundwater and the fluids were readily mixed, as no density gradients between the fluids were observable. Figure 2-1 gives the schematic overview for all these processes.

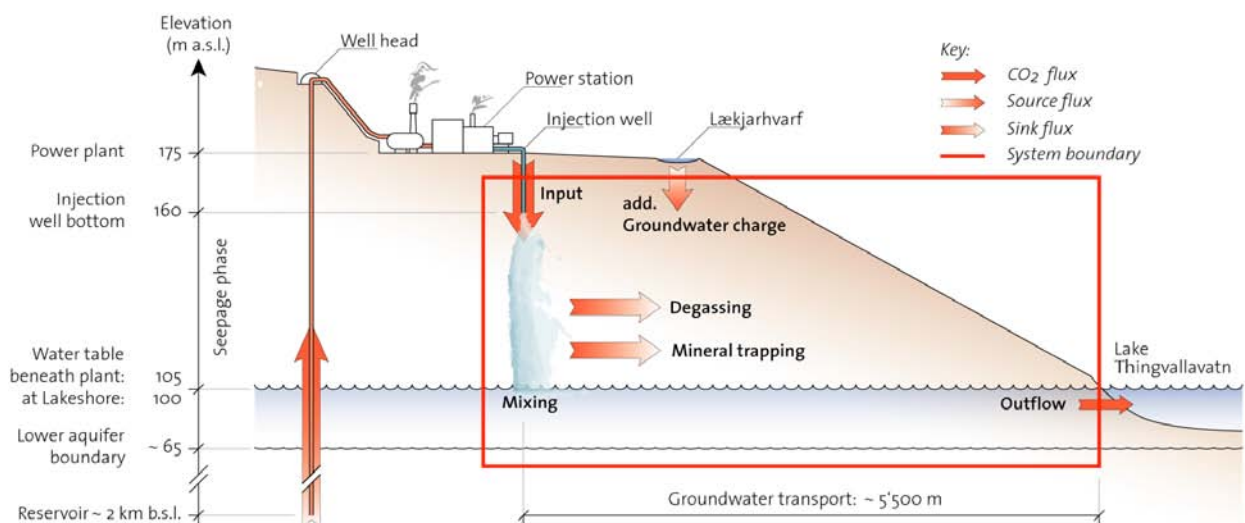


Figure 2-1: Mass balance scheme for the containment area from the plant to lake Thingvallavatn.

2.1. Input evaluation

Data recovery

Data was recovered and compiled from OR's former database *VDATA*, which was established and maintained by members of the research department. These entries stem from measurements taken by the plant operators on a weekly basis, and in less regular time intervals from chemical analysis on behalf of the research department. Of interest were the amount of injected condensate, the CO₂- and H₂S-load, temperature and pH. Unfortunately, the logging of the time series went back only to October 1994, the remaining entries were not properly recorded. Instead, a full data set on a daily basis was available for the amount of hot water pumped to Reykjavík from 1990 till 1998.

It is to mention, that it was not possible to comment on the data quality and its documentation, since no influence could be exerted on the analysis methods and data logging processes for the time before and during the injection.

Condensate injection on daily resolution

In order to estimate the amount of injected condensate during the record gap, the ratio between hot water and condensate should allow for an extrapolation – provided this ratio exhibited a reasonably small variance. Indeed, figure 2-2 shows a good correlation for the time before January 1998, returning an average ratio of 8.42 ± 0.39 , i.e. less than 5% variance. In 1998, testing of the new plant design was intensified and a big part of the condensed steam was disposed through the new piping system, ending superficially in the brook. Thus, less condensate went through the injection well, while the hot water production remained on the same level in line with demand.

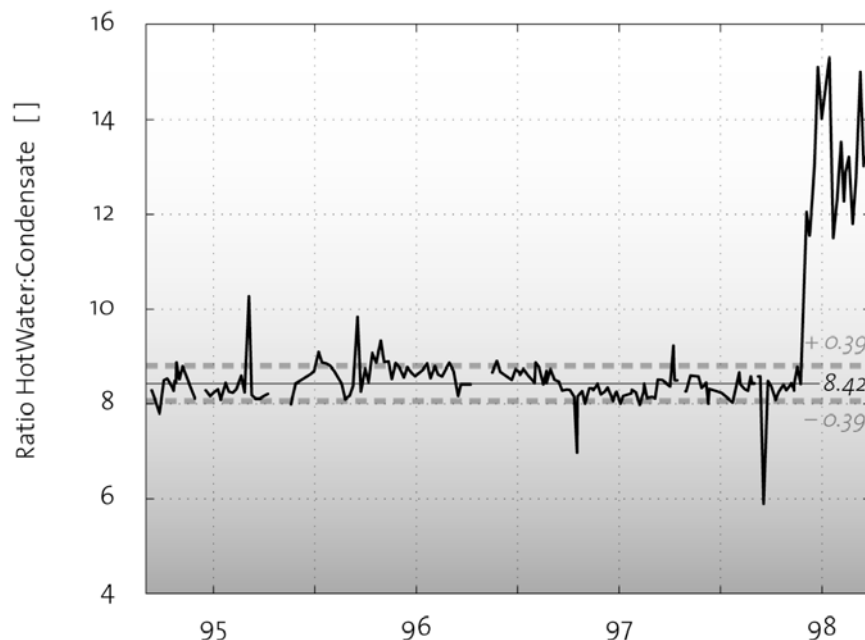


Figure 2-2: Ratio of injected condensate and produced hot water.

By means of this ratio, the condensate was extrapolated back to September 1990. Thus, an average condensate flow rate of 60 l sec^{-1} was obtained over the whole injection period. In order to have the time after 1994 on a daily resolution, too, the same procedure was applied to the rest of the hot water data, instead of extrapolat-

ing the weekly measurements from VDATA. After the changes in the production line in January 1998, the average ratio was found to be 13.05 ± 1.16 . Owing to these almost 10% variance, the VDATA measurements were extrapolated each week for the remaining injection time.

Temperature and pH of the condensate

The time series for the temperature revealed the following specifications:

Table 2-1: Temperature of the condensate.

[°C]	Average 1994-1998	Standard deviation	Median	Max imal	Minimal
Temperature	11.76	± 3.14	11	19	7

Only few data was available for the pH, which did not allow for statistical specifications. On average, a pH of 4.46 was measured and logged in VDATA.

Dissolved gases

Also the gas load of the condensate had been rarely analyzed. Figure 2-3 shows the available measurements.

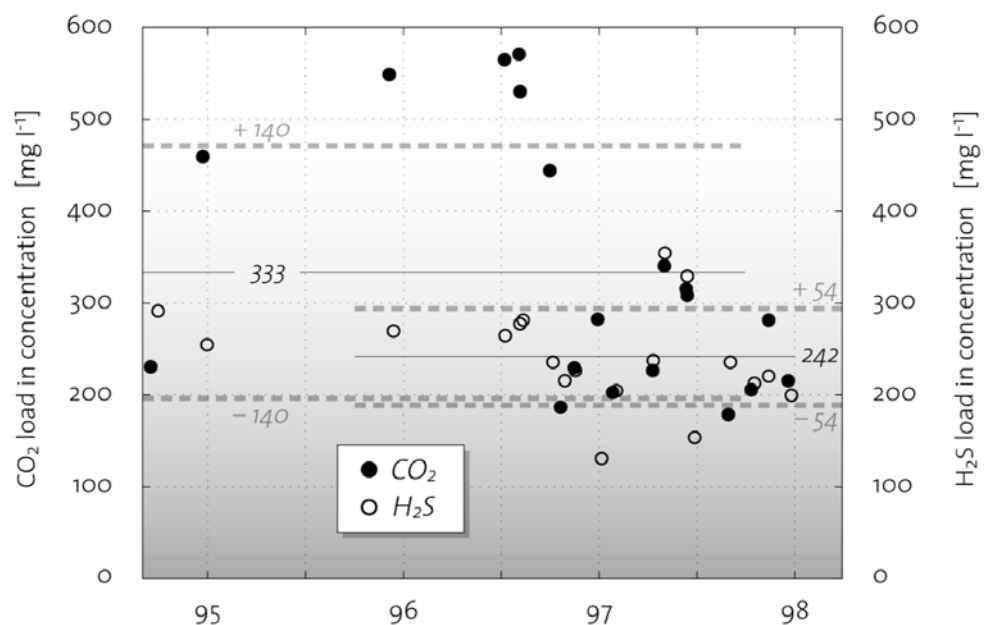


Figure 2-3: Dissolved CO₂ and H₂S in the condensate.

Obviously, these time series exhibit a large scatter, especially regarding the CO₂ measurements. On average, a mean concentration of 333 ± 140 mg l⁻¹ for CO₂ and 242 ± 54 mg l⁻¹ for H₂S was obtained. In order to validate the plausibility of these averages, the theoretical and actual composition of the atmosphere in the heat exchangers was compared as summarized in table 2-2. Henry coefficients for water air gas exchange were calculated for 12°C after Arnórsson et al. (1996), returning 20.0 l bar mol⁻¹ for CO₂, and 6.52 l bar mol⁻¹ for H₂S, respectively.

Table 2-2: Theoretical and actual gas composition in the heat exchangers.

	Actually measured in condensate [mg l ⁻¹]	Corresp. partial pressure [bar]	Theoretical gas composition [%]	Actually measured gas compos. [%]	Corresp. Partial pressure [bar]	Theoretical conc. in condensate [mg l ⁻¹]
CO ₂	333	0.151	73.7	75.6	0.151	332
H ₂ S	242	0.046	22.6	21.4	0.043	224

	Measured ratio C _{CO₂} :C _{H₂S} []	Corresp. total pressure [bar]		Based on the same total pressure [bar]	Theoretical ratio C _{CO₂} :C _{H₂S} []
	1.38	0.20		0.20	1.48

Composition of non-condensable gasses at Nesjavellir

The actually measured composition of the non-condensable gases at Nesjavellir stems from Olafsson (1992) and Gíslason (2000). Both authors reported a composition of 75.6 % CO₂, 21.4% H₂S and little amounts of H₂, N₂ and CH₄ (3-0.1%). These values are based on steam phase measurements by the staff of OR's research department.

Plausibility considerations

The low corresponding total pressure of 0.2 bar indicates firstly that residence time in the heat exchangers was not long enough to reach equilibrium, and secondly that the temperature drop down from 120°C to 12°C, which would affect the Henry constants, was neglected for the sake of simplicity. Olafsson (1992) reported concentrations in the Nesjavellir condensate of C_{CO₂}=2200 mg l⁻¹ and C_{H₂S}=1200 mg l⁻¹. These values are up to 10 times higher than the actually measured. One explanation might be that the author assumed the gas exchange in the heat exchangers to be in equilibrium for a total pressure between 1 and 2 bar. However, the aim was not to find absolute values, but to compare the ratio C_{CO₂}:C_{H₂S}, in order to evaluate the plausibility of the measured concentrations in the condensate. The relatively small difference between calculated and measured ratios indicates, that, despite the large data scatter in figure 2-3, at least the proportion of the calculated averages seems to comply with the gas composition that caused the condensate concentrations. This provided the needed confidence to allow for the calculation of the amount of injected CO₂ by multiplying the daily condensate injection with the average CO₂ concentration of 333 mg l⁻¹.

General

2.2. Sources and sinks: Containment area specifications

Following the condensate flow from the injection well to Lake Thingvallavatn should reveal possible sources and sinks of its CO₂ load. The flow path was characterized by various physical and chemical specifications that needed to be ascertained in advance. These were parameters such as the porosity, permeability, geological composition, the condition of the gas chemistry in the pore space and the background water chemistry in the aquifer. Normally, rock samples, so called drill chips, from any power plant related well are collected every few meters and stored in archives. For wells that don't reach high enthalpy depths, however, no geological analysis was carried out automatically. Also in situ measurements were hardly ever

taken and analyzed. Owing to the lack of such readily available data, trying to find ways to characterize the containment area was an integral part of the present mass balance.

Locations at Nesjavellir and surroundings

As illustrated in figure 2-1 on page 8 (mass balance scheme), the flow of condensate could be divided into two phases. First, it led 55 m through the vadose zone from the injection well bottom to the groundwater table at approximately 105 m a.s.l. (see appendix 5 for the groundwater level). Thereupon, it lost another 5 m of elevation on its 5.5 km long way northeastwards to the shores of Lake Thingvallavatn. A mapped air picture of the area under investigation is attached in appendix 2. It contains all information and locations of concern for any further specification.

Geology

The condensate seeped through geological formations that consist of postglacial basaltic lava flows formed during eruptions of Mount Hengill volcano, namely the 5'500 years old Hagavíkurhraun and Nesjahraun with an age of 2000 years. In appendix 4 the two available geological cross sections are presented, taken from the draft of a report about the geology at Nesjavellir for the area, which is under progress at ISOR, Iceland GeoSurvey (Hafstad et al., 2007). They mirror only two thirds of the distance between the power station and the lake (see appendix 2 for the exact location of the cross sections).

Basalt composition

Although not sampled directly at Nesjavellir, the unitary origin of Icelandic rock legitimated to assume the average composition of the basalts at Nesjavellir to be the same as found for post-glacial lava flow in the same part of the country². Table 2-3 lists the corresponding CIPW norm, given in volume percent (OR, 2007). This composition will also be used in the reaction path modeling for the Hellisheidi project.

Table 2-3: CIPW norm for a post-glacial lava flow in SW-Iceland (OR,2007).

Group	Mineral	Formula	% Volume
	Quartz	SiO ₂	0.26
Feldspar	Orthoclase	KAlSi ₃ O ₈	0.68
	Albite	NaAlSi ₃ O ₈	16.96
	Anorthite	CaAl ₂ Si ₂ O ₈	30.7
Diposide CaMgSi ₂ O ₆	Wollastonite	CaSiO ₃	12.97
	Enstatite	MgSiO ₃	6.99
	Foresterite	Mg ₂ SiO ₄	5.54
Hyperstene	Enstatite	MgSiO ₃	10.25
	Foresterite	Mg ₂ SiO ₄	8.16
Olivine	Foresterite	Mg ₂ SiO ₄	1.23
	Fayalite	Fe ₂ SiO ₄	1.05
Oxides	Magnetite	Fe ₃ O ₄	2.68
	Ilmetite	FeTiO ₃	2.69

² Sample taken near Krisuvík on Reykjanes peninsula, 45 km west of Nesjavellir; see appendix 2.

Chief composites were found to be Ca- and Mg-rich silicates such as anorthite, wollastonite, enstatite and forsterite, which predestined the material to be a good supplier of the basic cations needed for mineral sequestration (Matter et al, 2007).

Basaltic glass

Typically, fresh lava is glazed with basaltic glass, owing to the thermal shock it experienced during the eruption, i.e. when it got in sudden contact with air, water or ice (e.g. Marsh, 1981). Oelkers and Gíslason (2001) carried out a chemical analysis of Icelandic basaltic glass³, Table 2-4 shows their results. As to compare, the composition of MORB basalt after the geochemical earth reference model GERM is added⁴. All values are given in weight percent.

Table 2-4: The composition of Icelandic basaltic glass and MORB.

[oxide weight %]	Stapafell Iceland	[weight %]	Stapafell Iceland	MORB
SiO ₂	48.12	Si	22.493	23.3
TiO ₂	1.564	Ti	0.938	0.851
Al ₂ O ₃	14.62	Al	7.738	8.1
Fe ₂ O ₃	1.11	Fe(III)	0.776	
FeO	9.82	Fe(II)	7.633	
Fe (tot)		Fe (tot)	8.41	7.97
MnO	0.191	Mn	0.148	0.145
MgO	9.08	Mg	5.476	4.83
CaO	11.84	Ca	8.462	8.21
Na ₂ O	1.97	Na	1.461	1.93
K ₂ O	0.29	K	0.241	0.085
P ₂ O ₅	0.195	P	0.085	0.071

This composition corresponds to a chemical formula normalized to one Si as follows:



Fast weathering of glass and crystallinity effects

Thermo dynamical considerations as well as older studies suggest faster weathering of basaltic glass relative to material that had more time to crystallize (e.g. Gíslason and Eugster, 1987; Guy and Schott, 1989; Gíslason et al., 1996). In contrast to this, Wolf-Boenisch et al. (2005) found hardly an effect of crystallinity on the dissolution and solubility of ultra basic silicates (SiO₂ < 45%w), such as the Si-poor basalt at Nesjavellir. It was concluded that the high content of other cations inhibits a big influence on Si-polymerization in these silicates, i.e. slower solidification does not necessarily mean better-organized, thus more stable structures. Gíslason and Oelkers (2003) conceded that the enhanced weathering of basaltic glass might stem from two factors other than crystallinity. Firstly, although basaltic glass appears smooth on a micron scale, it exhibits a relatively high surface area on a 10-100 nm scale. They found BET measurements of their glass samples to be 92 times larger than the

³ Sample taken from Mount Stapafell on Reykjanes peninsula, 65 km west of Nesjavellir; see appendix 2.

⁴ GERM values were taken from Oelkers and Gíslason's, 2001.

geometrically calculated surface area⁵. This means, the introduction of a roughness factor in the same order of magnitude could make conventional surface estimations for basaltic glass more accurate. In this study, however, this consideration was omitted, as the general approach aimed not to hazard the consequences of overestimating poorly understood system parameters.

The second factor addresses the better access of basaltic glass to undersaturated aqueous solutions.

Scoria

Indeed, the permeability of a lava flow is always greatest along the glassy part (Sigurdsson and Ingimarsson, 1990), where the scoriaceous texture provides porosity values as high as 0.85 (Cashman and Mangan, 1994). Scoria is a textural term for sponge like macro-vesicular lava material. The same reason that causes the glaze of glass in fresh lava, i.e. the rapid chilling of its surface, is responsible for the formation of scoria. As a consequence, scoriaceous material is found on top and at the bottom of a lava flow - the latter due to the tumbling movement at the front, where clinkery surface material is buried by the advancing lava flow (Neuhoff et al., 1999).

At Nesjavellir, this fact is proven by the location of the aquifer within the zone of highest permeability, i.e. at the bottom of the lava flows Hagavíkurhraun and Nesjahraun (see the location of the groundwater table in the geological cross sections in appendix 4).

Porosity, hydraulic conductivity and permeability

Vatnaskil – Consulting Engineers, OR's contractor for hydrological issues evaluated an overall porosity of 0.15 between water table and surface, admitting this value to be rather vague⁶. Just underneath the injection well, Vatnaskil modeled an hydraulic conductivity of 0.13 m s⁻¹ at a local anisotropy value of 50, implicating a highly fractured rock matrix. Vatnaskil's hydraulic conductivity and anisotropy model for the layer between surface and lower aquifer boundary is attached in appendix 5. The modeled hydraulic conductivity corresponds to an extrinsic permeability of 10^{-3.8} cm² after the following equation:

$$K = \frac{\kappa \lambda}{\mu}, \quad (6)$$

where

K	= hydraulic conductivity	[m s ⁻¹],
κ	= intrinsic permeability of the material	[m ²],
λ	= specific weight of water (λ = 9.822e+3 at Nesjavellir)	[N m ⁻³],
μ	= is the dynamic viscosity of water (μ = 1.235e-3 at T = 12°C)	[kg m ⁻¹ s ⁻¹].

Discrepancy to literature

It is noteworthy that not even the intrinsic value of 10e-5.5 cm² (2.6 mm s⁻¹), i.e. neglecting the anisotropy, matches permeability ranges found in literature. Gustavsson (2006), for example, reviewed permeabilities between 10⁻⁷ and 10⁻¹¹ cm² (10^{-4.1} to 10^{-8.1} m s⁻¹) for porous zones within basaltic lavas, comparable to clean unconsolidated sand or karstic limestone. This discrepancy suggests the existence of

⁵ BET is an analytical method to measure surfaces by means of gas adsorption

⁶ Myer, E., Vatnaskil, 31.05.07; personal comment

	<p>either flow internal scoraceous zones (possible according to Gustavson, 2006) a highly fractured rock matrix throughout the whole lava body.</p>
Preferential flow beneath injection well	<p>No backwater was recorded in the injection well at any time. This suggests that the condensate drained off mainly through glassy, scoraceous zones and fractures, i.e. on preferential flow paths with high extrinsic permeability. With an average flow rate of 60 l s⁻¹ and an injection well diameter of 0.56 m, the minimum seepage velocity immediately after the well bottom had to be 0.24 m s⁻¹. Nevertheless, to account for an average flow velocity, Vatnaskil's mean hydraulic conductivity of 0.13 m s⁻¹ was assumed for the whole seepage distance.</p>
Groundwater model	<p>A groundwater model for the catchment area of the Nesjavellir valley exists since the late 1980s, when Vatnaskil was assigned to perform a tracer study and experimental drillings (Kjaran and Egilson, 1986,1987). According to their findings, drainage time from the power station to the lake is 8-10 weeks at an average background discharge of 1.6 m³ s⁻¹. Over the whole distance, the water table is unconfined, thus atmospheric pressure can be assumed throughout the overlying lava layers. Vatnaskil's groundwater model had been frequently updated by actual cognitions and computing methods. The latest version (Kjaran and Myer, 2005) and the version that was elaborated prior to the plant commissioning (Kjaran and Egilson, 1986) are attached in appendix 5.</p>
Outflow	<p>After the plant had been extended in 1998, discharge increased according to the higher energy output with increasing disposal of geothermal fluids. Therefore the flow in the 2005 version of the groundwater model appears to enter the lake within a broader zone than it actually did during the injection period. At that time, the main stream was confined within a rather narrow region (see the old version of the groundwater model in appendix 5). The core of the flow entered the lake at the small bay Varmagjá, meaning <i>warm-gully</i> (see photo documentation in appendix 1). Indeed, background temperature at Varmagjá was found to be 10°C and it never froze up (OR, 2007).</p>
Groundwater chemistry	<p>At Nesjavellir, background CO₂ concentrations as high as 160 mg l⁻¹ were measured in a borehole behind the powerhouse, but only few data was available for the time before the injection started. Towards the lake, background concentrations in boreholes decreased and reached an average value of 55 mgCO₂ l⁻¹ in the waters of the outflow at Varmagjá. Table 2-5 summarizes the developing of background measurements for CO₂ (i.e. the total dissolved inorganic carbon, DIC) and other chemical parameters of concern. As to expect from its inexistence in the free atmosphere, H₂S was not measurably present in its dissolved or dissociated form, neither in the ground- nor in the lake-water. Therefore, H₂S is not listed in table 2-5. Values in brackets do not indicate an average, as only a single measurement had been logged for the time before 1990. For the location of the test wells and monitoring station, see appendix 2.</p>

Table 2-5: Background water chemistry from plant to lake.

Well No°, Monitoring station	CO ₂ [mg l ⁻¹]	SO ₄ [mg l ⁻¹]	Ca ²⁺ [mg l ⁻¹]	Mg ²⁺ [mg l ⁻¹]	pH []	Temp [°C]
NN-1	157.2	11.6	23.4	10.1	7.5	4
NL-4	72.6	25.8	9.5	3.4	8.3	-
NK-1	(42.4)	(17.0)	-	-	(8.9)	-
NK-2	(22.6)	(4.4)	-	-	(7.3)	-
Varmagjá	54.0	12.2	11.2	5.85	7.7	9.9

It was to accept that the base data for table 2-5 is rather weak. Moreover, influences on these parameters are hardly reconstructable, which made it difficult to comment on. At least, the observed temperature difference between the plant and Varmagjá indicates the existence of thermal water rising through fractures, faults and dykes downstream the plant. The issue about background concentration developing is content of subchapter 2.4 and 3.3.

Pore air composition

For the investigation of the possible gas exchange, it was essential to characterize the pore air composition with regard to the gases of concern. These are CO₂, H₂S and oxygen (O₂), the latter to account for the change from anaerobic (prior to injection) to aerobic conditions (upon injection).

CO₂ in pore air

As aforementioned, CO₂ is steadily released from solidifying magma, especially in high temperature areas with magma chambers close to the surface (e.g. Kerrick et al., 1995). Buoyancy forces drive the gas upwards, where it dissolves into local aquifers. This explains the high background concentrations as measured in the well closest to the slopes of Mount Hengill volcano, i.e. well NN-1. Once the CO₂ reaches the unsaturated zone, it forms a gas phase that is denser than the ambient pore air (Oldenburg and Unger, 2003). This suggests the pore air composition in the containment area to differ significantly from atmospheric conditions with regard to CO₂. If equilibrium is assumed, its partial pressure above the groundwater table at Nesjavellir is with $p_{\text{CO}_2} = 0.07$ bar 180 times higher than the atmospheric partial pressure of $p_{\text{CO}_2, \text{atm}} = 380 \times 10^{-6}$ bar. Such an additional gas pressure normally overcomes the density contrast, causing the CO₂ to discharge at the ground surface (Oldenburg and Unger, 2003). Support to this is derived from the high volatility of CO₂, i.e. gas diffusion proceeds sufficiently fast for a good gas exchange with the atmosphere⁷. As a consequence, gas concentration gradients would have been measured within the vadose zone; the closer to the surface the closer to atmospheric conditions. However, the uppermost 15 meters (injection well depth) were outside the system boundary. Moreover, air composition does not have an influence on the kinetics of gas exchange, but on the equilibrium concentrations. Obviously, equilibrium was not reached until a certain seepage distance had been reached. Accordingly, it was simplified that the condensate did not over-degas with respect to the background concentration of 160 mg l⁻¹.

⁷ Kipfer, R. (eawag – Aquatic Research), ETH Zurich, 02.09.07; personal comment

H₂S and O₂ in pore air

The same considerations would apply for H₂S, but neither the free atmosphere nor the groundwater contained the gas in measurable concentrations.

As O₂ is a main component of air, the partial pressure was assumed to be the same in the pore space as at the surface, leading to an equilibrium concentration of 11.2 mg l⁻¹ at 12°C.

General

2.3. Sinks: Modeling the seepage phase

The first flow phase, i.e. the seepage from well bottom to groundwater table, was believed to exhibit the strongest effects on the CO₂ load, especially regarding the degassing. Direct calculations would have been possible, only if the pore and fracture geometry was well known. To come up against the lack of in-situ information, simplified pore geometry was proposed. Therewith, gas exchange and water-rock interaction could be estimated. Of major interest was the CO₂ concentration developing, pH developing and the cation release by silicate dissolution.

The aim was to design a flexible model with variable pore geometry. This should minimize assumptions regarding the nature of the pore space and allowed for different scenarios and the calculation of ranges.

A step-by-step description of the model calculations is given below. For the scripts, see appendix 6.

Basic geometrical approach

2.3.1 Geometrical approach

Justified by the considerations about preferential flow, the pore geometry was simplified to a distinct number of little unitary pipes leading straight down to the groundwater. The bigger the number of flow pipes n , later referred to as *pores*, the bigger the surface that is wetted by the condensate, i.e. the more rock surface was exposed to dissolution.

As in terms of soil physics, the pore space could be water saturated to a certain degree, determining the tendency of the dissolved species to degas. The lower the pore water saturation, the faster the degassing.

Introducing the saturation demanded for the flexibility in the number of pores n . A saturation of 50%, for instance, referred to the need for the double amount of pores in order to drain the same amount of condensate.

Constants

The following parameters were set constant:

- Flow rate at 60 l s⁻¹
- Flow velocity at 0.13 m s⁻¹
- Temperature at 12°C

To recall, the flow rate and temperature represent average values over the whole injection period from 1990 till 1998. Changes in equilibrium constants and other chemical parameters due to the cooling from 12°C to 4°C (groundwater temperature) were not considered, for the sake of simplicity. If not further specified, chemical equilibrium constants were calculated for 12°C from tables in Atkins and Löpfle (2002).

Variables	<p>The following two geometry parameters were defined as variables, thus offering the possibility for different model scenarios:</p> <ul style="list-style-type: none"> • Saturation from 1% to 99% • Wetted surface area (A_{w}) from 0.061 to 1.5 m², mean at 0.41 m²
A _w area after Marini (2007)	<p>The range of the wetted surface area was adopted from Marini (2007, p.388&351) and therein from Cipolli et al. (2004, p.796), where these values represent the total surface area of serpentinic rock in contact with 1l of water. Marini (2007) used them for the reaction path modeling of basaltic glass, admitting that uncertainty is rather large. He pointed out, that the main difficulty in kinetic geochemical modeling is the characterization of reactive surface areas of the solid phases. In this study, calculations are run using the minimum, mean and maximum value proposed by Cipolli and Marini, in order to cover the range and the mean coevally.</p>
No° of pores and pore radius at given A _w	<p>While holding the pore surface fixed at the three wetted surface area levels, the number of pores n and the corresponding radius was calculated after the following simple geometrical equations:</p> $A_{w} = \frac{2\pi r v_f n_{100}}{10^3 f}, \quad (7)$ $r = \sqrt{\frac{A_c}{\pi}}, \quad (8)$ $A_c = \frac{V_p}{v_f}, \quad (9)$ $V_p = \frac{f}{n_{100}}, \quad (10)$ <p>where</p> <p>A_w = 1 liter wetted surface area after Marini (2007) [m²],</p> <p>r = pore radius [m],</p> <p>v_f = flow velocity [m s⁻¹],</p> <p>n₁₀₀ = number of pores at saturation = 100% [],</p> <p>f = flow [m³ s⁻¹],</p> <p>A_c = cross section area of one pore [m²],</p> <p>V_p = volume of 1 pore for 1 sec of flow [m³].</p>
Visualization of the geometrical approach	<p>The following two figures visualize the geometrical approach, pointing out the values that correspond to the three considered A_w values.</p>

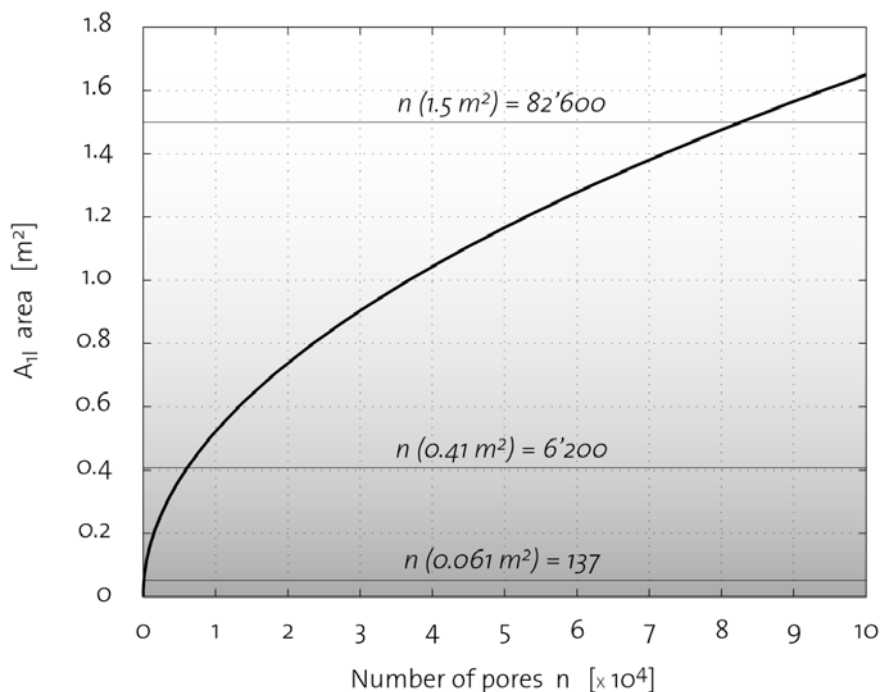


Figure 2-4: A₁₁ surface vs. number of pores n at 100% pore water saturation.

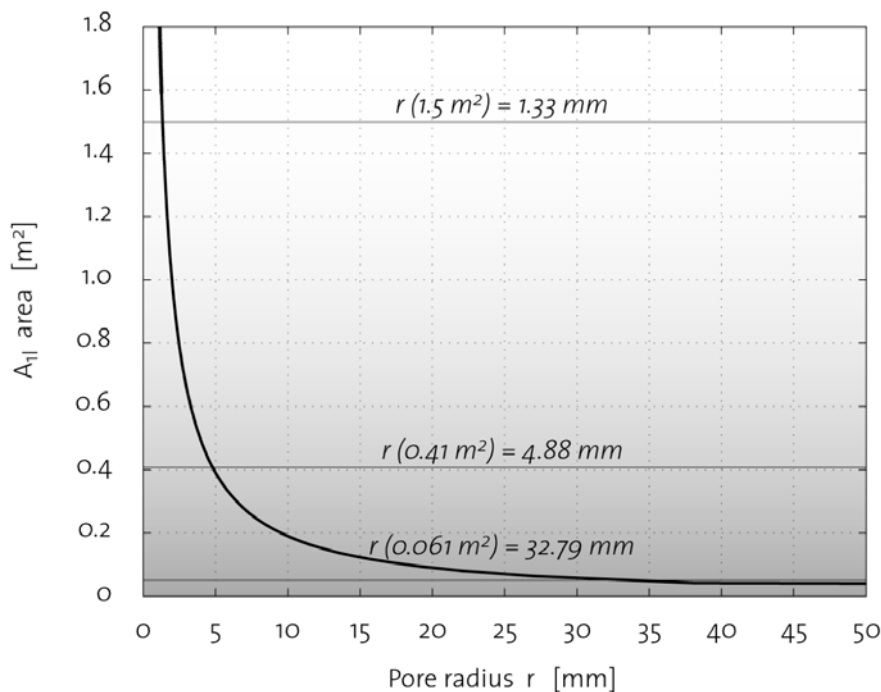


Figure 2-5: A₁₁ surface vs. pore radius at 100% pore water saturation.

Starting from these basic calculations, a proportional increase in n accounted for saturation < 100%, whereas the pore radius remained fixed. Hence, the wetted area for saturation < 100%, i.e. the total reactive surface area that is available for silicate dissolution, changes according to figure 2-6.

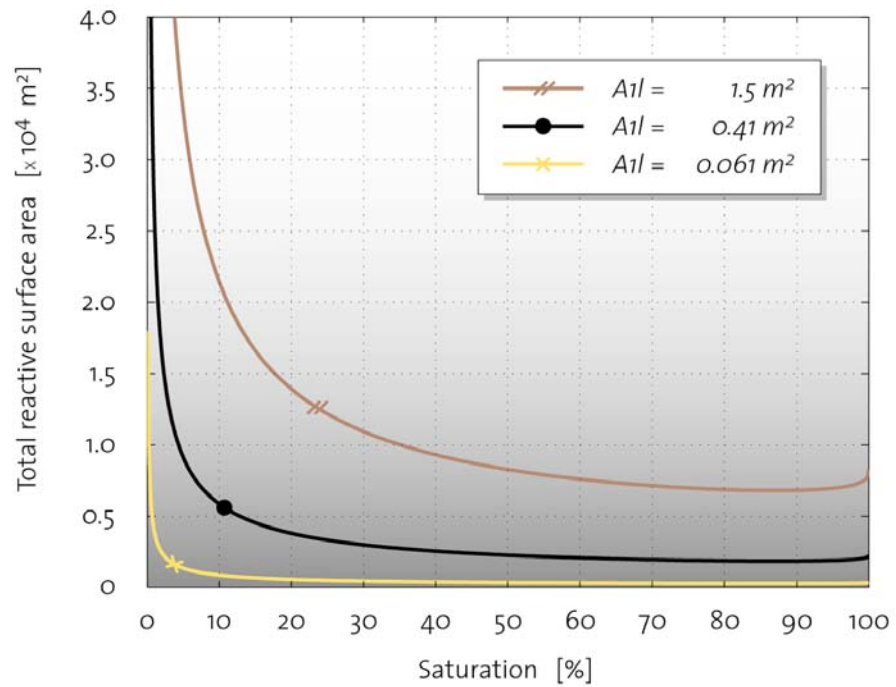


Figure 2-6: Total reactive surface area vs. pore saturation at given A_{II} area.

Total reactive surface area

Here, the ordinate represents the reactive surface area of the whole flow, not only for one pore, calculated via the following equation:

$$A_{tot} = \alpha_w r v_f n, \quad (11)$$

where additionally

A_{tot} = reactive surface area for 1 sec of total flow [m² sec⁻¹],

α_w = angle of the water filled segment [rad],

n = number of pores [.].

2.3.2 Degassing model

The species to consider for the gas exchange between condensate and pore air are:



River model

In order to model the degassing, a surface renewal gas exchange model for rivers was applied. In this model, the river cross section is assumed to be an ideal rectangle, i.e. constant depth over the whole width. Together with the gas specific transfer velocity, the river depth determines the exchange rate. The deeper the river and the slower the transfer velocity, the more time is needed for the whole water profile to be equilibrated. Core of the model is the following differential equation (Imboden and Kipfer, 2003):

$$\frac{dC_i}{dt} = -k_{g,i} (C_i - C_{eq,i}), \quad (15)$$

$$k_{g,i} = \frac{v_{w,i}}{h}, \quad (16)$$

with the solution:

$$C_i(t) = (C_{0,i} - C_{eq,i})e^{-k_{g,i}t} + C_{eq,i}, \quad (17)$$

where

C_i	= concentration of species i	[mol l ⁻¹],
$C_{eq,i}$	= equilibrium concentration	[mol l ⁻¹],
$C_{o,i}$	= concentration at t=0	[mol l ⁻¹],
$k_{g,i}$	= gas exchange rate	[sec ⁻¹],
$v_{w,i}$	= transfer velocity	[m sec ⁻¹],
h	= river depth	[m].

Gas transfer velocity

Gas transfer velocities depend strongly on the degree of turbulence in the liquid phase. The subscript w indicates a fluid-film controlled exchange behavior, as the dimensionless Henry-coefficient of all 3 gases is $K_H > 10^{-3}$ within the considered temperature range (Imboden and Kipfer, 2003). Normally, turbulence is expressed by the wind speed u_{10} (10m above water level). Values for 3 different degrees of turbulence ($u_{10} = 15, 10, 5 \text{ m s}^{-1}$) were obtained graphically from a study about transfer velocities of O₂ at 10°C (see appendix 7). As the boundary layer thickness at given turbulence is the same for all gases, it was possible to calculate the corresponding transfer velocities for CO₂ and H₂S via the following equation (Aeschbach-Hertig, 2005):

$$v_i = \frac{D_i}{\delta_{u_{10}}}, \quad (18)$$

where

D_i	= molecular diffusion coefficient of species i	[m ² sec ⁻¹],
$\delta_{u_{10}}$	= boundary layer thickness at given u_{10}	[m].

The molecular diffusion coefficients are $D_{CO_2}=10^{-8.72}$, $D_{H_2S}=10^{-8.80}$ and $D_{O_2}=10^{-8.70} \text{ m}^2 \text{ s}^{-1}$, respectively (Cunningham and Rockford, 2006).

Turbulence assumption

In this study, calculations were run using the transfer velocities at the high degree of turbulence, i.e. $u_{10} = 15 \text{ m s}^{-1}$, in order to account for the heavy perturbation water will experience that flows vertically through pore. It was to accept, that the u_{10} measure is rather far from a physical meaning of the flow perturbation in a pipe-shaped pore with delimited space for pore air.

Adapting the river depth

The river depth, i.e. the gas exchange distance, had to be adapted in order to match the half pipe shaped water volume of a partly filled pore. Figure 2-7 illustrates the geometrical problem.

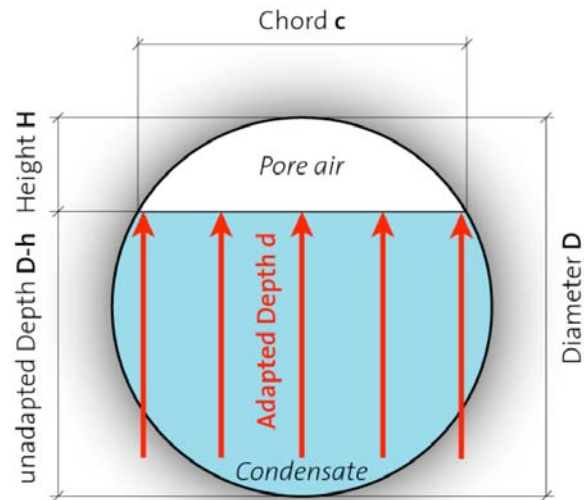


Figure 2-7: Pore geometry and adapted depth.

The following adaptation was found:

$$d = (D - H)\varepsilon\left(\frac{D}{c}\right)^\eta, \quad \text{for saturation} > 50\%, \quad (19)$$

$$d = (D - H)\varepsilon\left(\frac{c}{D}\right)^\eta, \quad \text{for saturation} < 50\%. \quad (20)$$

where

d	= adapted depth (exchange distance)	[m],
D	= pore diameter	[m],
H	= height of the air filled segment	[m],
c	= chord of the air filled segment	[m],
ε	= additional correction factor btw. 0.8–1.0	[],
η	= additional correction term btw. 0.6–1.0	[].

Meaning of the factors

The factor D/c implements an infinity effect towards the top of the pore at saturation close to 100%, where degassing is inhibited by the lack of air, i.e. by the equilibration of dissolved gas with the remaining pore air. Towards the bottom of the pore at saturation close to 0%, the factor c/D leads to a faster convergence of the depth d to zero, which means a facilitation of degassing relative to the unadapted exchange distance $(D-H)$.

The additional correction factor ε generally lowers $D-H$ in order to account for a hypothetical average depth of the pore water (i.e. it determines the length of the red arrows in figure 2-7 on page 22). A reasonable range was found to be 0.8–1.0, whereas $\varepsilon = 0.9$ was chosen for the calculations. The other additional correction term η delays the infinity effect towards the top of the pore, so that degassing is inhibited only at very high saturation. A wider range was proposed for the ε -factor, from 0.6–1.0, and it was set at $\eta = 0.8$.

Illustration of the adaptations

Figure 2-8 shows how the adaptations affect the adapted exchange distance D-H.

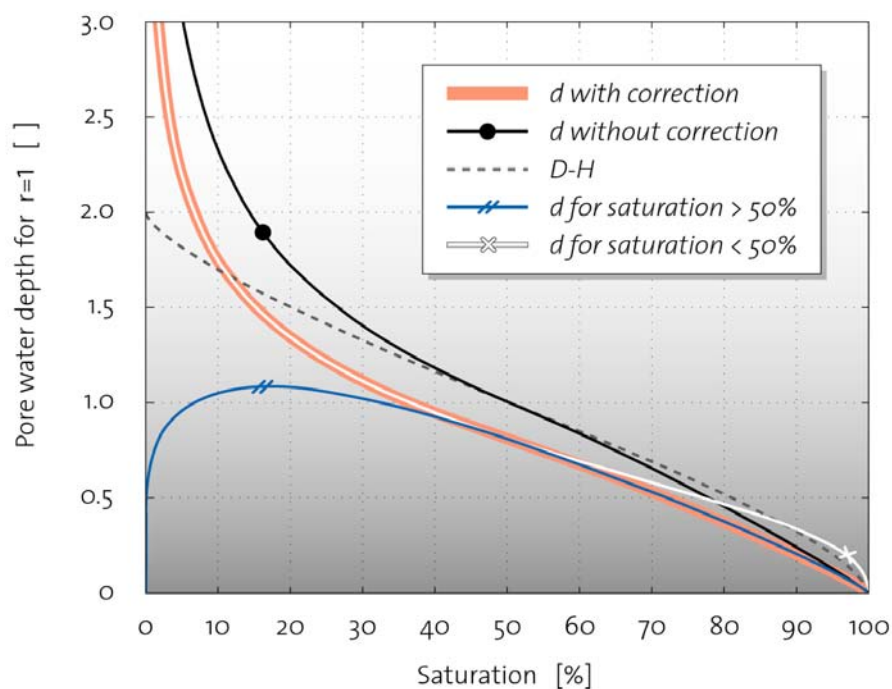


Figure 2-8: Adapted and unadapted exchange distance and effects of the additional correction terms.

Gas exchange in both directions

Gas exchange proceeds always in both directions, i.e. from water to gas phase and vice versa. Only probabilistic assumptions would determine, how much CO₂ at 55 m below well bottom actually stemmed from the input and how much had been replaced by the background CO₂ in the pore air. Such assumptions were not justifiable, since the tendency of an injected CO₂ molecule to re-diffuse into the condensate – once it had degassed – remained unknown. The quantification of the degassing was therefore given by a range between the two extreme cases of a total (scenario 1) and a zero (scenario 2) replacement (i.e. all injected CO₂ molecules escaped into the ambient pore air immediately upon degassing or they were the only ones to exchange back and forth).

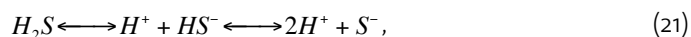
2.3.3 pH developing

So far, the mass transfer of CO₂ could be computed at the given input, equilibrium concentration and variable hypothetical geometry of the pore space. The same geometrical approach applied for the calculations of the silicate dissolution, provided a good estimation of the pH developing in the condensate could be found.

Initial pH at well bottom

The condensate entered the lava in acidic condition, as aforementioned at a measured initial pH of 4.46.

This was caused by the present H₂CO₃ (after reaction 1) and H₂S. The latter dissociates to bisulfide (HS⁻) and further to sulfide (S₂⁻) after the following reaction:



At a pH of 4.46, the chief part of total carbon and sulfur is present as H₂CO₃ and H₂S, respectively. The measured value is in good accordance with the theoretical pH

values of 4.26 and 4.66, which were calculated as follows for $C_{\text{CO}_2,0}=333 \text{ mg l}^{-1}$ and $C_{\text{H}_2\text{S},0}=242 \text{ mg l}^{-1}$ (Angst et al., 2002):

$$pH = \frac{1}{2} \left(pK_{a1} - \log \left(\frac{C_{a1}}{C^0} \right) \right), \quad (22)$$

where

$$\begin{aligned} pK_{a1} &= \text{acidic strength of acid a (} pK_{\text{H}_2\text{CO}_3}=6.40, pK_{\text{H}_2\text{S}}=7.18) & [], \\ C_{a1} &= \text{concentration of the acid a} & [\text{mol l}^{-1}], \\ C^0 &= \text{standard concentration} & [1 \text{ mol l}^{-1}]. \end{aligned}$$

Three possible influences on the pH were identified as described below.

Influence of CO₂ and H₂S degassing

According to equation (22), the pH had to increase while CO₂ and H₂S proceeded to degas. Unlike CO₂ with $C_{\text{CO}_2,\text{eq}}=160 \text{ mg l}^{-1}$, H₂S could degas completely, according to its equilibrium concentration $C_{\text{H}_2\text{S},\text{eq}}=0 \text{ mg l}^{-1}$. Furthermore, the two pK_a values, indicating that H₂S is an 8 times weaker acid than H₂CO₃. Hence, the protons from the carbonic acid system were predominant for the influence on the pH.

State of the carbonic acid system

At acidic conditions, the concentrations of HCO₃⁻ and CO₃²⁻ are orders of magnitudes below the one of H₂CO₃, the species from where CO₂ can degas (see reaction 1). The pH would have to rise until a value higher than 5 before a further increase would result in the formation of significant amounts of HCO₃⁻. This would slow down the degassing by increasing the solubility. Provided pH=5 was not exceeded, the modelled C_{CO₂}, i.e. C_{tot}, could be equalized to C_{H₂CO₃}, as summarized below:

$$C_{\text{H}_2\text{CO}_3} \cong C_{\text{CO}_2} = C_{\text{C}_{\text{tot}}} = C_{\text{H}_2\text{CO}_3} + C_{\text{HCO}_3^-} + C_{\text{CO}_3^{2-}}, \quad (23)$$

where

$$\begin{aligned} C_{\text{H}_2\text{CO}_3} &= \text{concentration of H}_2\text{CO}_3 & [\text{mol l}^{-1}], \\ C_{\text{CO}_2} &= \text{concentration of CO}_2 & [\text{mol l}^{-1}], \\ C_{\text{C}_{\text{tot}}} &= \text{concentration of total DIC} & [\text{mol l}^{-1}], \\ C_{\text{HCO}_3^-} &= \text{concentration of HCO}_3^- & [\text{mol l}^{-1}], \\ C_{\text{CO}_3^{2-}} &= \text{concentration of CO}_3^{2-} & [\text{mol l}^{-1}]. \end{aligned}$$

Deriving the degassing influence

Hence, the gas exchange model (equation 15) could be directly applied for the evaluation of the degassing influence on the pH at any time during the seepage phase. The following equation was derived:

$$\frac{dC_{\text{H}^+,g}}{dt} = -\frac{z}{2} (C_{\text{CO}_2})^{-1/2} \frac{dC_{\text{CO}_2}}{dt}, \quad (24)$$

with

$$z = 10^{-1/2 pK_{\text{H}_2\text{CO}_3}}, \quad (25)$$

$$\frac{dC_{\text{CO}_2}}{dt} = -k_{g,\text{CO}_2} (C_{\text{CO}_2} - C_{\text{CO}_2,\text{eq}}), \quad (26)$$

where

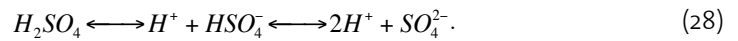
$$\begin{aligned} C_{\text{H}^+,g} &= \text{concentration of H}^+ \text{ influenced by CO}_2\text{-degassing} & [\text{mol l}^{-1}], \\ C_{\text{CO}_2} &= \text{concentration of CO}_2 & [\text{mol l}^{-1}], \\ C_{\text{CO}_2,\text{eq}} &= \text{equilibrium concentration of CO}_2 & [\text{mol l}^{-1}], \\ k_{g,\text{CO}_2} &= \text{gas exchange rate of CO}_2 & [\text{sec}^{-1}]. \end{aligned}$$

Influence of H₂S oxidation

The second influence was the possible oxidation of H₂S to sulfuric acid (H₂SO₄) as follows:



In aqueous solutions, H₂SO₄ dissociates to bisulfate (HSO₄⁻) and sulfate (SO₄²⁻) according to the following reactions:



H₂SO₄ deprotonates almost completely to HSO₄⁻, owing to its very low acidic strength (pK_{H₂SO₄} = -2.87). Much fewer protons in the solution stem from the thus formed HSO₄⁻ (pK_{HSO₄⁻} = 2.06). Therefore, it could be assumed that the oxidation of every H₂S increased the total amount of protons by one H⁺, thus lowering the pH accordingly.

H₂S oxidation kinetics

In an anaerobic environment, such as deep aquifers and similar formations, dissolved H₂S has no effects on the processes of mineral sequestration (Knauss et al., 2005). Instead, oxygen was present in the vadose zone at Nesjavellir as mentioned above. Although literature has been intensively searched, all oxidation rates within the initial pH and temperature conditions that were found consider reaction kinetics of pseudo first order, assuming oxygen to be sufficiently present. Millero et al. (1987), for instance, studied chemical oxidation rates of H₂S in air saturated water as a function of pH from 4 to 8 and temperature from 5°C to 65°C. The kinetics was described as follows:

$$\frac{dC_{H_2S}}{dt} = k'_{ox} C_{H_2S} \quad (29)$$

with

$$k'_{ox} = k_{ox} C_{O_2,eq} \quad (30)$$

$$\log(k_{ox}) = \frac{1}{60^2} \left(10.50 + 0.16 pH - \frac{3000}{T} \right) \quad (31)$$

where

C_{H₂S} = concentration of H₂S [mol l⁻¹],

C_{O_{2,eq}} = equilibrium concentration of O₂ [mol l⁻¹],

k'_{ox} = pseudo first order oxidation rate [sec⁻¹],

k_{ox} = oxidation rate [sec⁻¹],

T = temperature [°K].

Initially anaerobic conditions and biological oxidation

At Nesjavellir, oxygen first had to diffuse into the condensate before oxidation could take place. This would clearly demand oxidation kinetics of second order, i.e. adding the time depended concentration of O₂ to equation (29) and using a k_{ox} different than given in equation (31). Biological oxidation of H₂S might occur as well, but as corresponding rates are given in the same order of magnitude in literature (e.g. Plas et al., 1991), possible biological enhancement of the H₂S oxidation was negligible.

Deriving the H₂S oxidation influence

The calculations were tested using the oxygen saturation concentration of 11.2 mg l⁻¹, and thereupon modified to kinetics of true second order, using the same reaction rates but the actually present O₂ concentrations. Despite this could be in error, it would at least not lead to an overestimation of the pH decrease. A system of ordinary first order differential equations was set up as follows:

$$\frac{dC_{H_2S}}{dt} = -k_{g,H_2S}C_{H_2S} - k_{ox}C_{H_2S}C_{O_2}, \quad (32)$$

$$\frac{dC_{H^+,ox}}{dt} = +k_{ox}C_{H_2S}C_{O_2}, \quad (33)$$

$$\frac{dC_{O_2}}{dt} = +k_{g,O_2}(C_{O_2,eq} - C_{O_2}) - k_{ox}C_{H_2S}C_{O_2}, \quad (34)$$

with

$$k_{ox} = 10^{\frac{1}{60^2} \left(10.5 - 0.16 \log(C_{H^+}) - \frac{3000}{T} \right)}, \quad (35)$$

where additionally

$C_{H^+,ox}$ = concentration of H⁺ influenced by oxidation [mol l⁻¹],

C_{O_2} = concentration of O₂ [mol l⁻¹],

k_{g,H_2S} = gas exchange rate of H₂S [sec⁻¹],

k_{g,O_2} = gas exchange rate of O₂ [sec⁻¹].

Influence of silicate
dissolution

Silicate dissolution takes place via proton exchange reactions. Thus it represents a proton consuming process and exhibits an influence on the pH itself, provided the aqueous solution is unbuffered (which was the case in the condensate).

Basaltic glass dissolution rates

Oelkers and Gíslason (2001) and Gíslason and Oelkers (2003) studied the dissolution of the aforementioned sample of basaltic glass from Stapafell, SW-Iceland under laboratory conditions. They found dissolution rates to depend chiefly on the pH, with a characteristic asymmetric U-shape and a shift of the minimum rate towards lower pH with increasing temperature, as visualized below.

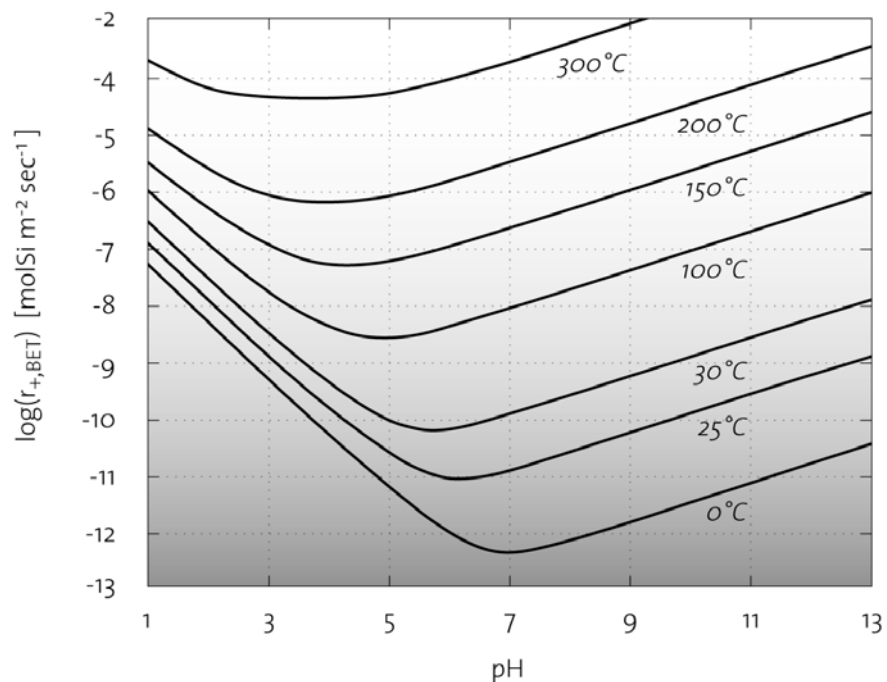


Figure 2-9: Dissolution rates of Icelandic basaltic glass (Gíslason and Oelkers, 2003).

Below pH 5.5, this dependency could be locally linearized as follows (graphically assessed):

$$\log k_{diss, Si} = -3.99 - 0.95 pH, \quad (36)$$

where

$$k_{diss, Si} = \text{dissolution rate of Si} \quad [\text{molSi m}^{-2} \text{sec}^{-1}].$$

Deriving the silicate dissolution influence

The same studies found the release of one mole Si to consume 1.08 moles of protons. The normalization of the dissolution rate to molSi per square meter demanded to following adaptation, in order to calculate the influence on the proton concentration gradient (given in mol l⁻¹):

$$\frac{dC_{H^+, Si}}{dt} = -1.08 \frac{A_w}{V_w} k_{diss, Si}, \quad (37)$$

with

$$A_w = \alpha_w r v_f, \quad (38)$$

$$V_w = r^2 (\alpha_w - \sin \alpha_w) v_f, \quad (39)$$

where additionally

$$C_{H^+, Si} = \text{concentration of H}^+ \text{ influenced by silicate dissolution} \quad [\text{mol l}^{-1}],$$

$$A_w = \text{reactive surface area for 1 pore in 1 sec} \quad [\text{m}^2 \text{sec}^{-1}],$$

$$V_w = \text{water volume in 1 pore in 1 sec} \quad [\text{l sec}^{-1}].$$

Overall pH calculation

To repeat and conclude, summing the 3 influences up lead to the following system of ordinary first order differential equations:

$$\frac{dC_{CO_2}}{dt} = -k_{g, O_2} (C_{CO_2} - C_{O_2, eq}), \quad (40)$$

$$\frac{dC_{H_2S}}{dt} = -k_{g, H_2S} C_{H_2S} - k_{ox} C_{H_2S} C_{O_2}, \quad (41)$$

$$\frac{dC_{O_2}}{dt} = +k_{g, O_2} (C_{O_2, eq} - C_{O_2}) - k_{ox} C_{H_2S} C_{O_2}, \quad (42)$$

$$\frac{dC_{H^+}}{dt} = +k_{ox} C_{H_2S} C_{O_2} - \frac{z}{2} (C_{CO_2})^{-1/2} \frac{dC_{CO_2}}{dt} - 1.08 \frac{A_w}{V_w} k_{diss, Si}. \quad (43)$$

This system was to solve numerically and returned the overall pH developing for different pore geometries.

2.3.4 Mineral trapping

Estimating the mineral trapping demanded for the Ca²⁺, Mg²⁺ and CO₃²⁻ concentration developing to be calculated.

Calcium and magnesium release

The calculation of the calcium and magnesium release tied in with the considerations about silicate dissolution induced proton consumption stated above.

Assuming stoichiometric release of Ca²⁺ and Mg²⁺ (see formula 5), Ca²⁺ and Mg²⁺ concentration could be derived in accordance with equation (37):

$$\frac{dC_{Ca^{2+}}}{dt} = +0.26 \frac{A_w}{V_w} k_{diss,Si}, \quad (44)$$

$$\frac{dC_{Mg^{2+}}}{dt} = +0.28 \frac{A_w}{V_w} k_{diss,Si}, \quad (45)$$

where

$k_{diss,Si}$ = dissolution rate of Si [molSi m⁻² sec⁻¹].

C_{Ca} = concentration of Ca²⁺ [mol l⁻¹],

C_{Mg} = concentration of Mg²⁺ [mol l⁻¹].

Calculating the CO₃²⁻ concentration

Since the carbonic acid system equilibrates within milliseconds, the CO₃²⁻ concentrations were calculated without using a kinetic model. The simplification in equation (23) was used to determine the carbonate concentration as follows (Wehrli and Fuchs, 2005):

$$C_{CO_3^{2-}} = C_{tot} \frac{K_{H_2CO_3} K_{HCO_3^-}}{K_{H_2CO_3} K_{HCO_3^-} + K_{H_2CO_3} C_{H^+} + C_{H^+}^2}, \quad (46)$$

where additionally

$K_{H_2CO_3}$ = 1st dissociation constant, $K_{H_2CO_3} = 10^{6.40}$ [],

$K_{HCO_3^-}$ = 2nd dissociation constant, $K_{HCO_3^-} = 10^{10.47}$ [],

C_{tot} = modeled CO₂ concentration after equation (15) [mol sec⁻¹].

Equation (46) is valid for a closed carbonic acid system or, as the case at Nesjavellir, far from equilibrium conditions with immediate equilibration.

Precipitation of the carbonates

Accepting silicate dissolution to be rate limiting, as widely believed in literature (e.g. Goff and Lackner, 1998; O'Connor et al., 2002; Park and Fan, 2004; Hänchen et al., 2006&2007), precipitation of calcite (CaCO₃) and magnesite (MgCO₃) does not control the mineral sequestration process. But, precipitation is only possible, if the aqueous solution is oversaturated with respect to the present Ca²⁺/Mg²⁺ and CO₃²⁻ concentrations. Hence, the investigation of precipitation (reaction 3) had to be based on equilibrium calculations, also due to the lack of suitable kinetics.

The solubility product

Saturation conditions were estimated from the solubility product of reaction (3) (implicating an activity divisor of 1 for the solid carbonates):

$$K_{S,CaCO_3} = [Ca^{2+}][CO_3^{2-}] = 10^{-8.38}, \quad (47)$$

$$K_{S,MgCO_3} = [Mg^{2+}][CO_3^{2-}] = 10^{-8.14}, \quad (48)$$

where

K_S = solubility equilibrium constants [],

[x] = concentrations of the species of concern [mol l⁻¹].

In other words, precipitation took then place, when the concentration products reached a value higher than 10^{-8.38} and 10^{-8.14}, respectively.

If this condition was fulfilled and if immediate precipitation upon silicate dissolution was assumed, it had been possible to calculate, for instance, how much kilos of sequestered CO₂ was to expect at each m below the well bottom. To foreshadow the

findings from the saturation condition investigation, such calculations were a priori highly hypothetical and therefore omitted.

2.4. Sources, sinks and outflow: Groundwater transport

General

So far, the processes during the seepage phase had been investigated on high level of detail. It was beyond the scope of the present study to examine the 5.5 km long groundwater transport in the same manner. Numerous background impacts would have been not reconstructable and thus, a high-resolution mathematical model would only pretend accuracy and would not lead to reliable estimations. Instead, two ways were proposed in order to evaluate the further fate of remaining CO₂ input and to validate the results from the seepage phase modeling.

First, a qualitative discussion of the existing outflow monitoring data was considered reasonable, taking both the findings from the seepage modeling and the data from the water monitoring at Lækjarhvarf into account.

Secondly, the mixing for the given input and background concentrations could be calculated and normalized with the conditions before 1990. This of course simplified the actual processes, but allowed for a direct comparison with the actually measured situation at the outflow.

Preliminary to these two approaches, the additional groundwater charge at Lækjarhvarf shall be described, in order to include it as the key source for CO₂ and other species of concern to the containment area.

2.4.1 Groundwater charge at Lækjarhvarf

Disposal of geothermal brine

As aforementioned, the separated geothermal brine was disposed in the brook Nesjvallalækur at a rate of approximately 40 l sec⁻¹ at the beginning, rising up to 90 l sec⁻¹ by 1998. This natural brook carries the surface drainage of the valley, typically at 90 l sec⁻¹, depending on runoff conditions, which may lead to flows as high as 1000 l sec⁻¹ (Kjaraan and Egilson, 1986). The water flows 2 km along the eastern side of the valley before it disappears underground at the shallow pond Lækjarhvarf. The seepage is visibly confined to a gully like zone (see the photo documentation in appendix 1), where the flow follows a vertical fault 40 m down to the groundwater (Hafstad et al., 2007).

Water chemistry monitoring at Lækjarhvarf

Right at that place, water samples were taken twice a year and analyzed. Hence, the mixing with the brine and any chemical process in the brook did not have to be evaluated to depict the impact of this charge to the containment area. Average concentrations were calculated and could be used to interpret the measured concentrations in the outflow. For an average flow rate of the brine, 60 l sec⁻¹ was assumed. Appendix 8 contains plots of the time series for the species of concern. These are CO₂, Mg²⁺, Ca²⁺, SO₄²⁻ as well as the pH and temperature.

2.4.2 Qualitative considerations

Monitoring stations

As aforementioned, a time series was available for the water chemistry at the outflow, i.e. at the shores of Lake Thingvallavatn, going back as far as the 1980ies. The purpose of these measurements was the monitoring of possible impacts of the plant on the adjacent lake. Each summer and each winter, a water sample was taken from

6 places, namely Markagjá, Varmagjá, Eldvík, Sigguvík, Stapavík and Markatangi. All stations were located around the estimated extent of the run off from Nesjavellir valley and the freshwater pump station Grámelur (see overview in appendix 2). To investigate the outflow conditions before and during the injection period, it was enough to consider the data from Varmagjá.

Monitored parameters

The same parameters as at Lækjarhvarf were monitored; to repeat, the concentration of CO₂, H₂S, Mg²⁺, Ca²⁺ and SO₄²⁻. All time series were plotted and attached in appendix 8.

They could be put into relation with the calculated input from the condensate and with the plots from Lækjarhvarf and the input from the condensate.

Uncertainty

Again, having in mind to be careful when interpreting this data was vitally important. Many background processes, such as abnormal precipitation events, long term changes in reservoir properties or short-term natural geothermal variations due to seismic activity might have influenced the water chemistry substantially. Thus, an expected trend might have been blurred or even superposed.

2.4.3 Quantitative estimations

Background concentrations changes

The same uncertainty was faced when trying to validate the model assumptions, i.e. to find a way to calculate the impacts from the wastewaters of Nesjavellir and compare the resulting concentration mixes with the average concentrations measured at Varmagjá. First to be done was the evaluation of the available background measurements from the time before 1990, in order to quantify average changes in concentrations from the plant to the lake.

Table 2-5 on page 16 already foreshadowed the unknown background processes, revealing rather strong changes. In order to keep the further descriptions concise, the distance between plant and lake was split in several parts and key stations with corresponding concentrations as indicated by figure 2-10.

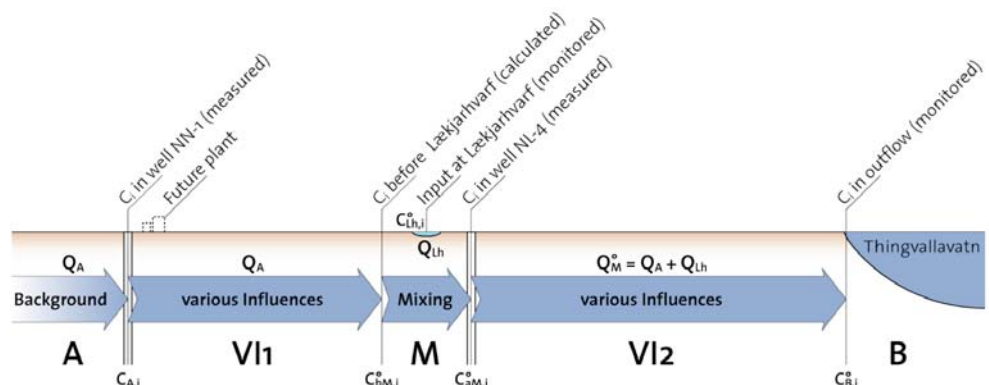


Figure 2-10: Background concentration scheme.

Calculations for the background concentration scheme

The concentration changes due to various influences VI1 and VI2 were quantified by simply building the differences from A to M and M to B, respectively. From the measured average background concentrations in the wells NN-1 and NL-4, the conditions just before Lækjarhvarf were estimated. The following equations were derived:

$$VI1_i = C_{A,i} - C_{bM,i}^o \quad (50)$$

$$C_{bM,i}^o = \frac{Q_M^o C_{aM,i}^o - Q_{Lh}^o C_{Lh,i}^o}{Q_A} \quad (51)$$

$$VI2_i = C_{aM,i}^o - C_{B,i}^o \quad (52)$$

where

$C_{x,i}$ = concentration of species i, as indicated in figure 2-10 [mg l⁻¹],

Q_x = flow rate, as indicated in figure 2-10 [l sec⁻¹],

$VI1,2_i$ = various influences on concentration of species i [mg l⁻¹].

With $Q_A = 1600$ l sec⁻¹, $Q_{Lh} = 90$ l sec⁻¹ and $Q_M = Q_A + Q_{Lh}$, background concentration developings are obtained as summarized in Table 2-6.

Table 2-6: Background concentration developing.

Background changes	CO ₂ [mg l ⁻¹]	SO ₄ [mg l ⁻¹]	Ca ²⁺ [mg l ⁻¹]	Mg ²⁺ [mg l ⁻¹]	pH []
C_A	157.2	11.6	23.4	10.1	7.50
$VI1$	-83.2	+13.0	-13.8	-6.7	+0.85
C_{bM}^o	74.1	24.6	9.5	3.4	8.35
C_{Lh}^o	46.3	47.0	9.1	3.63	8.16
C_{aM}^o	72.6	25.8	9.5	3.4	8.34
$VI2$	-18.7	-13.6	+1.7	+2.5	-0.69
C_B^o	54.0	12.2	11.2	5.9	7.7

Three points were to accept. First of all, the exact cause of the concentration changes, i.e. the various influences $VI1$ and $VI2$, remained uncertain. Nevertheless, it was tried to draw conclusions from the interpretation of the concentration developing in the outflow and in the additional charge at Lækjarhvarf, as described below in subchapter 3.3.1. Secondly, possible lateral or geothermal influxes were not included in the flow rates of equation (51). Thirdly, the results in Table 2-6 had to be assumed constant over the years, in order to use them for the normalization of the calculations of the conditions during the injection period.

Concentration developing during injection

To account for the new discharge impacts after the plant had started its production, figure 2-10 was redesigned as follows:

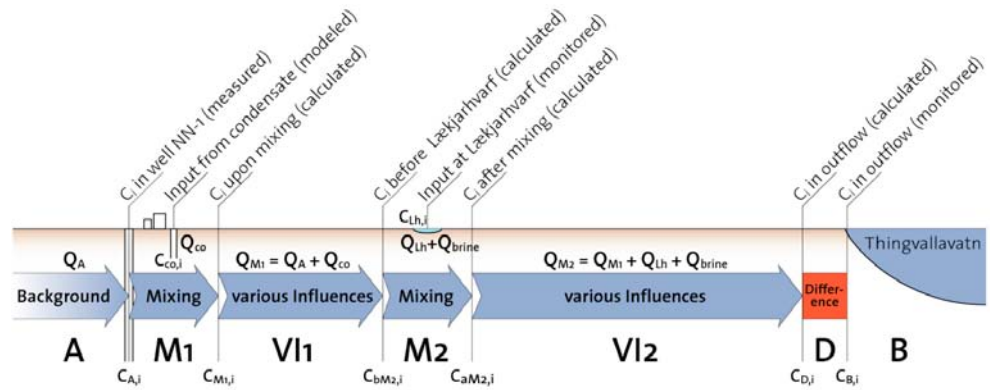


Figure 2-11: Concentration developing scheme during injection period.

Now there were two mixing events and the additional input at Lækjarhvarf increased by the amount of disposed geothermal brine from the separators.

Calculations for the concentration developing scheme during injection

60 l sec⁻¹ and the modeled concentrations at 55m below well bottom were taken for the condensate input (M1 mixing event). 150 l sec⁻¹ ($Q_{Lh} + Q_{brine}$) and average concentrations from the water chemistry monitoring at Lækjarhvarf denoted the new additional groundwater charge at the pond (M2 mixing event). Before and after M2, the changes from the background concentration evaluation were included, in order to make the resulting concentrations C_D comparable to the average values from the lake water monitoring at Varmagjá between 1990 and 1998 (C_B). To following equations were derived:

$$C_{M1,i} = \frac{Q_{CO_2} C_{CO_2,i} + Q_A C_{A,i}}{Q_{M1}} \quad (53)$$

$$C_{bM2,i} = C_{M1,i} - VI1_i \quad (54)$$

$$C_{aM2,i} = \frac{Q_{M1} C_{bM2,i} + (Q_{Lh} + Q_{brine}) C_{Lh,i}}{Q_{M2}} \quad (55)$$

$$C_{D,i} = C_{aM2,i} - VI2_i \quad (56)$$

where

$C_{x,i}$ = concentration of species i, as indicated in figure 2-11 [mg l⁻¹],

Q_x = flow rate, as indicated in figure 2-11 [l sec⁻¹].

VI1 and VI2 follow from equation (50) and (52), respectively.

Maximum and minimum impact

The calculations were run using first the maximal possible impact on concentration conditions from the processes during the seepage phase, regardless that different maximal values might stem from different pore geometry scenarios. Maximum impact means the highest modeled concentrations at 55 m below well bottom for CO₂, SO₄²⁻ (slowest H₂S degassing), Ca²⁺, Mg²⁺ and H⁺ (lowest pH).

Thereupon, the same calculations were run using the minimal possible impact concentrations (fastest H₂S degassing and highest pH). As for the pore water saturation conditions, values lower than 10% and higher than 90% were not regarded reasonable to describe the nature of the pore space, thus they were not considered for the maximal and minimal impact.

Saturation conditions for Ca/MgCO₃ precipitation during groundwater transport

In case the condensate did not reach equilibrium concentration, i.e. C_{CO_2} of the groundwater, the mixing process caused a small pH swing, which led to an increase in HCO_3^- and CO_3^{2-} relative to the concentrations before mixing. Nevertheless, also in these cases the fate of the remaining CO₂ input would have been complete degassing, unless the new conditions were such that saturation was reached with regard to the CaCO₃ or MgCO₃ solubility. Generally it was to find out, whether mineral trapping was a possible sink during the groundwater transport. This meant to test saturation conditions via the solubility product (equations 47 and 48) at all key stations downstream the plant.

Model validations

Finally, the maximal and minimal difference between the obtained concentrations $C_{D,i}$ and the actually measured $C_{B,i}$ (denoting the parameter D in figure 2-11) made it possible to draw conclusions about the validity of the model assumptions or possible other interference.

3. Results and discussion

3.1. Input

Daily input

The daily input of CO₂ is visualized in figure 3-1 for the whole injection period:

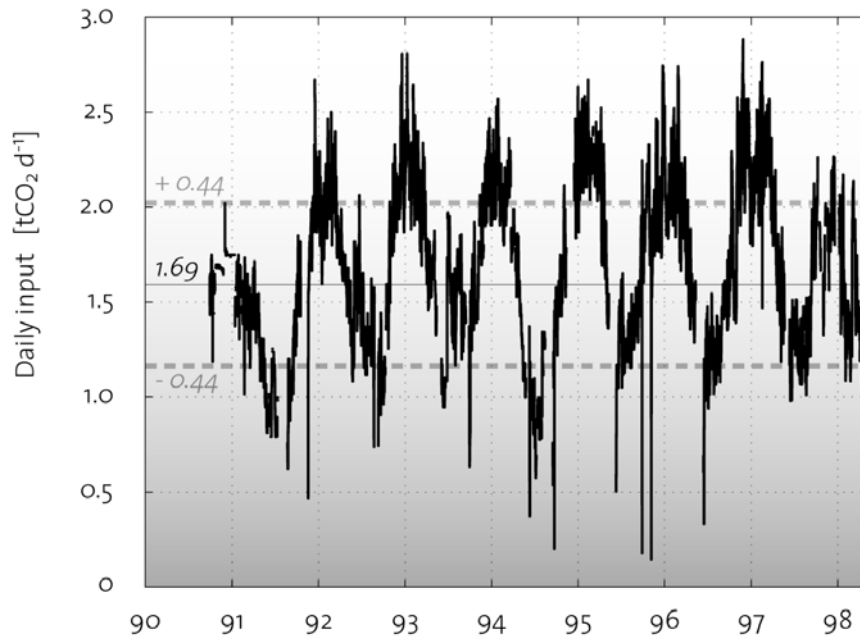


Figure 3-1: Daily input of CO₂ from condensate injection.

Table 3-1 shows the statistical description of the input presented above.

Table 3-1: Input statistics.

[kg d ⁻¹]	Average 1990-1998	Standard deviation	Median	Maximal	Minimal
CO ₂ injection	1690	± 440	1693	2870	130

Total input

To answer the first research question of this study, over the whole injection period of 7.5 years (2770 days), the daily injection could be summed up to a total amount of 4'500 tCO₂.

Figuring this CO₂ was meant to be sequestered, such an input would qualify the Nesjavellir event to be listed amongst other geological storage projects worldwide - the total injection would rank before the smallest projects mentioned in the IPCC special report on CCS (IPCC, 2005; therein table 5.1).

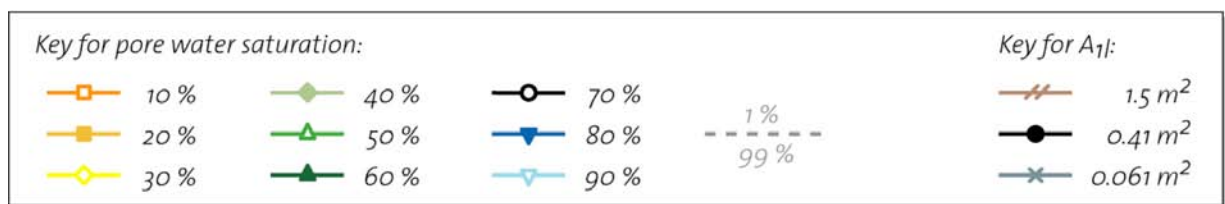
3.2. Sinks during seepage phase

General

In the following, the results from the seepage phase modeling are presented. In order to cover the variability of the proposed pore geometry, four plots were prepared for each process considered. To recall, these were the degassing, the pH developing and the Ca²⁺/ Mg²⁺-release. Three plots stand for of the minimum, mean and maximum A₁₁ area of 0.061, 0.41 and 1.5 m², respectively. Each of them contains 9 graphs, covering the full range of pore water saturation conditions from 10 to 90%, framed

by the boundary values of 1% and 99%. In the fourth plot, the 70% saturation condition is visualized for all three A_{1l} scenarios, thus allowing for a direct comparison of these. Again, permeability was set constant at 0.13 m sec⁻¹, thus in all cases the condensate reached groundwater after 55m of seepage in 423 sec. In other words, the ordinates in all plots represent both the seepage time and depth, whereas depth was chosen for better illustration.

The following key applies to all visualizations of the model results, namely figure 3-2 to 3-5. The addressed figures are content of this subchapter 3.1.1.



Degassing

To sum up shortly, the speed of degassing in the proposed model depends firstly on the degree of turbulence and molecular diffusion coefficient, both expressed in the gas specific transfer velocity, and secondly on the gas exchange distance, depicted by the water depth in the pore. The latter was specially adapted to account for the simplified pipe-shaped pore geometry. Figure 3-2 shows the computed developing of the CO₂ concentration in the vadose zone upon injection.

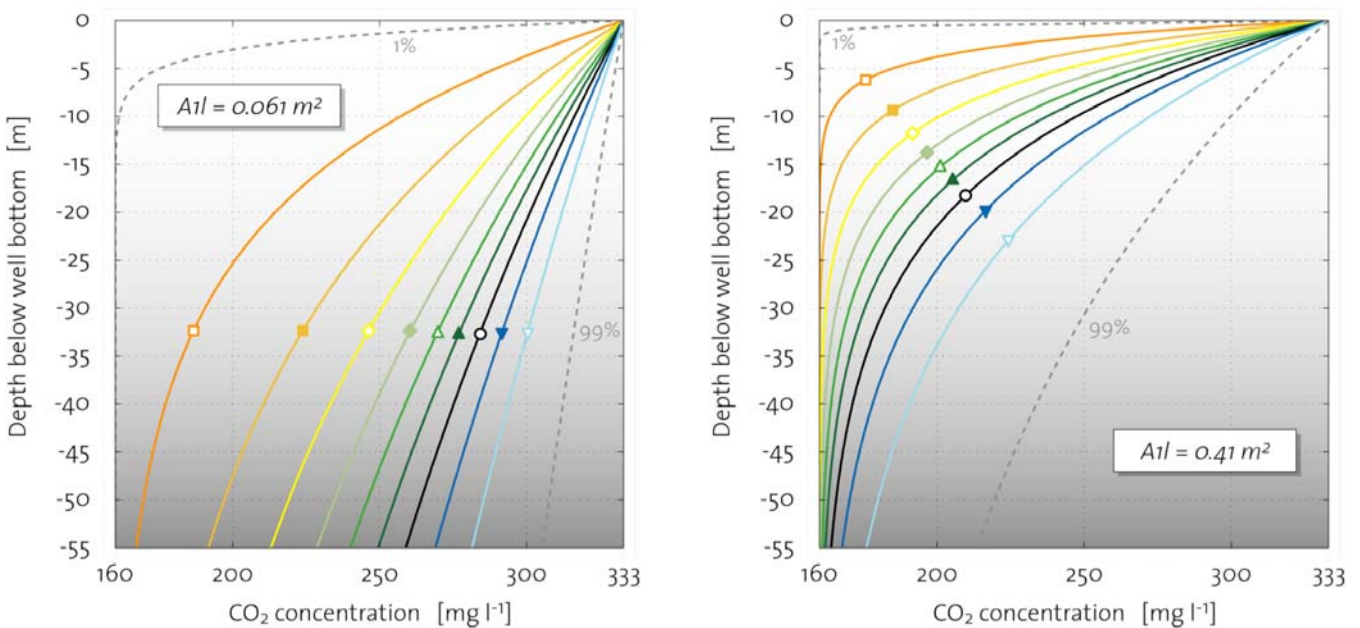


Figure 3-2 to be continued next page.

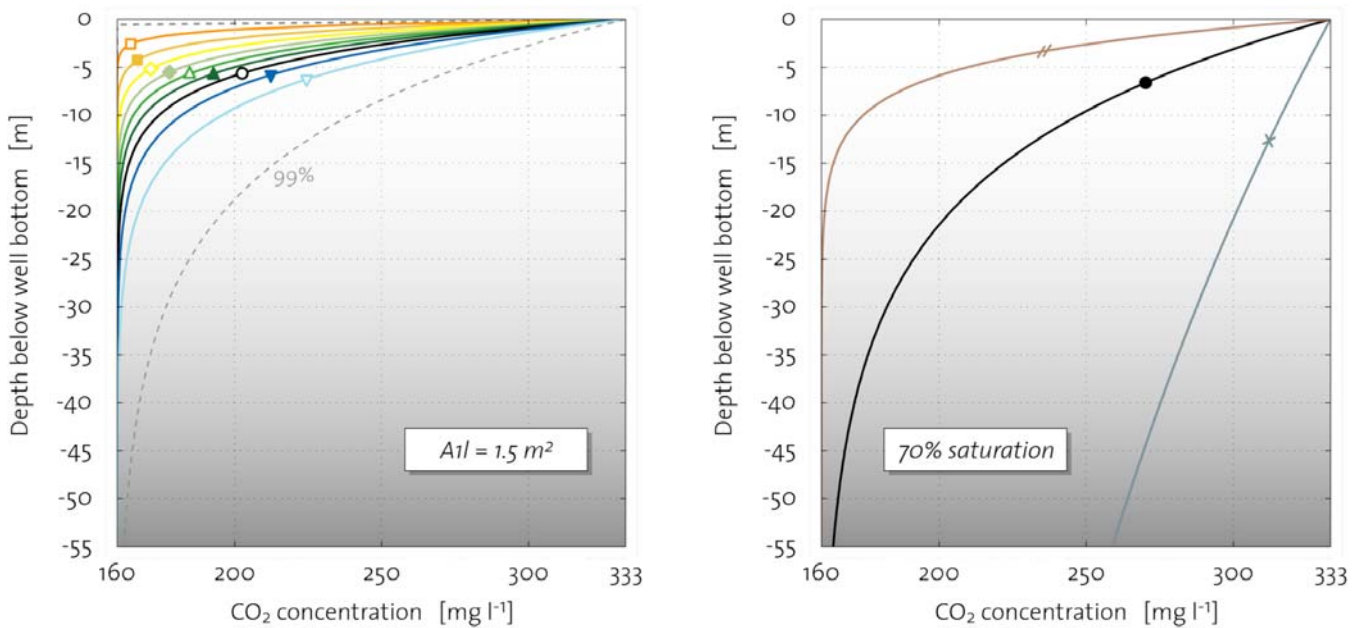


Figure 3-2: Developing of CO₂ concentration during seepage phase.

As to expect and artificially imposed by the adaptations of the gas exchange distance (equations 19 and 20), the higher the pore water saturation, the slower the gas exchange. The maximum A_{1l} scenario exhibits fastest degassing, since the corresponding small pore diameter does not allow for a long gas exchange distance.

Figure 3-2 reveals a degassing between 30% and 100% for gas exchange scenario 1 (full replacement of the injected CO₂ by molecules from the ambient pore air), and between 16% and 52% for scenario 2 (zero replacement). This corresponds to an end concentration at 55 m below well bottom of 281 mg l⁻¹ for the slowest gas exchange and 160 mg l⁻¹ for the fastest.

pH developing

The pH was modeled using the same pore geometry scenarios as for the gas exchange, including the three influences of CO₂ degassing, H₂S oxidation and silicate dissolution. Figure 3-3 shows the computed developing of the pH in the vadose zone upon injection.

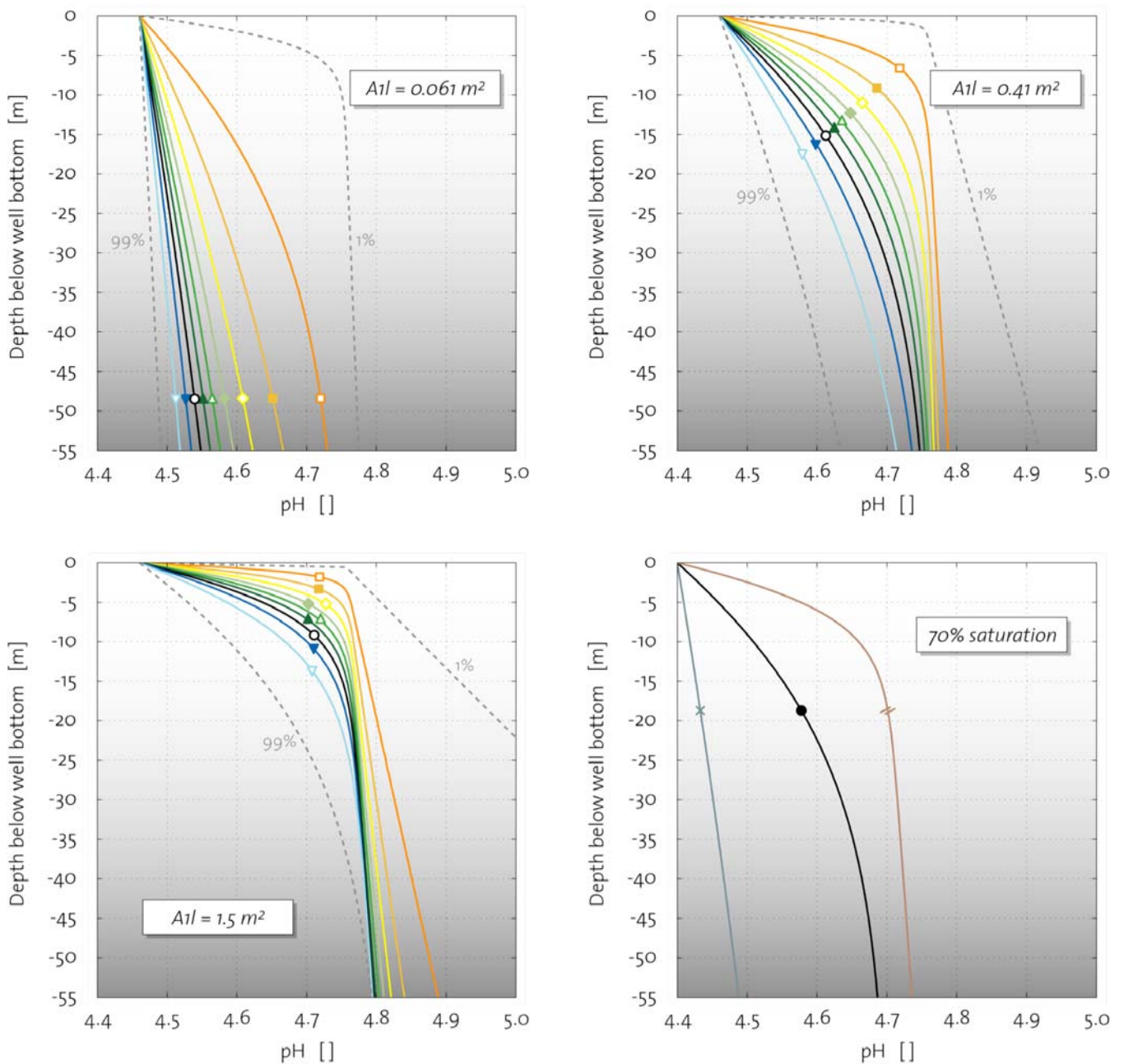


Figure 3-3: Developing of the pH during seepage phase.

Comparing the plots of the CO₂ deassing (figure 3-2) with the pH developing, it follows that the biggest influence stemmed from the decrease in CO₂. The model returns values for the pH between 4.52 and 4.89. It would have been wrong to compute the three influences separately, because each one is influenced by the others via the pH developing itself (see equations 40-43). Nevertheless, the small influences of H₂S oxidation and silicate dissolution shall be shortly described apart from the others, in order to illustrate their minor effects.

Influence of H₂S oxidation

The plots of the degassing of H₂S and the dissolving of O₂ are attached in appendix 9. These plots show that H₂S was present over a relatively long seepage distance in most cases. Oxygen on the other hand dissolved sufficiently fast into the condensate.

Instead, the SO₄²⁻ plots, as presented in figure 3-4, reveal that the kinetics of the H₂S oxidation is too slow to exhibit a substantial influence. Even if the condensate were assumed to be O₂ saturated from the beginning on, H₂S oxidation would barely affect the pH.

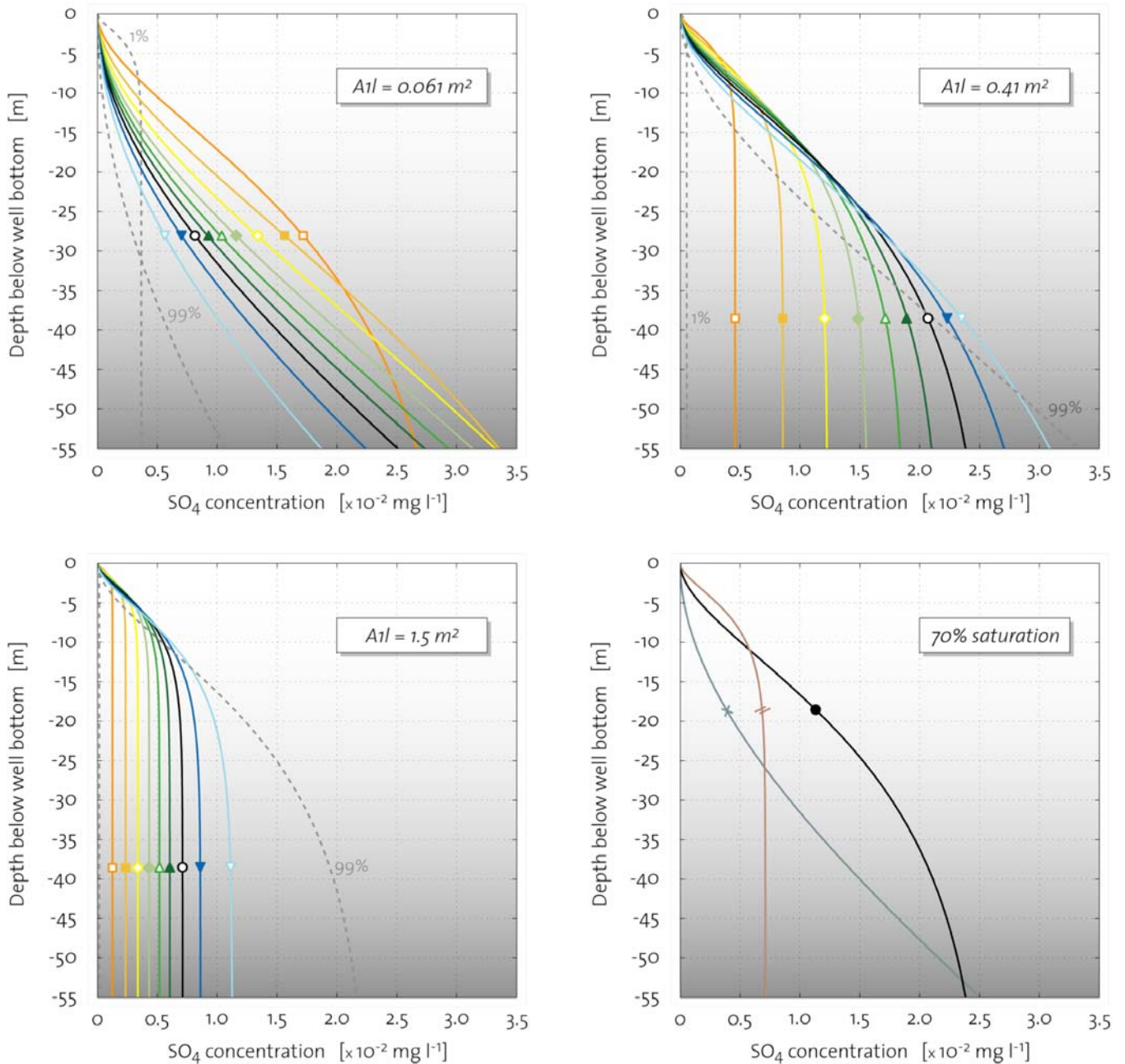


Figure 3-4: Developing of the formation of SO₄²⁻ during seepage phase.

According to the model, the end concentrations of SO₄²⁻ at 55 m below well bottom reached a minimum as low as 0.0013 mg l⁻¹ and a maximal value of 0.034 mg l⁻¹. Assuming one additional proton per SO₄²⁻ formed, these values correspond to a pH decrease between 0.00017 and 0.0043 log units.

Influence of silicate dissolution

The proton consumption by silica dissolution turned out to be a minor effect, too, but at least it is distinguishable in figure 3-3. If this influence were excluded, no further pH increase would have resulted once H₂S had completely degassed. This is best observable in the $A_{11}=1.5 \text{ m}^2$ plot of in figure 3-3, since at $A_{11}=1.5 \text{ m}^2$ degassing proceeds fastest. The separate influence of silicate dissolution follows from figure 3-5, where the release of Ca²⁺ is as presented.

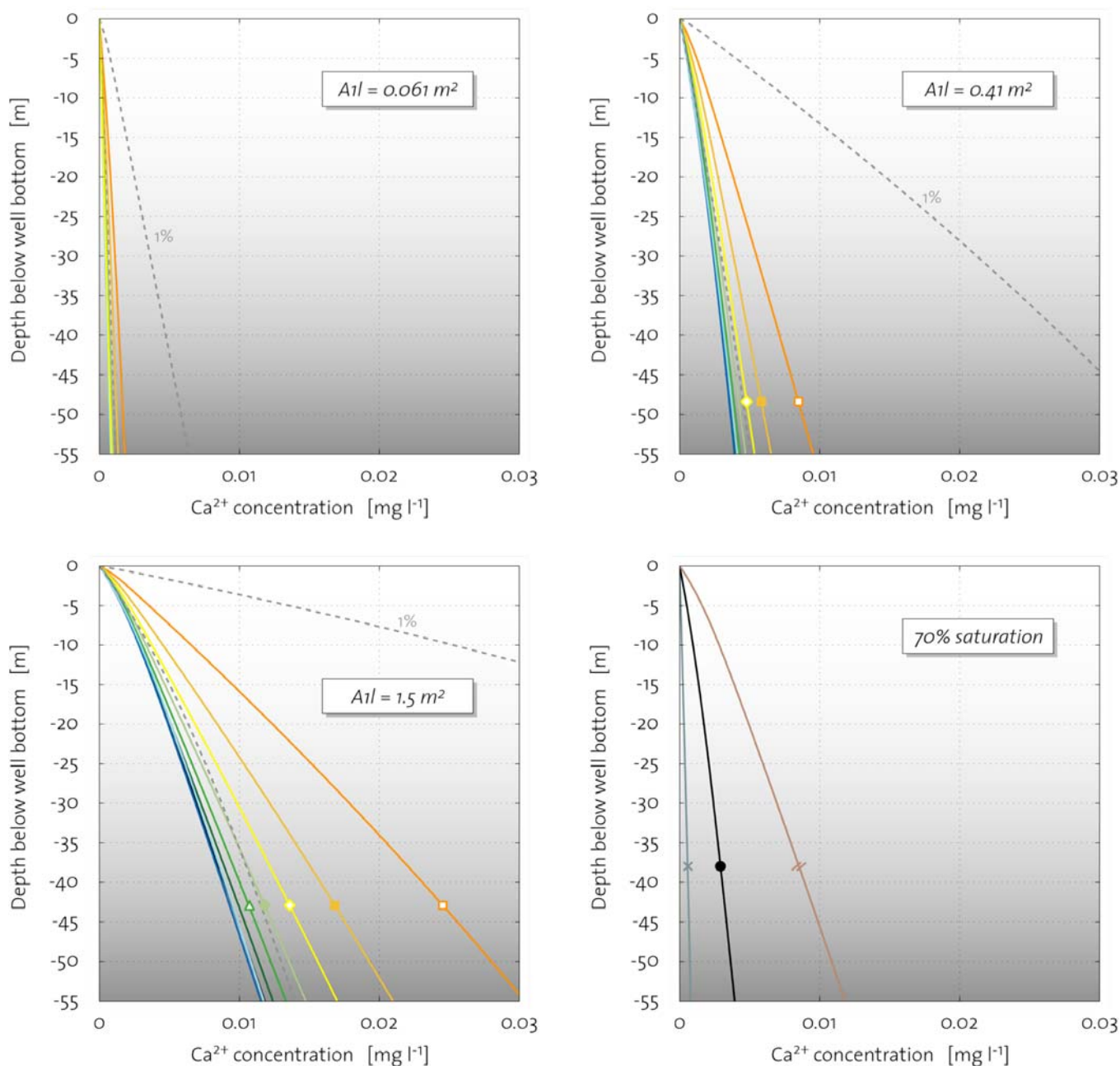


Figure 3-5: Developing of the Ca²⁺ concentration during seepage phase.

Figure 3-5 is further described in the next clause.

Since the dissolution of 1 molSi corresponds to the release of 0.26 molCa²⁺ and consumes 1.08 molH⁺, the minimum and maximum end concentration of Ca²⁺ corresponds to a pH increase between 0.0019 and 0.066 log units log units.

Ca²⁺ and Mg²⁺ release

As temperature was assumed constant, the release of Ca²⁺ and Mg²⁺ (i.e. silicate dissolution) during the seepage was only depending on the pH. To recall, calculations had to be normalized by the total reactive surface area and the water volume in a pore per second of flow, which are both determined by the pore radius (i.e. A_i) and water saturation. The plots of the Ca²⁺ release was already presented above. Since the graphs of Mg²⁺ do not differ in character from those in figure 3-5, they are attached in appendix 9.

The model returned end concentrations at 55 m below well bottom between 0.0012 and 0.047 mg l⁻¹ for Ca²⁺ and between 0.0008 and 0.030 mg l⁻¹ for Mg²⁺.

Mineral trapping:
Saturation conditions for
carbonate precipitation

Such a low cation release suggested mineral trapping to be impossible, considering that saturation conditions with regard to Ca/Mg²⁺ and CO₃²⁻ species needed to be reached for carbonate precipitation being a possible sink of CO₂. The CO₃²⁻ concentration was calculated according to the pH developing after equation (43). Here, the question about saturation conditions is fully answered table 3-2, where the results from the solubility equilibrium calculations of the maximum end concentrations are presented, as undersaturation would only increase for other scenarios.

Table 3-2: Solubility equilibrium calculations.

	K _{sol}	C _{CO₃} [mol l ⁻¹]	C _i [mol l ⁻¹]	Solubility Product	Under- saturation
CaCO ₃	10 ^{-8.38}	10 ^{-14.43}	10 ^{-5.93}	10 ^{-20.36}	x 10 ^{-11.98}
MgCO ₃	10 ^{-8.14}		10 ^{-5.90}	10 ^{-20.33}	x 10 ^{-11.95}

To conclude, the condensate was 10¹² times undersaturated with regard to the solubility equilibrium of the CaCO₃ and MgCO₃. Hence no mineral trapping ever took place during the seepage phase.

3.3. Sources and sinks during groundwater transport

3.3.1 Qualitative interpretations

So far, the model revealed that Ca²⁺, Mg²⁺ and SO₄²⁻ was released and formed only to a very small extent. The end concentrations at 55 m below well bottom were orders of magnitudes smaller than the natural background concentrations in this area, i.e. a dilution of the groundwater with respect to these species was the consequence rather than vice versa. The qualitative interpretation of the monitoring plots for Lækjarhvarf and Varmagjá in appendix 8 led to a general idea of the dilution and mixing processes. The following trends were found:

Water chemistry trends at
Lækjarhvarf

1. At Lækjarhvarf, seasonal variations were generally high.
2. SO₄²⁻ concentration initially increased substantially, and then remained on a value around 60 mg l⁻¹, exhibiting large variations.
3. The concentrations of Ca²⁺ and Mg²⁺ decreased by half from 1990 till 1998, but increased only slowly after this.
4. The developing of the pH can be described with an increase until 1998, followed by a slight decrease.

Water chemistry trends at Varmagjá

5. Similarly, temperature increased from 10°C to 30°C during the injection period, followed by a decrease.
6. At Varmagjá, the SO₄²⁻ concentration doubled from 12 to approx. 25 mg l⁻¹ from 1990 till 1998. Afterwards, the C_{SO4} remained on that high level.
7. In the same period, concentrations of CO₂, Ca²⁺ and Mg²⁺ increased by a few milligrams per liter at Varmagjá (CO₂ mainly denotes HCO₃⁻ at the a pH around 7.6). After the extension of the plant, these concentrations showed a striking decrease.
8. The pH was well buffered throughout the monitoring period at Varmagjá. Moreover, a flattening of the time series, i.e. an even better buffering, is observable after 1990.
9. Until 1998, temperature at Varmagjá showed only a small increase, but it climbed up to 30°C after the plant extension.

Interpreting the trends

Trend No°1 depicts the fact, that conditions at Lækjarhvarf are under a winter-summer influence by changing natural runoff and hot water demand (leading to more or less disposal of geothermal brine).

Trend No°2 stems from the high H₂S content in the brine (up to 90 mg l⁻¹), which oxidizes on the way from the separators to the pond. Hence, trend No°6 can be explained entirely by the impact from the disposed brine.

Measured concentrations of Ca²⁺ and Mg²⁺ in the disposed geothermal brine are very low, comparable with the end concentrations in the condensate and well below the background in the brook, which is around 20 mgCa l⁻¹ and 6 mgMg l⁻¹. Moreover, the disposal of brine steadily increased, owing to new boreholes that were connected to the system for testing purpose. This explains the dilution as described in trend No°3. After 1998, the brine was used in the heat exchangers and disposed in a new shallow well, thus reaching the groundwater not via Lækjarhvarf. The expectedly simultaneous increase at the pond was delayed by the then starting temporal disposal of condensate in the brook (see description of figure 2-2 on page 9). The same considerations explained trend No°4 for the pH, as the H⁺ concentration in the brine below background, too ((in brook pH=7.7, in brine pH=8.8).

The 100°C hot brine caused also the temperature increase in the pond before the plant was redesigned (trend No°5), which on the other hand caused the small increase measured at Varmagjá (trend No°9). The extension to a co-generating plant increased the disposal of geothermal fluids massively, which led to the observed step-up of the temperature at Varmagjá.

Uncertainty concerning trend No°7

Trend No°7 was the most difficult to reconstruct. It was found, that the disposal of both condensate and geothermal brine had a diluting effect on the concentrations of Ca²⁺, Mg²⁺ and CO₂ in the groundwater. The step-up in discharge of both brine and condensate after the plant extension increased the diluting impact accordingly. This is well proven by the abrupt decrease of Ca²⁺ and Mg²⁺ at Varmagjá after 1998. But then it was to explain, what could have caused the monitored increase in theses concentrations at prior to the plant extension. It followed from the simultaneity that it must be a signal caused by the discharge from the plant. It might have originated

from an increased silicate dissolution, which is not to exclude but unlikely, since conditions were not such that dissolution was specially enhanced. Considering the slow dissolution rate, 10 weeks between plant and lake would have been not enough time to dissolve the observed concentrations. The same applies to the thinkable conclusion, that the modeled condensate concentrations are in error, meaning orders of magnitudes higher than calculated.

Theory about dissolution of present carbonates

A careful explanation could be to assume that the pores of the basalts at Nesjavellir already contained some precipitated carbonates, in spite of their young age. Furthermore assuming the background aqueous solution was close to solubility equilibrium, a small diluting impact would have caused an equilibrium shift and the dissolution of the carbonates to a certain extent. Support to this was derived from trend No°8, since carbonate dissolution is an effective buffering system. The increase in CO₂ concentration was smaller than for Ca²⁺ and Mg²⁺, but dissolution of carbonates would have affected the carbonic acid system, i.e. a part of the additional CO₂ would have already been degassed at the outflow. This theory, however, is also lacking a more profound knowledge about the actual nature of the containment area and the processes therein.

Concentration developing from maximum impact

3.3.2 Quantitative calculations

Recalling figure 2-11 on page 32 for the notations, table 3-3 summarizes the results from calculations after the concentration developing scheme, considering the maximum impact scenario.

Table 3-3: Concentration developing for maximum impact.

Max. impact 1990-1998	CO ₂ [mg l ⁻¹]	SO ₄ [mg l ⁻¹]	Ca ²⁺ [mg l ⁻¹]	Mg ²⁺ [mg l ⁻¹]	pH []
C _A	157.2	11.6	23.4	10.1	7.50
C _{co(max)}	281.45	0.03	0.05	0.03	4.52
C _{M1}	161.72	11.18	22.52	9.75	5.95
C _{bM2}	78.57	24.19	8.68	3.02	5.96
C _{Lh}	38.14	61.54	9.34	2.53	8.08
C _{aM2}	75.22	27.29	8.74	2.98	6.00
C _D	56.57	13.73	10.44	5.43	5.99
C _B	57.47	13.27	11.49	6.15	7.51
D	0.91	-0.45	1.06	0.72	1.52
D [%]	1.578	-3.419	9.206	11.638	-

Concentration developing
with minimum impact

Table 3-4 summarizes the results for minimum impact.

Table 3-4: Concentration developing for minimum impact.

Min. impact 1990-1998	CO ₂ [mg l ⁻¹]	SO ₄ [mg l ⁻¹]	Ca ²⁺ [mg l ⁻¹]	Mg ²⁺ [mg l ⁻¹]	pH []
C _A	157.2	11.6	23.4	10.1	7.50
C _{co(min)}	157.23	1.30E-03	1.20E-03	8.00E-04	4.89
C _{M1}	157.23	11.18	22.52	9.75	6.30
C _{bM2}	74.08	24.19	8.68	3.02	6.33
C _{Lh}	38.14	61.54	9.34	2.53	8.08
C _{aM2}	71.10	27.29	8.73	2.98	6.36
C _D	52.45	13.73	10.43	5.43	6.35
C _B	57.47	13.27	11.49	6.15	7.51
D	5.02	-0.45	1.06	0.72	1.16
D [%]	8.742	-3.411	9.219	11.654	-

Table 3-5 repeats the obtained differences for maximum and minimum impact in order to make them better comparable.

Table 3-5: Differences between measured and calculated outflow concentrations.

Differences 1990-1998	CO ₂ [mg l ⁻¹]	SO ₄ [mg l ⁻¹]	Ca ²⁺ [mg l ⁻¹]	Mg ²⁺ [mg l ⁻¹]	pH []
D(max)	0.91	-0.45	1.06	0.72	1.52
D(max) [%]	1.578	-3.419	9.206	11.638	-
D(min)	5.02	-0.45	1.06	0.72	1.16
D(min) [%]	8.742	-3.411	9.219	11.654	-

Conclusions from the
resulting estimations

It follows, that the release of Ca²⁺ and Mg²⁺, and the formation of SO₄ were too small to exhibit significant differences between maximum and minimum scenario. In the case of CO₂, the maximum impact scenario leads to a supposedly smaller D.

It suggests itself, that table 3-5 reveals the same uncertainty about the increase in Ca²⁺, Mg²⁺ and CO₂ concentrations and the pH buffering in the outflow as found and described in the qualitative analysis in subchapter 3.3.1. Here as well, these concentrations are 10% in error and the pH is 15-30 times too low. Even the small error of 1.6 % for CO₂ is presumably an artifact, as it is not likely to consider maximum impact in this case, meaning that only a minor part of the CO₂ load had degassed in the vadose zone. Scenarios with more degassing would lead to errors up to 8.7% (minimum impact), which fits better in the unexplained observed increase in CO₂ at Varmagjá.

Under these circumstances, the saturation condition calculations that should have revealed the possibility of mineral trapping during the groundwater transport could be omitted, as they would only return results in error with respect to the too low Ca²⁺, Mg²⁺ and CO₂ (i.e. CO₃²⁻) concentrations table 3-3 and table 3-4. The monitored increase of these species in the outflow is anyway proof for the inexistence of carbonate precipitation.

Remains of the model validation

The only parameter of which the monitored concentration could be put in proper correlation to the plant's impact, i.e. SO₄, exhibits a D below 5%. This gave the confidence in the model assumptions for the seepage phase that was sought by calculating the quantitative estimations in table 3-3 and table 3-4.

Degassing during groundwater transport

3.4. Mass balance summary

As mineral trapping could be excluded as a possible sink throughout the containment area, it followed that in case the CO₂ did not entirely degas during the seepage phase, the remains were lost to the vadose zone upon mixing. The same considerations about gas exchange in both directions, as mentioned in subchapter 2.3.2, applied also for the further degassing upon mixing. In the case of degassing from the aquifer, where CO₂ is steadily delivered from the background flux, it was safe to assume that once a CO₂ molecule that stems from the input had degassed, it rose to the surface and did not re-diffuse. Thus, no such molecules would have reached the outflow, and the final destination of the remaining CO₂ was the vadose zone short after the power station.

Concerning the source at Lækjarhvarf

This made it unnecessary, to quantify the CO₂ stemming from the additional groundwater charge at Lækjarhvarf, as it had no influence on the mass balance. Though it was important to include it to the qualitative and quantitative considerations about the processes during the groundwater transport.

Reducing the mass balance

Hence, the mass balance after equation (4) simplifies to:

$$Input = Dg \quad (57)$$

It was shown, that between 15% and 100% of the input had degassed even before the condensate reached the groundwater table, depending on the tendency of the injected CO₂ to escape into the vadose zone or rediffuse once it had degassed. Thus it was possible to localize the final destination and corresponding quantities for the CO₂ input of the Nejavellir injection event.

Final destination of the input

Table 3-6 gives the answer to the second research question.

Table 3-6: Final destination and corresponding quantities for the CO₂ injection at Nesjavellir..

[tCO ₂]	Input 1990-1998	Vadose zone beneath injection	Vadose zone from plant to lake	Outflow
at the least	4'500	700	0	0
at the most		4'500	3'800	

Rising from the vadose zone, the gas sooner or later reached the surface, and the true fate of the entire CO₂ input was the disadvantageous release to the atmosphere.

4. Conclusions

Two questions were addressed, related to the CO₂ input during the Nesjavellir injection event between the years 1990 and 1998: First, how much CO₂ had been disposed? And secondly, where was the final destination of this input and to what extent did it end up there? For both issues, the present study gives clear answers, despite the many uncertainties that were faced, due to the fact that the quasi experiment was unintended and took place a decade ago; hence no influence could be exerted on its set-up, documentation and the quality of the available data.

The input evaluation revealed a total amount of 4'500 tons CO₂ over the whole injection period of 7.5 years. This would qualify the event to be comparable with other geological storage pilot projects worldwide.

It was shown, that mineral trapping was inexistent throughout the containment area. All of the injected CO₂ had degassed to the pore space of the vadose zone, most of it within short distance to the input. Thus, it was inevitably lost to the atmosphere, and it is safe to say, that the Nesjavellir injection event does not allow for research of change mitigation. Neither would any further investigation, for instance by a profound geochemical modeling, the analysis of drill-chips or even new core-drillings, contribute to Iceland's research efforts on geological storage in basalt. For this reason, the authors do not recommend further research on the Nesjavellir injection event.

References

- Aeschbach-Hertig, W., 2005. Skript zur Vorlesung *Physik aquatischer Systeme I*, Kapitel Gasaustausch, 5.1–5.26. (in German)
- Allinson, W.G, Nguyen, D.N., Bradshaw, J., 2003. The economics of geological storage of CO₂ in Australia, *APPEA Journal* **623**.
- Angst, W., Diem, Diem, D., Meister, E., Togni, A., Uhlig, W., 2002. Skript zur Vorlesung *CHEMIE I*. (in German)
- Arnórsson, S., Geirsson, K., Andrésdóttir, A., Sigurdsson, S., 1996. Compilation and evaluation of thermodynamic data on aqueous species and dissociational equilibria in aqueous solutions I. The solubility of CO₂, H₂S, H₂, CH₄, N₂, O₂, and Ar in pure water. *Science Institute*, Univ. of Iceland, Report RH-17-96. 20pp.
- Atkins, P.W., Höpfer, A., 2002. *Physikalische Chemie*, 3. korr. Auflage. Wiley-VCH, Weinheim, Germany, 1130pp. (in German)
- Baccini, P., Brunner, P.H., 1991. *Metabolism of the Anthroposphere*, Springer-Verlag, Berlin/Heidelberg/New York.
- Bachu, S., Gunter, W. D., Perkins, E.H., 1994. Aquifer disposal of CO₂: hydrodynamic and mineral trapping, *Energy Convers. Manage.* **35**(4), 269–279.
- Berner, R.A., Lasaga, A.C., 1989. Modeling the geochemical carbon cycle. *Sci. Am.* **260**, 74–81.
- Bodvarsson, G., 1951. Report on geothermal research in Hengill, Hveragerdi and surroundings. *J. Eng. Soc. Iceland*, 1947-1949.
- Cashman, K.V., Mangan, M.T., 1994. Physical aspects of magmatic degassing II. Constraints on vesiculation processes from textural studies of eruptive products. In: Carroll, M.R., and Holloway, J.R. (eds) *Volatiles in magmas: Mineralogical Society of America, Reviews in Mineralogy* **30**, 447–478.
- Cipolli, F., Gambardella, B., Marini, L., Ottonello, G., Vetuschi Zuccolini, M., 2004. Geochemistry of high-pH waters from serpentinites of the Gruppo di Voltri (Genova, Italy) and reaction path modeling of CO₂ sequestration in serpentinite aquifers. *Appl. Geochem.* **19**, 787–802.
- Cunningham, A.B., Rockford, J.R., 2006. Table 4-1: Diffusion coefficients in water at 25°C. In: *BIOFILMS: The Hypertextbook*. Center for Biofilm Engineering, Montana State University. http://www.erc.montana.edu/biofilmbook/MODULE_04/Table4-1_DiffCoeffH2O.htm (viewed 06.01.2008)
- Dunsmore, H.E., 1992. A geological perspective on global warming and the possibility of carbon dioxide removal as calcium carbonate mineral. *Energy Convers. Manage.* **33**(5–8), 565–572.
- GERM, 2000. The Geochemical Earth Reference Model. <http://earthref.org/GERM/index.html>
- Gíslason, G., 2000. Nesjavellir Co-Generation Plant, Iceland - Flow of Geothermal Steam and Non-Condensable Gases. In: *Proceedings World Geothermal Congress*, May 28 - June 10, 2000, Kyushu - Tohoku, Japan.
- Gíslason, S.R., Eugster H.P., 1987. Meteoric water-basalt interactions: a laboratory study. *Geochim. Cosmochim. Acta* **51**, 2827–2840.
- Gíslason, S.R., Arnórsson, S., Armannsson, H., 1996. Chemical weathering of basalt in southwest iceland: effects of runoff, age of rocks and vegetative/glacial cover. *Am. J. Sci.* **296**, 837–907.
- Gíslason, S.R., Oelkers, E.H., 2003. The mechanism, rates, and consequences of basaltic glass dissolution. II. An experimental study of the dissolution rates of basaltic glass as a function of pH at temperatures from 6°C to 150°C. *Geochim. Cosmochim. Acta* **67**, 3817–3832.
- Gíslason, S.R., Gunnlaugsson, E., Broecker, W.S., Oelkers, E.H., Matter, J.M., Stefánsson, A., Arnórsson, S., Björnsson, G., Fridriksson, T., Lackner, K., 2007. Permanent CO₂ sequestration into basalt: the Hellisheidi, Iceland project, *Geophysical Research Abstracts* **9**. (unpublished)
- Goff, F., Lackner K., 1998. Carbon dioxide sequestering using ultramafic rocks. *Env. Geosci.* **5**, 89–101.
- Gunnarsson, A., Steingrímsson, B., Maack, R., Gunnlaugsson, E., Magnússon, J., 1991. Nesjavellir Geothermal Co-Generation Power Plant. Hitaveita Reykjavíkur. (unpublished)
- Gunter, W.D., Perkins, E.H., McCann, T.J., 1993. Aquifer disposal of CO₂-rich gases: reaction design for added capacity. *Energy Convers. Manage.* **34**, 941–948.
- Gustavsson, J., 2006. Analysis of porosity evolution during low temperature metamorphism of basaltic lavas and implications for fluid flow. Master Thesis, University of Florida.
- Guy, C., Schott, J., 1989. Multisite surface reaction versus transport control during hydrolysis of a complex oxide. *Chem. Geol.* **78**, 181–204.

- Hafstad, Th.H., Vilmundardóttir, E.G., Kristjánsson, B.R., 2007. Nesjavellir – Rannsóknarborholur í hraununum á affallssvæði virkjunarinnar. Unnið fyrir Orkuveitu Reykjavíkur - Prepared for Reykjavík Energy. *ISOR*. (in Icelandic, unpublished draft)
- Hänchen, M., Prigiobbe, V., Storti, G., Seward, T.M., Mazzotti, M., 2006. Dissolution kinetics of fosteritic olivine at 90–150 °C including effects of the presence of CO₂. *Geochim. Cosmochim. Acta*, **70**, 4403–4416.
- Hänchen, M., Krevor, S., Mazzotti, M., Lackner, K.S., 2007. Validation of a population balance model for olivine dissolution. *Chem. Eng. Sci.*, **62**, 6412–6422.
- Imboden, D., Kipfer, R., 2003. Skript zur Vorlesung *Physik aquatischer Systeme*, Kapitel Gas exchange. 4.1–4.16. (in German)
- IPCC, 2005. IPCC Special Report on Carbon Dioxide Capture and Storage. Prepared by Working Group III of the Intergovernmental Panel on Climate Change. *Cambridge University Press*, Cambridge, United Kingdom and New York, NY, USA, 442 pp.
- IPCC, 2007. Climate Change 2007: The Physical Science Basis. Contribution of Working Group I to the Fourth Assessment Report of the Intergovernmental Panel on Climate Change. *Cambridge University Press*, Cambridge, United Kingdom and New York, NY, USA, 996 pp.
- IPCC, 2007. Climate Change 2007: Impacts, Adaptation and Vulnerability. Contribution of Working Group II to the Fourth Assessment Report of the Intergovernmental Panel on Climate Change. *Cambridge University Press*, Cambridge, UK, 976 pp.
- ISOR, 2007. Natural CO₂-sequestration in 3 high temperature systems, Iceland. (unpublished)
- Kerrick, D.M., McKibben, M.A., Seward, T.M., Caldeira, K., 1995. Convective hydrothermal CO₂ emission from high heat flow regions. *Chem. Geol.* **121**, 285–293.
- Kjaran, S.P., Egilson, D., 1986. Nesjavellir - Áhrif affallsvatns frá fyrirhugadri jarðvarmavirkjun á vatnsból við Grámel. *Vatnaskil*, **86-03**. (in Icelandic)
- Kjaran, S.P., Egilson, D., 1987. Ferlun Grunnvatns á Nesjavöllum. *Vatnaskil*. (in Icelandic)
- Kjaran, S.P., Myer, E.M., 2005. Nesjavellir - Árleg endurskoðun á grunnvatnslíkani fyrir árið 2003. Unnið fyrir Orkuveitu Reykjavíkur - Prepared for Reykjavík Energy. *Vatnaskil*, **05.02**. (in Icelandic)
- Knauss, K.G., Johnson, J.W., Steefel, C.I., 2005. Evaluation of the impact of CO₂, co-contaminant gas, aqueous fluid and reservoir rock interactions on the geologic sequestration of CO₂. *Chem. Geol.* **217**(3–4), 339–350.
- Lackner, K.S., Wendt, C.H., Butt, D.P., Joyce, E.L., Sharp, D.H., 1995. Carbon-dioxide disposal in carbonate minerals. *Energy* **20**, 1153–1170.
- Lasaga, A.C., 1981. Dynamic treatment of geochemical cycles: global kinetics. In: Lasaga, A.C., Kirkpatrick, R.J. (Eds.), *Kinetics of Geochemical Processes*. *Reviews in Mineralogy* **8**, 69–110.
- Lichtner, P.C., 1998. Modeling reactive flow and transport in natural systems. In: Marini, L., Ottonello, G. (eds.), *Proceedings of the Rome Seminar on Environmental Geochemistry*, 22–26 May, 1996, Castelnuovo di Porto, Pisa, Italy: Pacini, 5–72.
- Matter, J. M., Takahashi, T., Goldberg, D., 2007. Experimental evaluation of in situ CO₂-water-rock reactions during CO₂ injection in basaltic rocks: implications for geological CO₂ sequestration. *Geochem. Geophys. Geosyst.* **8**.
- Marini, L., 2007. Geological sequestration of carbon dioxide: thermodynamics, kinetics, and reaction path modeling. *Elsevier, Developments in Geochemistry* **11**, 453pp.
- Marsh, B.D., 1981. On the crystallinity, probability of occurrence, and rheology of lava and magma. *Contrib. Miner. Petrol.* **78**, 85–98.
- McGrail, B.P., Martin, P.F., Saripalli, K.P., Bryant, S.L., Sass, B.M., 2001. Use of Forced Mineral Trapping for Sequestration of CO₂. In: *Proceedings of the First National Conference on Carbon Sequestration*, 14–17 May, 2001, Washington DC, USA.
- Millero, F.J., Hubinger, S., Fernandez, M., Garnett, S., 1987. Oxidation of H₂S in seawater as a function of temperature, pH and ionic strength. *Env. Sci. Tech.* **21**, 439–443.
- Neuhoff, P. S., Fridriksson, T., Arnorsson, S., 1999. Porosity evolution and mineral paragenesis during low-grade metamorphism of basaltic lavas at Teigarhorn, Eastern Iceland. *Am. J. Sci.* **299**, 467–501.
- Newall, P.S., Clarke, S.J., Haywood, H.M., Scholes, H., Clarke, N.R., King, P.A., Barley, R.W., 2000. CO₂ storage as carbonate minerals, report PH3/17 for IEA Greenhouse Gas R&D Programme, CSMA Consultants Ltd, Cornwall, U.
- O'Connor, W.K., Dahlin, D.C., Nilsen, D.N., Rush, G.E., Walters, R.P., Turner, P.C., 2000. CO₂ storage in solid form: a study of direct mineral carbonation. In: *Proceedings of the 5th international conference on greenhouse gas technologies*, August 14–18, 2000, Cairns, Australia.

- Oelkers, E.H., Gíslason, S.R., 2001. The mechanism, rates and consequences of basaltic glass dissolution: I. An experimental study of the dissolution rates of basaltic glass as a function of aqueous Al, Si and oxalic acid concentration at 25 °C and pH=3 and 11. *Geochim. Cosmochim. Acta* **65**, 3671–3681.
- Ólafsson, J., 1992. Chemical characteristics and trace elements of Thingvallavatn. *Oikos* **64**, 151-161.
- Oldenburg, C.M., Unger, A.J.A., 2003. On leakage and seepage from geologic carbon sequestration sites: unsaturated zone attenuation. *Vadose Zone J.*, **2**, 287–296.
- OR press release, 2007. Nature Imitated in Permanent CO₂ Storage Project.
<http://hugin.info/138185/R/1156978/223423.pdf> (download 04.01.2008)
- Park, A.A-H., Fan, L-S., 2004. CO₂ mineral sequestration: physically activated dissolution of serpentine and pH swing process. *Chem. Eng. Sci.* **59**, 5241-5247.
- Plas, C., Harant, H., Danner, H., Jelinek, E., Wimmer, K., Holubar, P., Braun, R., 1994. Ratio of biological and chemical oxidation during the aerobic elimination of sulphide by colourless sulphur bacteria. *Env. Biotech.*, **36**, 817–822.
- Seifritz, W., 1990. CO₂ disposal by means of silicates. *Nature* **345**, 486.
- Sigurdsson, F., Ingimarsson, J., 1990. The hydraulic conductivity of Icelandic rocks. In: Water and the Country (ed. G. Sigbjarnarson), National Energy Authority, Reykjavik, 121–128. (in Icelandic)
- Spane, F.A., McGrail, B.P., Sullivan, E.C., Goldberg, D.S., McLing, T.L., Weeks, R.S., Smith, R.W., 2007. Field Activity Plan: characterization Test for CO₂ Sequestration in the Columbia River Basalt Group. Prepared for Big Sky Regional Carbon Partnership. Battelle Pacific Northwest Division.
- Wehrli, B., Fuchs, L., 2005. Skript zur Vorlesung *Umweltchemie I*, 20–24.
- Wolff-Boenisch, D., Gíslason, S.R., Oelkers, E.H., 2006. The effect of crystallinity on dissolution rates and CO₂ consumption capacity of silicates. *Geochim. Cosmochim. Acta* **70**, 858–870.

Appendices	page
Appendix 1: Photo documentation	A1
Appendix 2: Maps	A5
Appendix 3: Original technical drafts	A6
Appendix 4: Geological cross-sections	A7
Appendix 5: Groundwater model	A8
Appendix 6: Scripts for seepage phase modeling	A9
Appendix 7: Gas exchange transfer velocity for O ₂	A15
Appendix 8: Plots monitoring at Lækjarhvarf and Varmagjá	A16
Appendix 9: Additional plots of the seepage phase modeling	A17

Appendix 1: Photo documentation

Nesjavellir geothermal power plant and its vicinity



Panorama of the power station; separators in the front to the right, power-house in the middle, behind stretches Nesjahraun and in the background Lake Thingvallavatn.



Main feature of the Mount Hengill area transmission lines, steaming production wells and natural geothermal activity.



The rough surface of Nesjahraun in the vicinity of the plant. In the background, today's location for the overflow disposal of condensate.

Documentation of the relevant locations at Nesjavellir



The closure head of the injection well Nidurrensslihola in front of the power-house.



Location of the disposal of geothermal brine into the brook Nesjavallalækur. In the background, the separators and excess steam chimneys.



The brook Nesjavallalækur..



The gully-like seepage zone at the pond Lækjarhvarf.



A research well (No° NL-3) between in the lava field Hagavíkurhraun between Lækjarhvarf and lake shore.



The small bay Varmagjá, where the main part of the discharge enters Lake Thingvallavatn (in the background to the right)..

The Carb-Fix project at
Hellisheidi



In the middle, the geothermal plant Hellisheidi under construction, in the background, below the dark conic hill, the designated injection site for the Carb-Fix project..



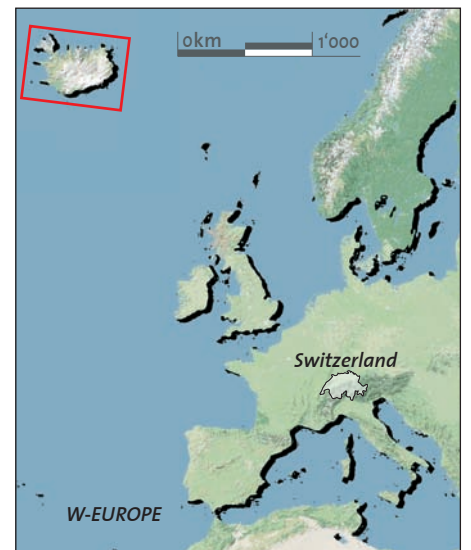
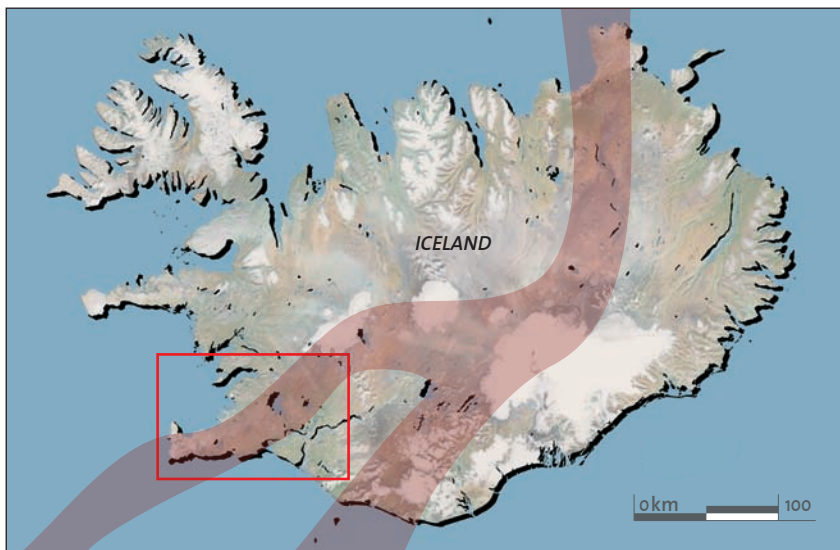
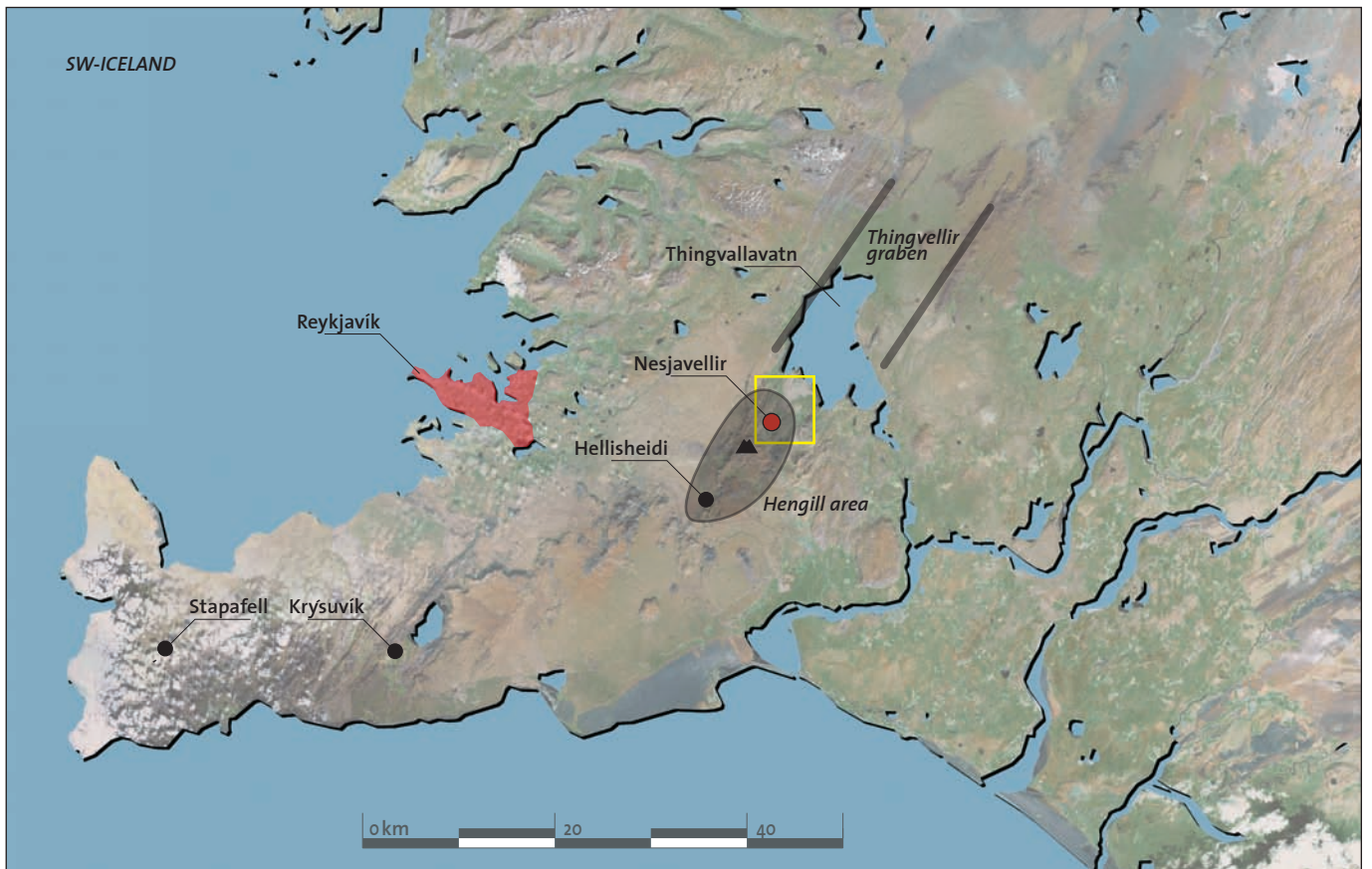
Stakeholders discussing the experimental set-up at the designated injection well HN-2.

Appendix 2: Maps

Sheet 1: Mapped air picture of SW-Iceland, with corresponding orientation maps

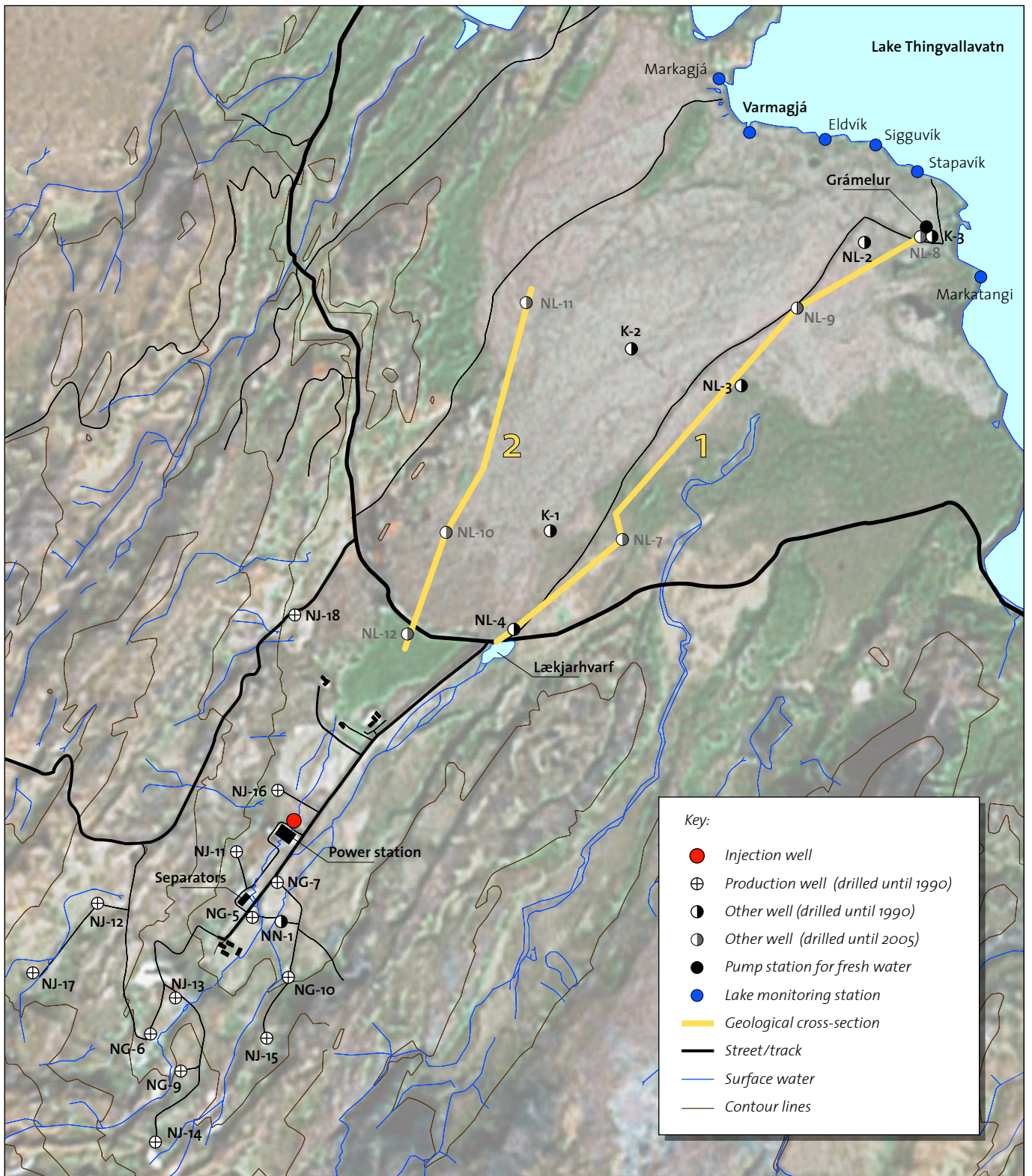
Sheet 2: Overview Nesjavellir valley

Sheet 1: Mapped air picture of SW-Iceland with corresponding orientation maps



Key:

- Framing the detailed maps
- Framing the
 - overview Nesjavellir valley
 - Groundwater model sheets
- Neo-volcanic zone
- Mount Hengill Volcano



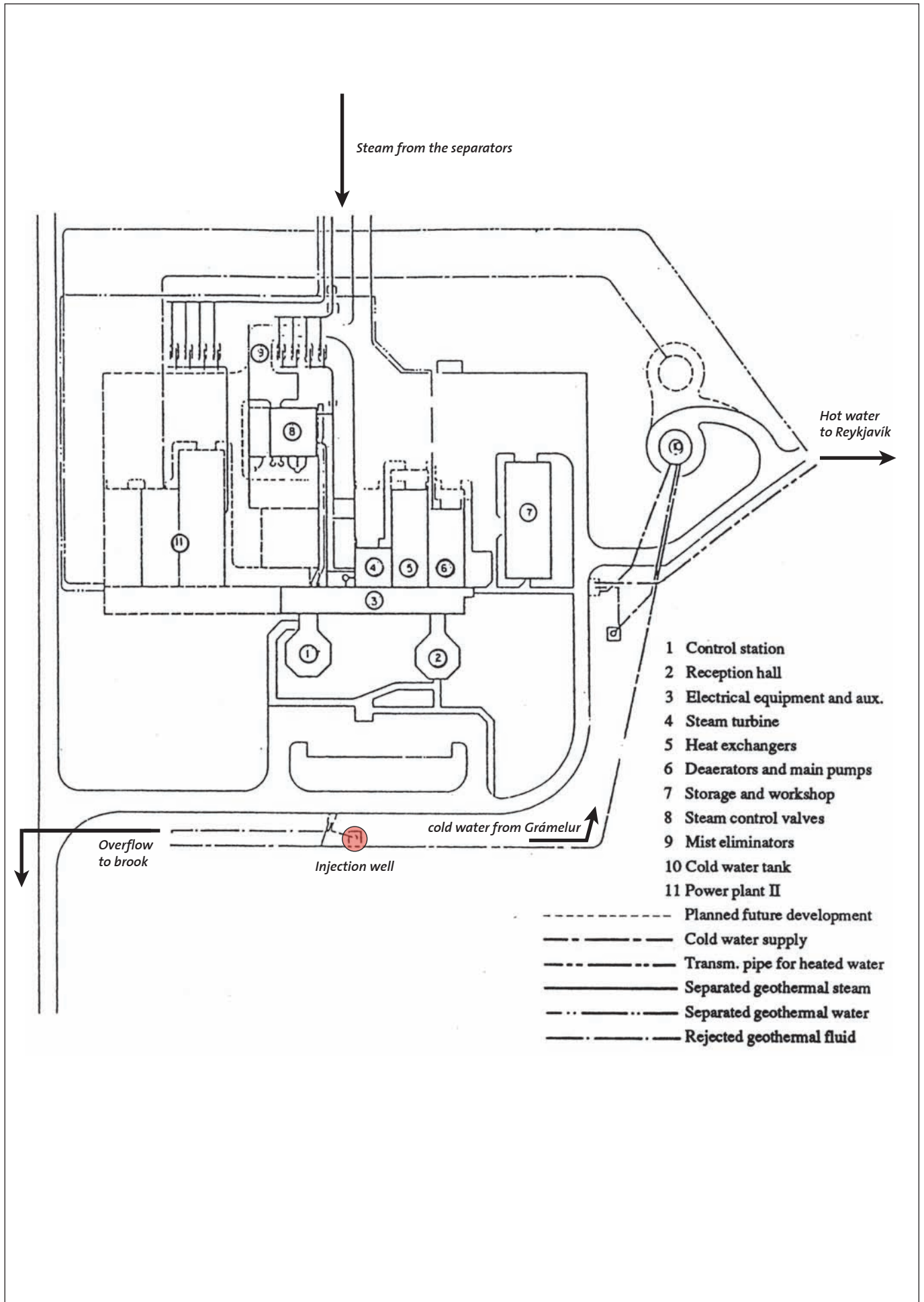
Appendix 3: Original technical drafts

Sheet 1: Draft of the powerhouse 1991

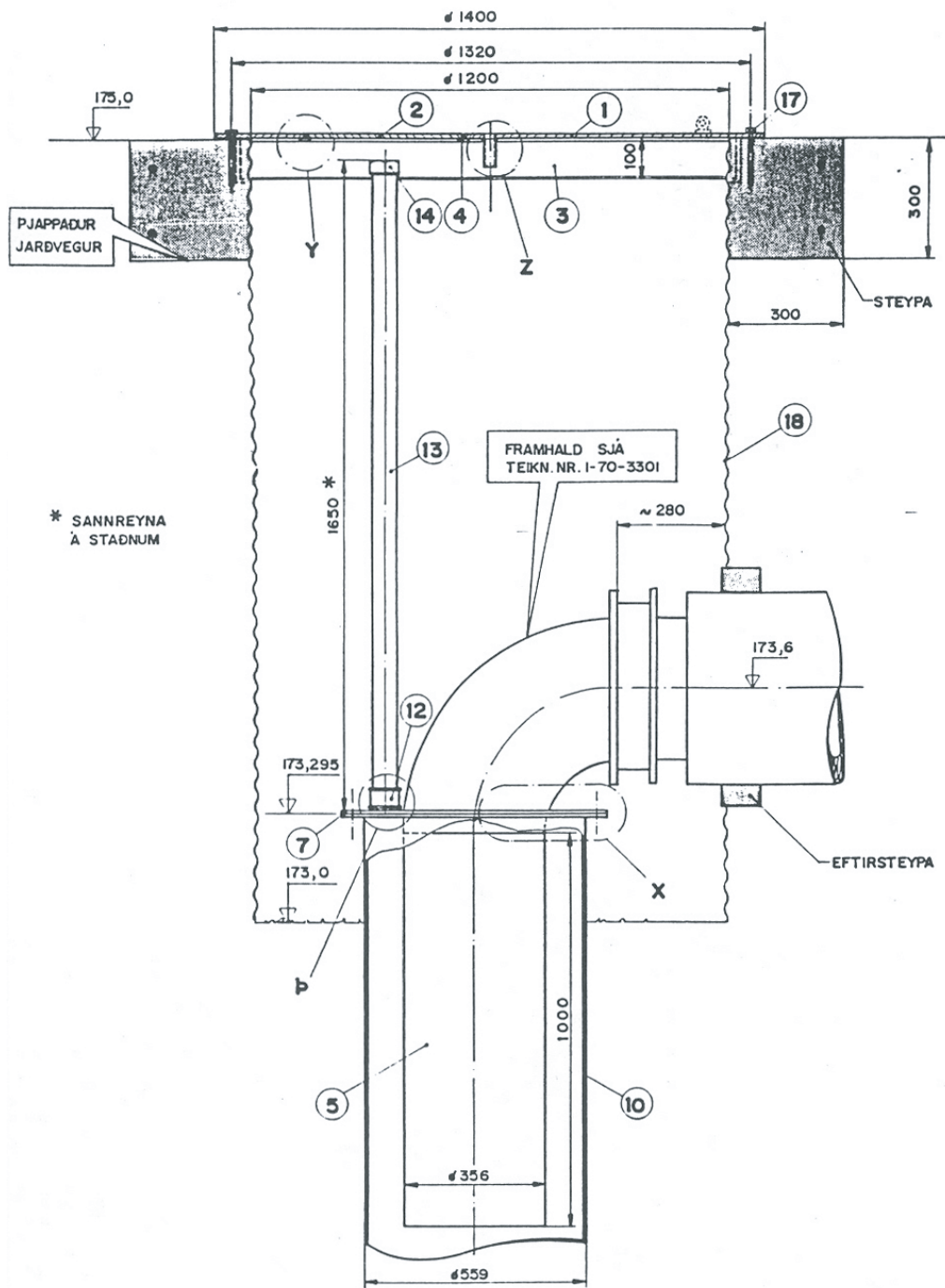
Sheet 2: Draft of the injection well Nidurrenslihola

References:

Sheet 1&2: OR, 2007



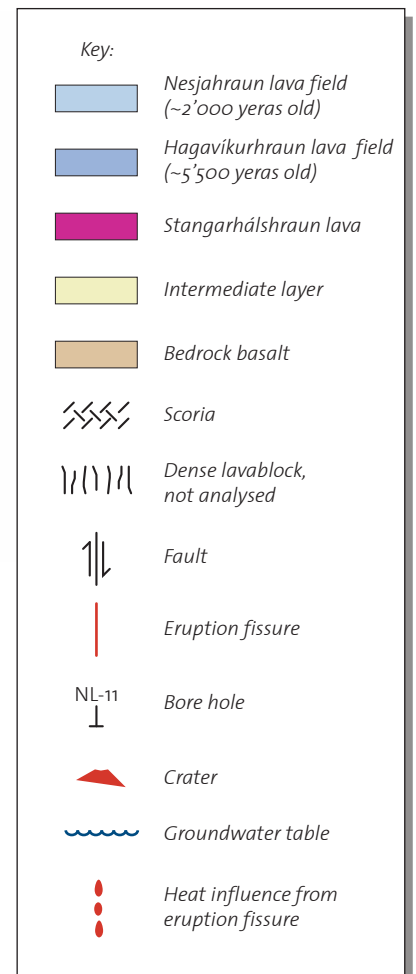
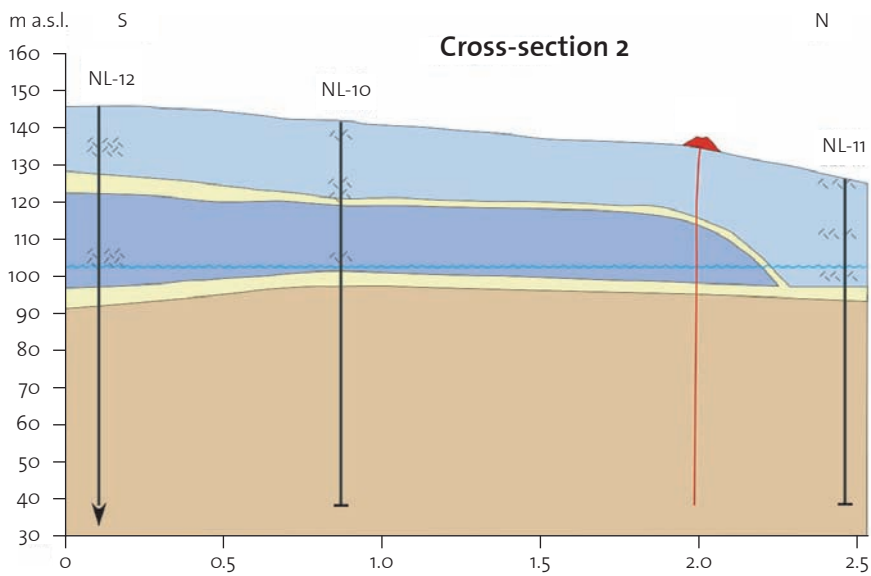
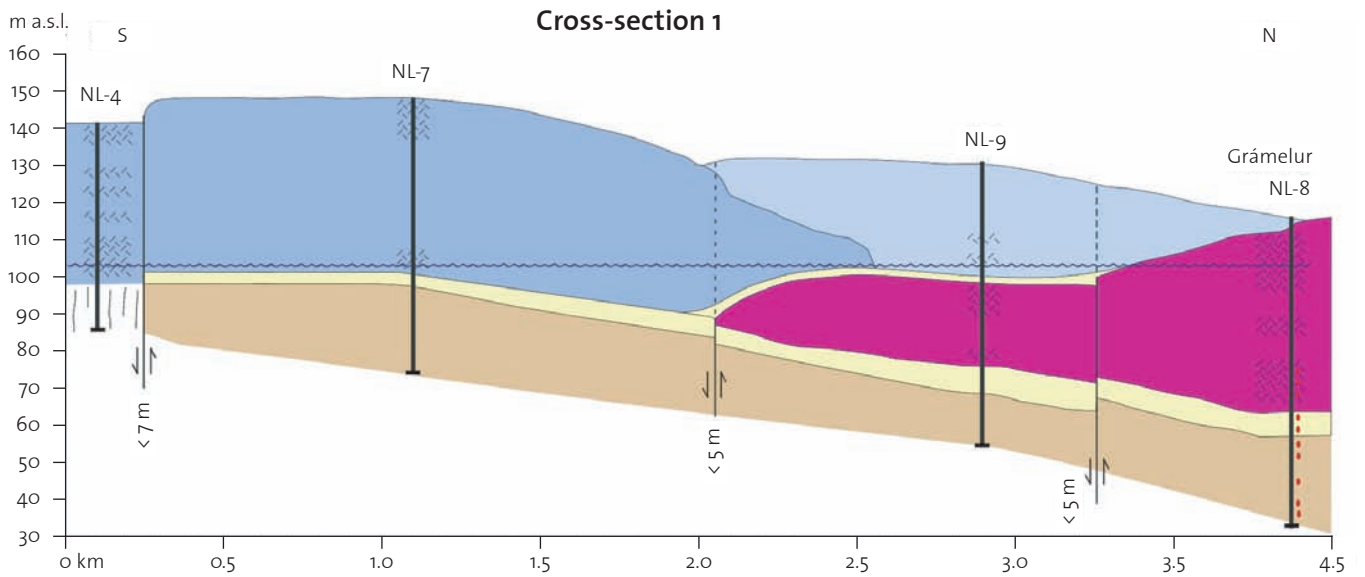
Sheet 2: Draft of the injection well Nidurrennslihola



Appendix 4: Geological cross-sections through the containment area

Reference:

after Hafstad et al., 2007



See Appendix 2, Sheet 2, overview Nesjavellir valley for exact location of cross-sections.

Appendix 5: Groundwater model

Sheet 1: Runoff, 2005 version

Sheet 2: Groundwater table

Sheet 3: Hydraulic conductivity in model layer 1 (from surface to lower aquifer boundary)

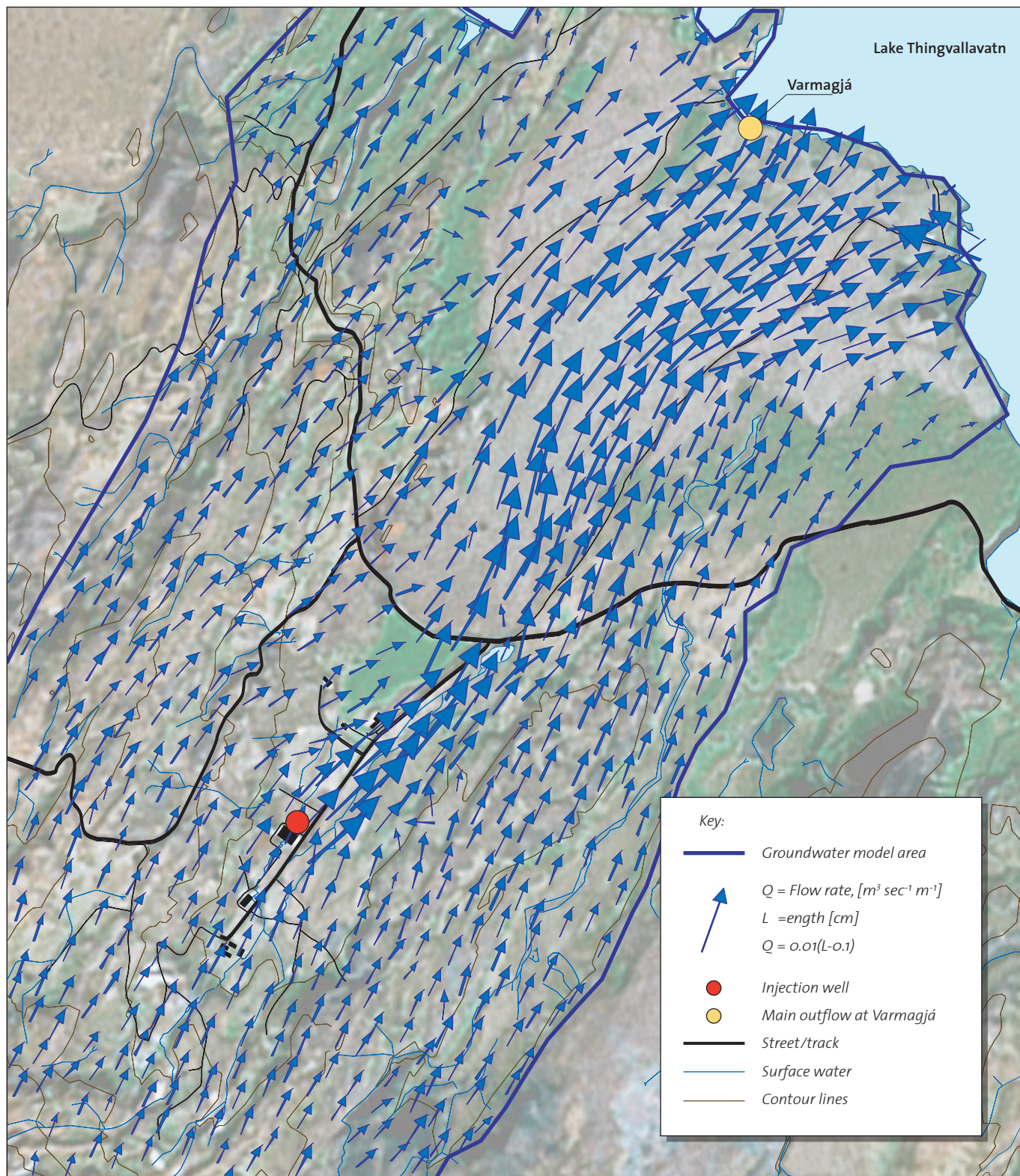
Sheet 4: Anisotropy in model layer 1 (from surface to lower aquifer boundary)

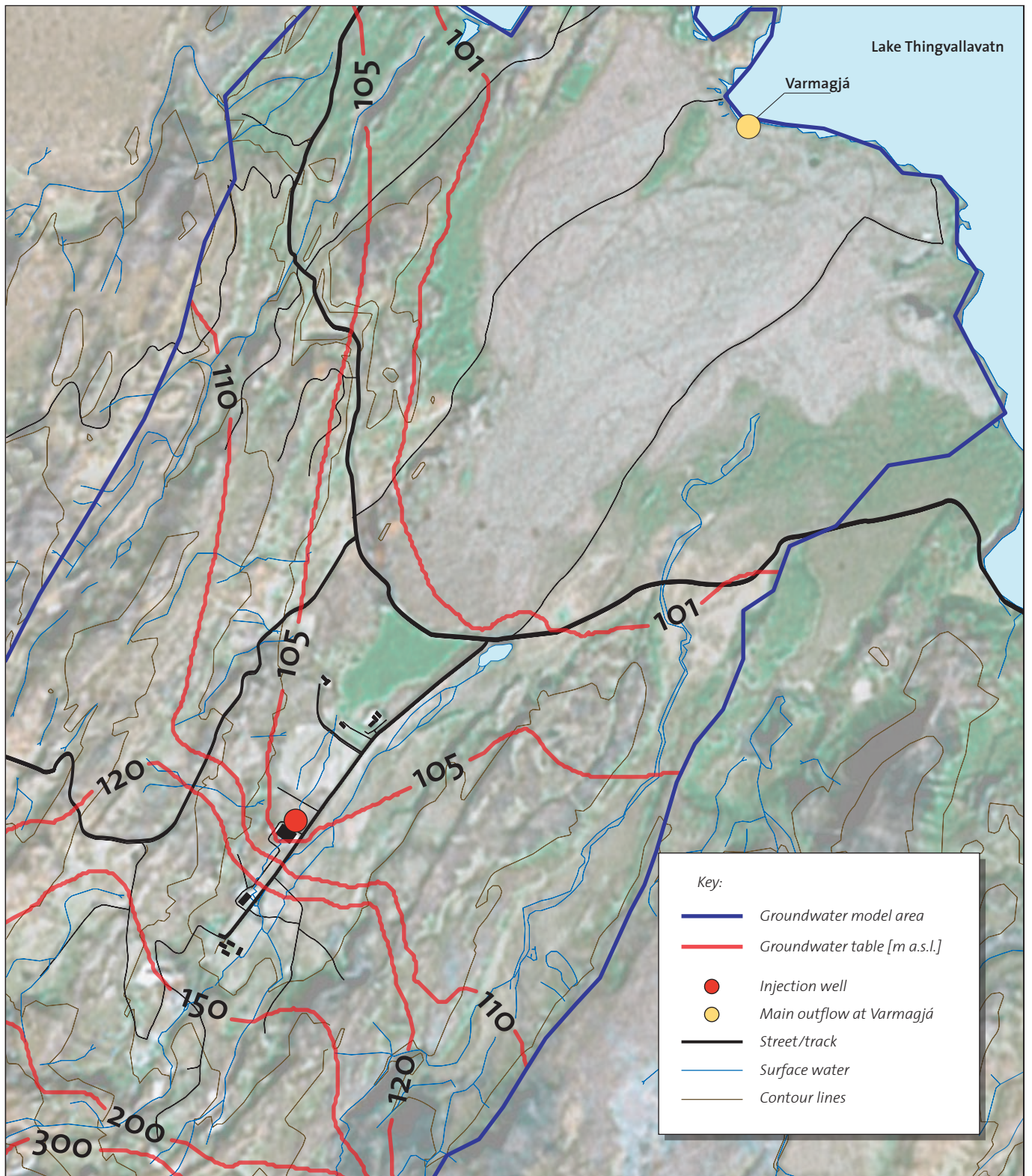
Sheet 5: Runoff prior to plant commissioning

References:

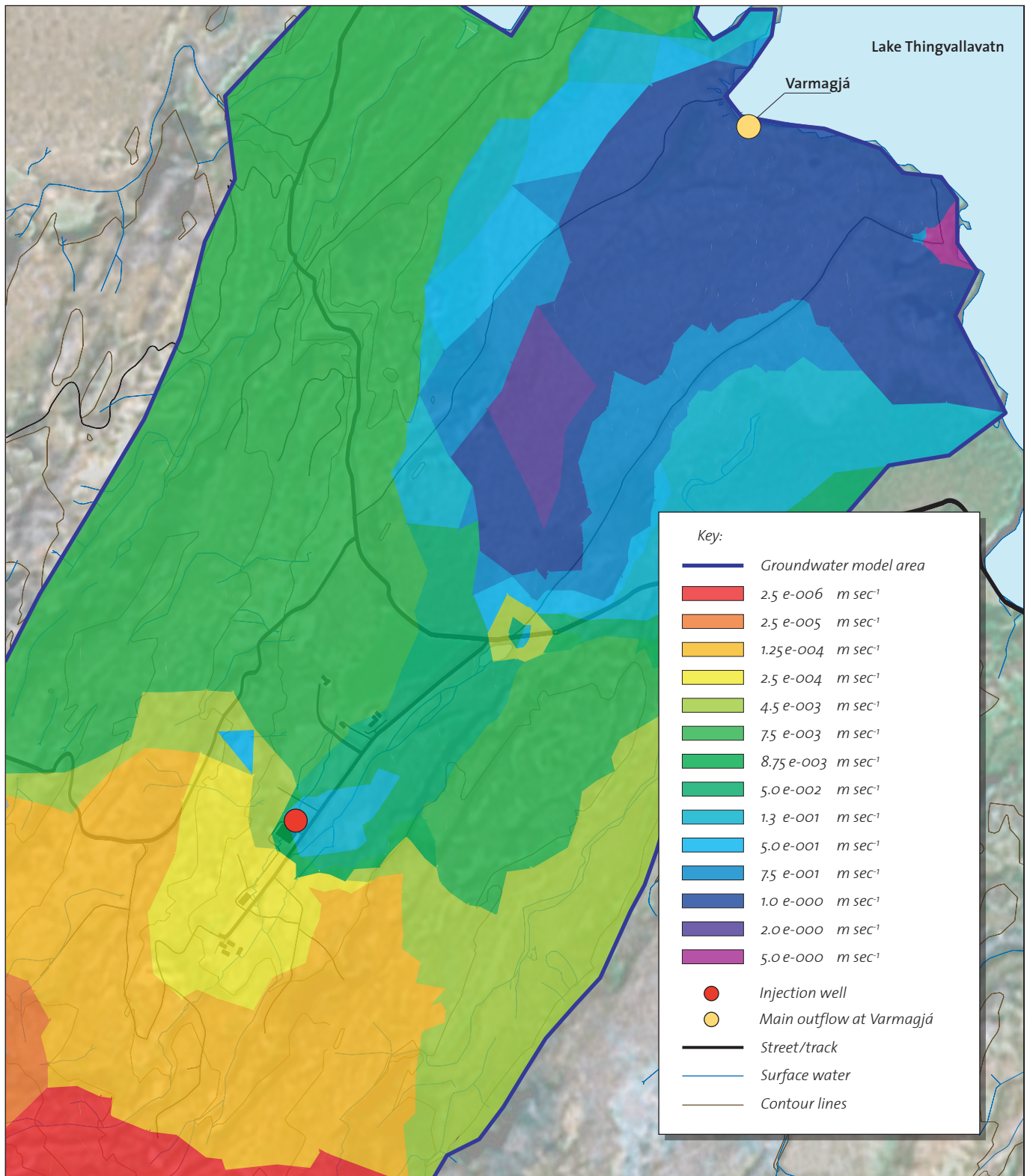
Sheet 1–4 after Kjaran and Myer, 2005

Sheet 5: Kjaran and Egilsson, 1986

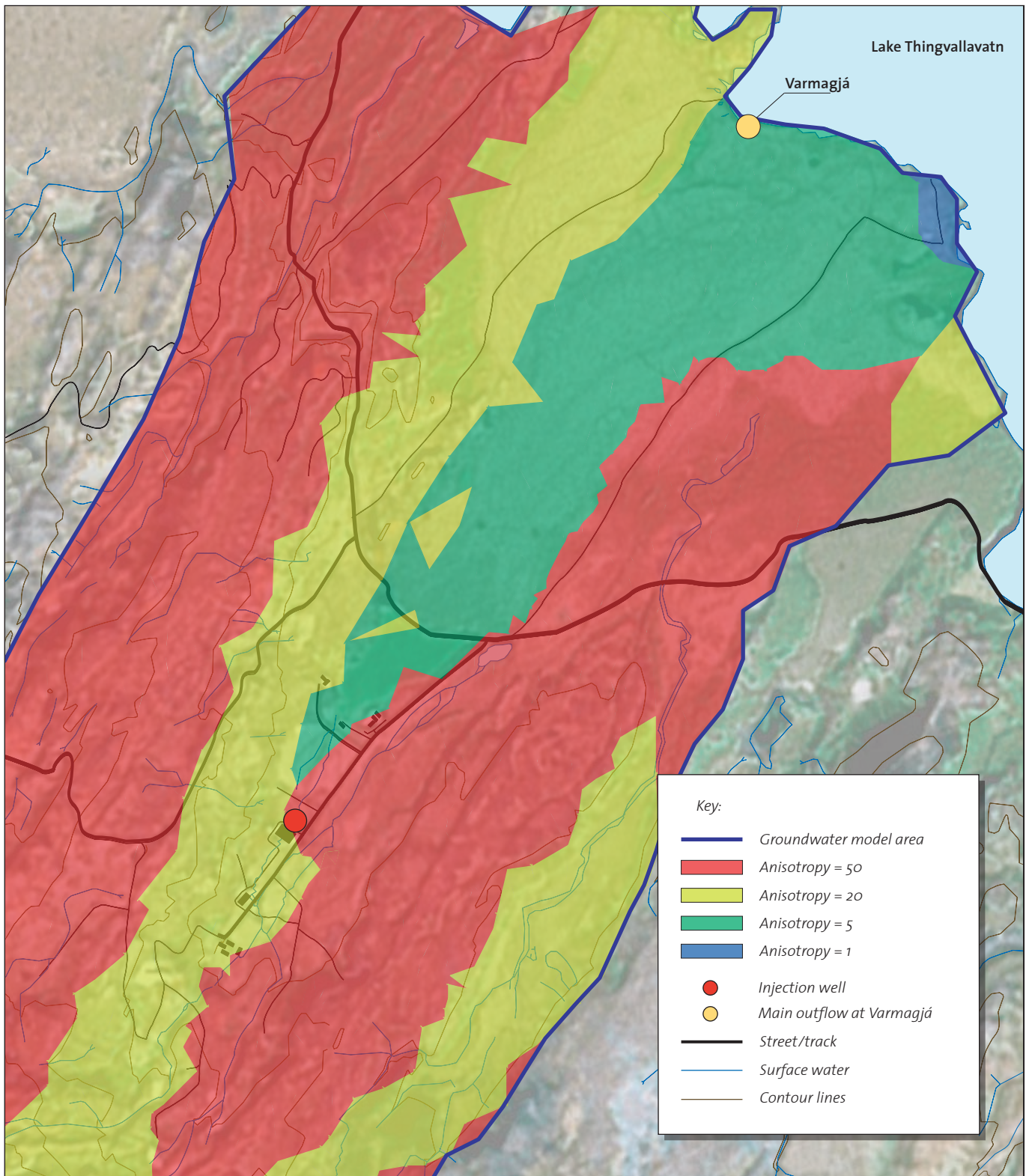




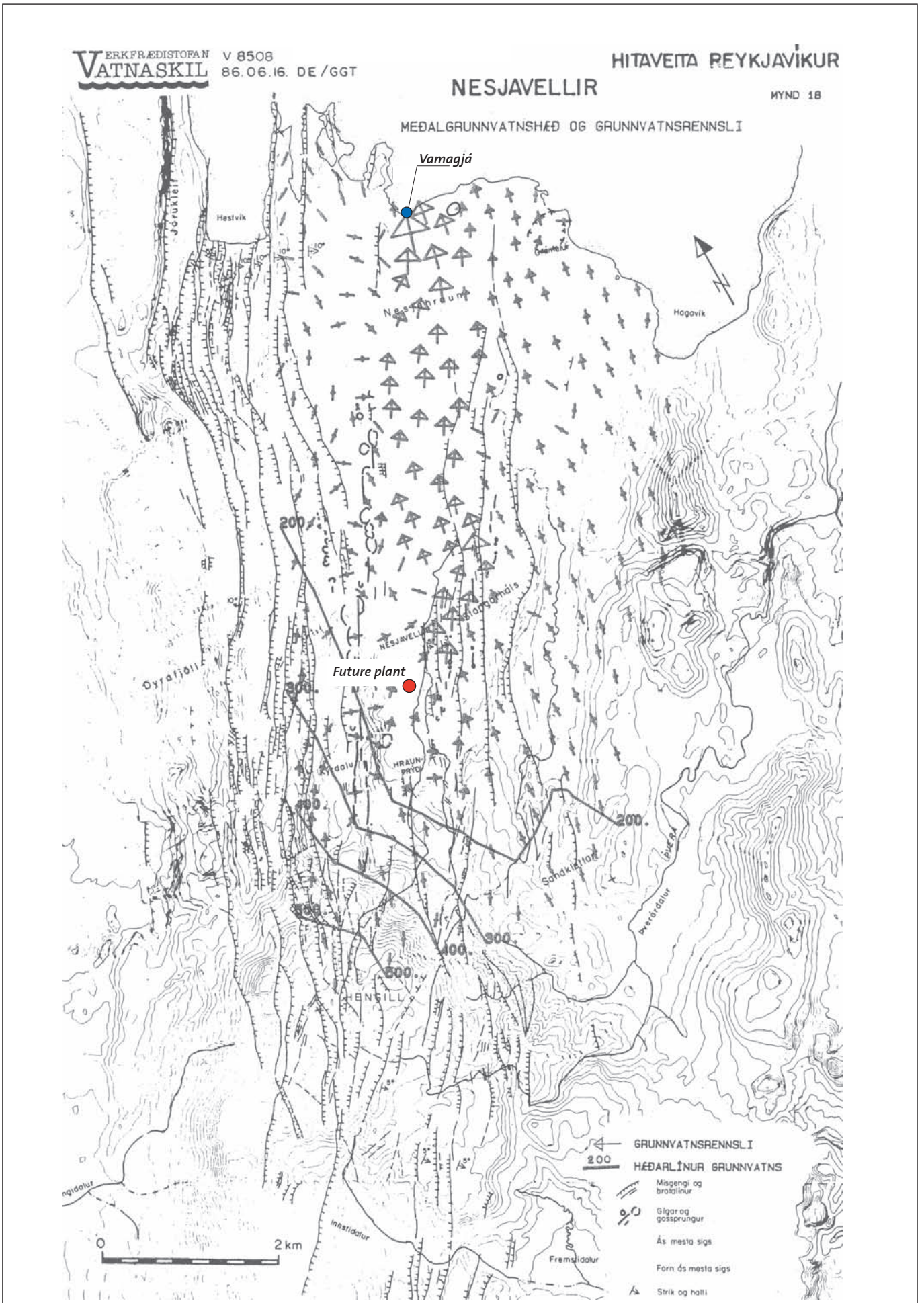
Sheet 3: Hydraulic conductivity in model layer 1 (from surface to lower aquifer boundary)



Sheet 4: Anisotropy in model layer 1 (from surface to lower aquifer boundary)



Sheet 5: Runoff prior to plant commissioning



Appendix 6: Scripts for seepage phase modeling

```

%%%%%%%%%%%%%%%%%%%%%%%%%%%%%%%%%%%%%%%%%%%%%%%%%%%%%%%%%%%%%%%%%%%%%%%%%%
%% Model conditions
%%%%%%%%%%%%%%%%%%%%%%%%%%%%%%%%%%%%%%%%%%%%%%%%%%%%%%%%%%%%%%%%%%%%%%%%%%

flow = 0.06; %[m3/sec]
    %average flow of condensate
vflow = 0.13; %[m]
    %flow velocity given by permeability
rough = 92; %[]
    %the roughness factor for basaltic glass surface area

saturation = [0.01 0.1 0.2 0.3 0.4 0.5 0.6 0.7 0.8 0.9 0.99]; %[]
    %vector for different airfill of the pore space
marinis = [0.061 0.41 1.5]; %[m^2]
    %vector for different marini-surfaces, i.e. the surface defined
    %by 1 liter of porevolume

%%%%%%%%%%%%%%%%%%%%%%%%%%%%%%%%%%%%%%%%%%%%%%%%%%%%%%%%%%%%%%%%%%%%%%%%%%
%% No of Flows, Pore geometry, Reactive surface area
%%%%%%%%%%%%%%%%%%%%%%%%%%%%%%%%%%%%%%%%%%%%%%%%%%%%%%%%%%%%%%%%%%%%%%%%%%

geometry = zeros(length(saturation),9,length(marinis));
    %3D matrix (length(saturation),9,length(marinis)) returning the
    %geometry specifications
for k = 1:length(marinis)
    marini = marinis(k);
    % calculate n for given marini, 100 % saturation; see script calcAll.m
    f = @(n) calcAll(n,flow,vflow)-marini;
    %n = fzero(f,n0(k))
    n = fzero(f,[1 100000000]);

    VPwater = flow/n; %[m^3]
        %water volume of 1 sec of flow at 100% saturation, denoting
        %the pore volume also for saturation < 100%

    Awater = VPwater/vflow; %[m^2]
        %corresponding cross-section area, at 100% saturation this is
        %the whole cross-section of the pore

    radius = (Awater/pi)^0.5; %[m]
        %radius for marini, i.e. 100% saturation original formula from
        %Awater=Acirc-Asegm: r =(Awater/(pi-0.5*(x-sin(x))))^0.5
        %if the total flow and marini wouldn't fix the radius at
        %0%airfill, i.e. x=0, sin(0)=0

    for i = 1:length(saturation)
        f = @(x) 1/(pi*2)*(x-sin(x))-(1-saturation(i));

        rad = fzero(f,pi); %[rad]
            %angle according to saturation in radians

            if rad < 0
                %this condition eliminates negative values the function
                %"fzero" finds around 0
                rad = 0.1; %[rad]
                    %a value as high as 0.1 instead of one closer to 0
                    %keeps the infinity effect moderate during the
                    %further calculations
                    %%%rad = rad*(-1); alternative correction
            end

        deg = rad*180/pi;
            %the angles in degrees

        nair = n/(saturation(i)); %[]
            %new n for saturation < 100% (the radius found for 100%
            %saturation is kept constant while the number of flows (n)
            %increases with decreasing % saturation)

        height = radius - (radius*cos(rad/2)); %[m]
            %the height of the airfilled segment
    end
end

```



```

    chord = 2*radius*sin(rad/2); %[m]
        %the chord of the airfilled segment, i.e. the free water
        %surface
    if rad == 0.1
        %this condition countermands the condition in line 50, as an
        %angle of 0.1 for 100% saturation returns the wrong marini
        %surface
        reactivea = (2*pi*radius-radius*0)*vflow*nair*rough; %[m^2]
            %the total surface for n flows that the given flow
            %is wetting
    else
        reactivea = (2*pi*radius-radius*rad)*vflow*nair*rough; %[m^2]
    end

    geometry(i,:,k) = [marini radius rad deg saturation(i) nair height
chord reactivea];
        %defines the columns of the geometry matrix
    end
end
geometry;

%%%%%%%%%%%%%%%%%%%%%%%%%%%%%%%%%%%%%%%%%%%%%%%%%%%%%%%%%%%%%%%%%%%%%%%%
%% Calculations: "River Depth" for Degassing Model
%%%%%%%%%%%%%%%%%%%%%%%%%%%%%%%%%%%%%%%%%%%%%%%%%%%%%%%%%%%%%%%%%%%%%%%%

correct = 0.9; %[]
    %lowers the riverdepth relative to Diameter-height in order to
    %account for a hypothetical average "depth" of the water in the
    %pore; reasonable range = 0.6-1.0

delayinf = 0.8; %[]
    %delays the infinity-effect towards top of the pore (see below)
    %reasonable range = 0.6-1.0

referencedepts = zeros(length(saturation),length(marinis)); %[m]
    %2D matrix(length(saturation),length(marinis)) returning
    %the uncorrected degassing-distance, in order to tune the
    %modifications used in the model
riverdepths = zeros(length(saturation),length(marinis)); %[m]
    %2D matrix(length(saturation),length(marinis)) returning the
    %degassing-distance, i.e. the riverdepth in the degassing
    %model for rivers used in this study
for i=1:length(saturation)
    for j=1:length(marinis)
        if geometry(i,3,1) < pi %if saturation higher than 50%
            riverdepths(i,j) = ((2*geometry(1,2,j))-
geometry(i,7,j))*correct*((2*geometry(1,2,j))/geometry(i,8,j))^delayinf;
                %river depth for low airfill, the factor
                %diameters/chords implements an infinity-
                %effect towards the top of the poor, where
                %degassing is inhibited by the lack of air
                %and the equilibration of dissolved gas and
                %partial pressure in the remaining pore-air
        else
            riverdepths(i,j) = ((2*geometry(1,2,j))-
geometry(i,7,j))*correct*(geometry(i,8,j)/(2*geometry(1,2,j)))^delayinf;
                % river depth for high airfill
                %the factor chords/diameters flattens the
                %dropdown-effect towards the bottom of the,
                %which means a facilitation of degassing
                %owing to faster convergence of the
                %"riverdepth" towards 0
        end
        referencedepts(i,j) = (2*geometry(1,2,j))-geometry(i,7,j);
    end
end
referencedepts;
riverdepths;

%%%%%%%%%%%%%%%%%%%%%%%%%%%%%%%%%%%%%%%%%%%%%%%%%%%%%%%%%%%%%%%%%%%%%%%%
%% Degassing Model Specifications
%%%%%%%%%%%%%%%%%%%%%%%%%%%%%%%%%%%%%%%%%%%%%%%%%%%%%%%%%%%%%%%%%%%%%%%%

temp = 285; %[°K]
    %average temperature of the condensate

```

```

CO20mg = 333; %[mg/l]
CO20mol = CO20mg/0.044e+6; %[mol/l]
        %CO2 concentration of the condensate at t=0

H2S0mg = 242; %[mg/l]
H2S0mol = H2S0mg/0.034e+6; %[mol/l]
        %CO2 concentration of the condensate at t=0

O20mg = 0; %[mg/l]
O20mol = O20mg/0.032e+6; %[mol/l]
        %CO2 concentration of the condensate at t=0

SO40mg = 0; %[mg/l]
SO40mol = SO40mg/0.096e+6; %[mol/l]
        %CO2 concentration of the condensate at t=0

CO2EQmg = 160; %[mg/l]
CO2EQmol = CO2EQmg/0.044e+6; %[mol/l]
        %CO2 concentration at equilibrium

H2SEQmg = 0; %[mg/l]
H2SEQmol = H2SEQmg/0.034e+6; %[mol/l]
        %H2S concentration at equilibrium

O2EQmg = 11.19633523; %[mg/l]
O2EQmol = O2EQmg/0.032e+6; %[mol/l]
        %O2 concentration at equilibrium (T=12°C)

tvO2 = [0.0000075;0.000025;0.000056]; %[m/sec]
        %transfer velocity of CO2 in water at 10°C (Banks, 1975)
        %the 3 values stand for three different turbulence conditions,
        %literally expressed by different u10-velocities (wind in 10m
        %height above water level):
        %
        %      [ low turbulence (u10=5m/sec) ]
        %      tvO2 @ [middle turbulence (u10=10m/sec)]
        %      [ high turbulence (u10=15m/sec) ]

DCO2 = 1.92e-9; %[m^2/sec]
DH2S = 1.6e-9; %[m^2/sec]
DO2 = 2.0e-9; %[m^2/sec]
        %molecular diffusion coefficients in water at 25°C (after montana
        %state university)

layer = DO2./tvO2; %[m]
        %the boundary layer thickness for the 3 u10 values, which is
        %constant for all gases

tvCO2 = DCO2./layer; %[m]
        %transver velocities of CO2 for the 3 u10 values
tvH2S = DH2S./layer; %[m]
        %transver velocities of H2S for the 3 u10 values

TV = [tvCO2 tvH2S tvO2];
        %2D matrix (3,3) containing all transfer velocities, used in the
        %"surface renewal degassing model" for rivers

%%%%%%%%%%%%%%%%%%%%%%%%%%%%%%%%%%%%%%%%%%%%%%%%%%%%%%%%%%%%%%%%%%%%%%%%
%% Calculating the pH, degassing, H2SO4
%%%%%%%%%%%%%%%%%%%%%%%%%%%%%%%%%%%%%%%%%%%%%%%%%%%%%%%%%%%%%%%%%%%%%%%%

t = 0:4.23:423; %[sec]
        %time vector, reaching to the water tabel with 0.13 m/sec

lavadept = -t*0.13; %[m]
        %the seepage depth at time t

tv = TV(3,:); %choosing the degree of turbulence (1=low, 2=middle, 3=high)

kgCO2 = tv(1)./riverdepths; %[sec^-1]
        %2D matrix (length(airfill),length(marinis)) returning the gas
        %exchange rates of CO2 for the different pore geometries
kgH2S = tv(2)./riverdepths; %[sec^-1]
        %2D matrix (length(airfill),length(marinis)) returning the gas
        %exchange rates of H2S for the different pore geometries

```

```

kgO2 = tv(3)./riverdepths; %[sec^-1]
      %2D matrix (length(airfill),length(marinis)) returning the gas
      %exchange rates of O2 for the different pore geometries

pH0 = 4.46; %[]
      %pH concentration at time 0, when the condensate enters the lava
H0 = 10^-pH0; %[mol/l]
      %H+ concentration at time 0, when the condensate enters the lava

Ca0 = 0; %[mol/l]
Mg0 = 0; %[mol/l]
      %Ca/Mg concentration at time 0, when the condensate enters the lava

pKH2CO3 = 6.40; %[]
      %acidic strenght of H2CO3 at T = 12°C

rad = geometry(:,3,:); %[rad]
      %2D matrix (length(saturation),length(marinis)) returning the angles
      %of the air filled pore segment

radius = geometry(:,2,:); %[m]
      %2D matrix (length(saturation),length(marinis)) returning the
      %radii according to All

values0 = [H2S0mol H0 O20mol CO20mol Ca0 Mg0 SO40mol]; %[mol/l]
      %the initial conditions for the pH ODE system

solODES = zeros(length(t),7,length(saturation),length(marinis)); %[mol/l]
      %4D matrix (length(t),4,length(saturation),length(marinis))
      %returning the concentration development of H2S,H+,O2 and CO2.
      %For simplicity, the Ca/Mg/SO4-concentration development is also
      %calculated here, but will not be called before the next section
T = zeros(length(t),length(saturation),length(marinis));
for i = 1:length(saturation)
  for j = 1:length(marinis)
    [T(:,i,j),solODES(:, :, i, j)] = ode45(@(t,f) calcO-
DES(t,f,temp,kgCO2(i,j),kgH2S(i,j),kgO2(i,j),CO2EQ0mol,O2EQ0mol,radius(i,j),ra
d(i,j),pKH2CO3),t,values0);
  end
end
T;
solODES;

conccO2 = zeros(length(t),length(saturation),length(marinis)); %[mg/l]
      %3D matrix (length(t),length(saturation),length(marinis))
      %returning the development of the CO2 concentration
conch2S = zeros(length(t),length(saturation),length(marinis)); %[mg/l]
      %3D matrix (length(t),length(saturation),length(marinis))
      %returning the development of the H2S concentration
concsO4 = zeros(length(t),length(saturation),length(marinis)); %[mg/l]
      %3D matrix (length(t),length(saturation),length(marinis))
      %returning the development of the SO4 concentration
conco2 = zeros(length(t),length(saturation),length(marinis)); %[mg/l]
      %3D matrix (length(t),length(saturation),length(marinis))
      %returning the development of the O2 concentration
conch = zeros(length(t),length(saturation),length(marinis)); %[mol/l]
      %3D matrix (length(t),length(saturation),length(marinis))
      %returning the development of the H+ concentration
pH = zeros(length(t),length(saturation),length(marinis)); %[]
      %3D matrix (length(t),length(saturation),length(marinis))
      %returning the development of the pH
for k=1:length(t)
  for i=1:length(saturation)
    for j=1:length(marinis)
      concCO2(k,i,j) = solODES(k,4,i,j)*0.044e6;
      concH2S(k,i,j) = solODES(k,1,i,j)*0.034e6;
      concO2(k,i,j) = solODES(k,3,i,j)*0.032e+6;
      concSO4(k,i,j) = solODES(k,7,i,j)*0.096e+6;
      concH(k,i,j) = solODES(k,2,i,j);
      pH(k,i,j) = -log10(concH(k,i,j));
    end
  end
end
conccO2;
conch2S;
conco2;

```



```

%%%%%%%%%%%%%%%%%%%%%%%%%%%%%%%%%%%%%%%%%%%%%%%%%%%%%%%%%%%%%%%%%%%%%%%%
%% calcAC11 FUNCTION
%%%%%%%%%%%%%%%%%%%%%%%%%%%%%%%%%%%%%%%%%%%%%%%%%%%%%%%%%%%%%%%%%%%%%%%%

%this function calculates the surface area wetted by one liter of fluid at
%given number of flows n, flowrate and flow velocity, assuming 100%
%saturated pore space

function All = calcAll(n,flow,vflow)

VPwater = flow/n; %[m]
           %water volume of 1 sec of flow at 100% saturation, denoting
           %the pore volume also for saturation < 100%
Awater = VPwater/vflow; %[m^2]
           %corresponding cross-section area, at 100% saturation this is
           %the whole cross-section of the pore
radius = (Awater/pi)^0.5; %[m]
           %corresponding pore radius
VP = pi*radius^2*vflow; %[m^3]
           %corresponding pore volume
AC = 2*pi*radius*vflow; %[m^2]
           %corresponding reactive surface area (here, at 100% saturation = the
           %mantel area of a vflow-long pore piece
All = 0.001/VP*AC; %[m^2]
           %the area, that 1l of fluid is wetting in 1 sec

%%%%%%%%%%%%%%%%%%%%%%%%%%%%%%%%%%%%%%%%%%%%%%%%%%%%%%%%%%%%%%%%%%%%%%%%
%% END FUNCTION
%%%%%%%%%%%%%%%%%%%%%%%%%%%%%%%%%%%%%%%%%%%%%%%%%%%%%%%%%%%%%%%%%%%%%%%%

%%%%%%%%%%%%%%%%%%%%%%%%%%%%%%%%%%%%%%%%%%%%%%%%%%%%%%%%%%%%%%%%%%%%%%%%
%% calcODES FUNCTION
%%%%%%%%%%%%%%%%%%%%%%%%%%%%%%%%%%%%%%%%%%%%%%%%%%%%%%%%%%%%%%%%%%%%%%%%

%this function calculates the system of ordinary first order differential
%equations fort the modeling of the pH developing

function df = calcO-
DES(t,f,temp,kgCO2,kgH2S,kgO2,CO2EQmol,O2EQmol,radius,rad,pKH2CO3)

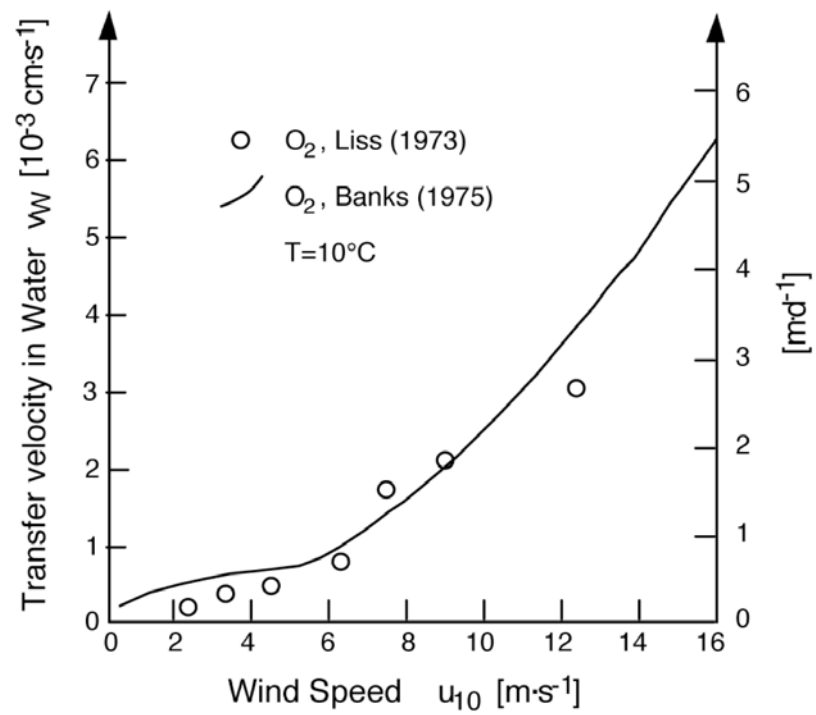
df = zeros(7,1);
df(1) = -(10^((10.5+0.16*(-log10(f(2))))-(3000/temp)))/3600)*f(1)*f(3)-
kgH2S*f(1);
df(2) = (10^((10.5+0.16*(-log10(f(2))))-(3000/temp)))/3600)*f(1)*f(3)-
(1.08*(2*pi-rad)/(1000*radius*(pi-0.5*(rad-sin(rad))))*10^(-3.99-0.95*(-
log10(f(2)))))-(10^-(pKH2CO3/2)*0.5*f(4)^-0.5*kgCO2*(f(4)-CO2EQmol));
df(3) = -(10^((10.5+0.16*(-log10(f(2))))-
(3000/temp)))/3600)*f(1)*f(3)+kgO2*(O2EQmol-f(3));
df(4) = -kgCO2*(f(4)-CO2EQmol);
df(5) = 0.26*(2*pi-rad)/(1000*radius*(pi-0.5*(rad-sin(rad))))*10^(-3.99-
0.95*(-log10(f(2)))));
df(6) = 0.28*(2*pi-rad)/(1000*radius*(pi-0.5*(rad-sin(rad))))*10^(-3.99-
0.95*(-log10(f(2)))));
df(7) = (10^((10.5+0.16*(-log10(f(2))))-(3000/temp)))/3600)*f(1)*f(3);

```

Appendix 7: Gas exchange transfer velocity for O₂ in water at 10°C

Reference:

Imboden and Kipfer, 2003, and reference therein



Appendix 8: Plots of the water chemistry monitoring at Lækjarhvarf and Varmagjá

Sheet 1: CO₂ concentration

Sheet 2: SO₄ concentration

Sheet 3: Ca²⁺ concentration

Sheet 4: Mg²⁺ concentration

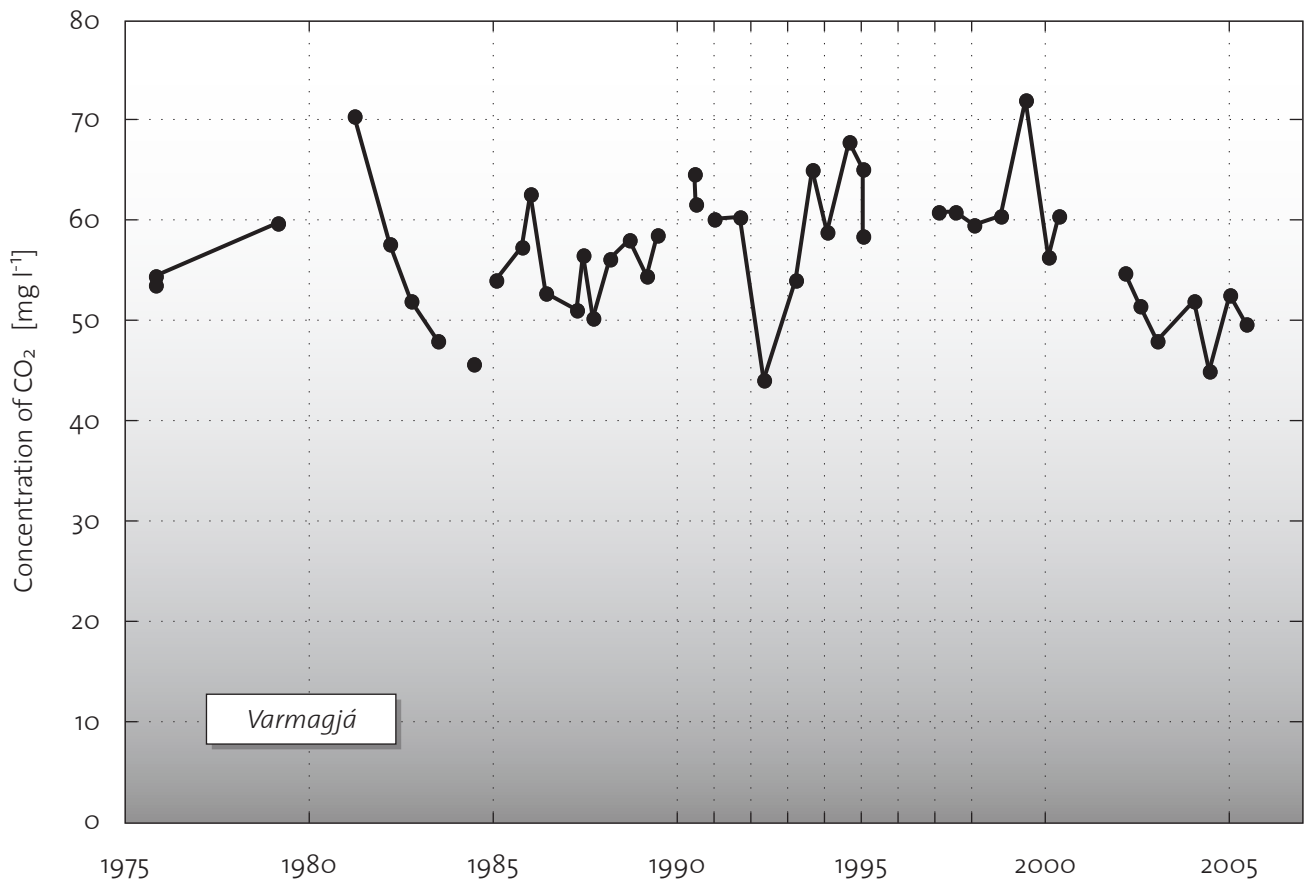
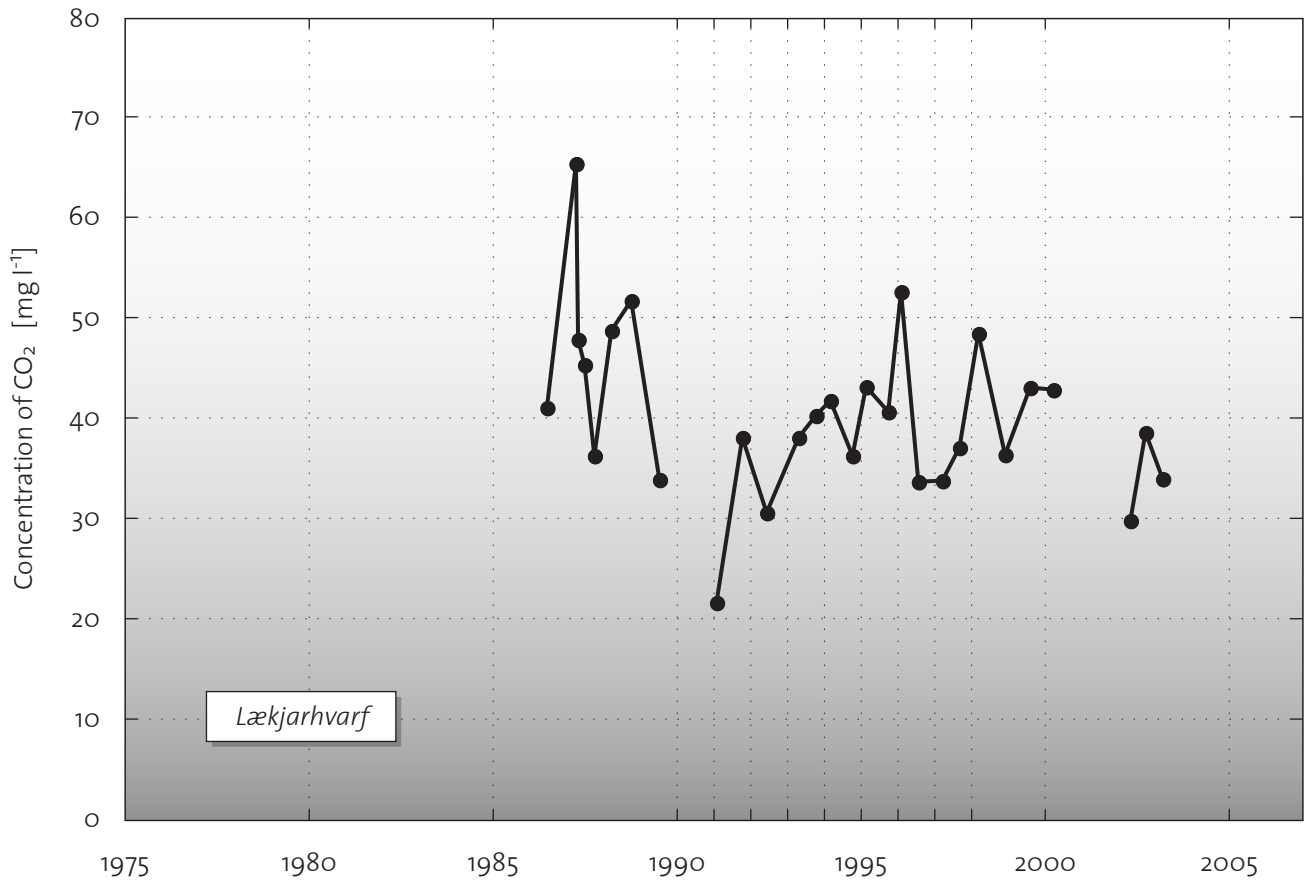
Sheet 5: pH developing

Sheet 6: Temperature developing

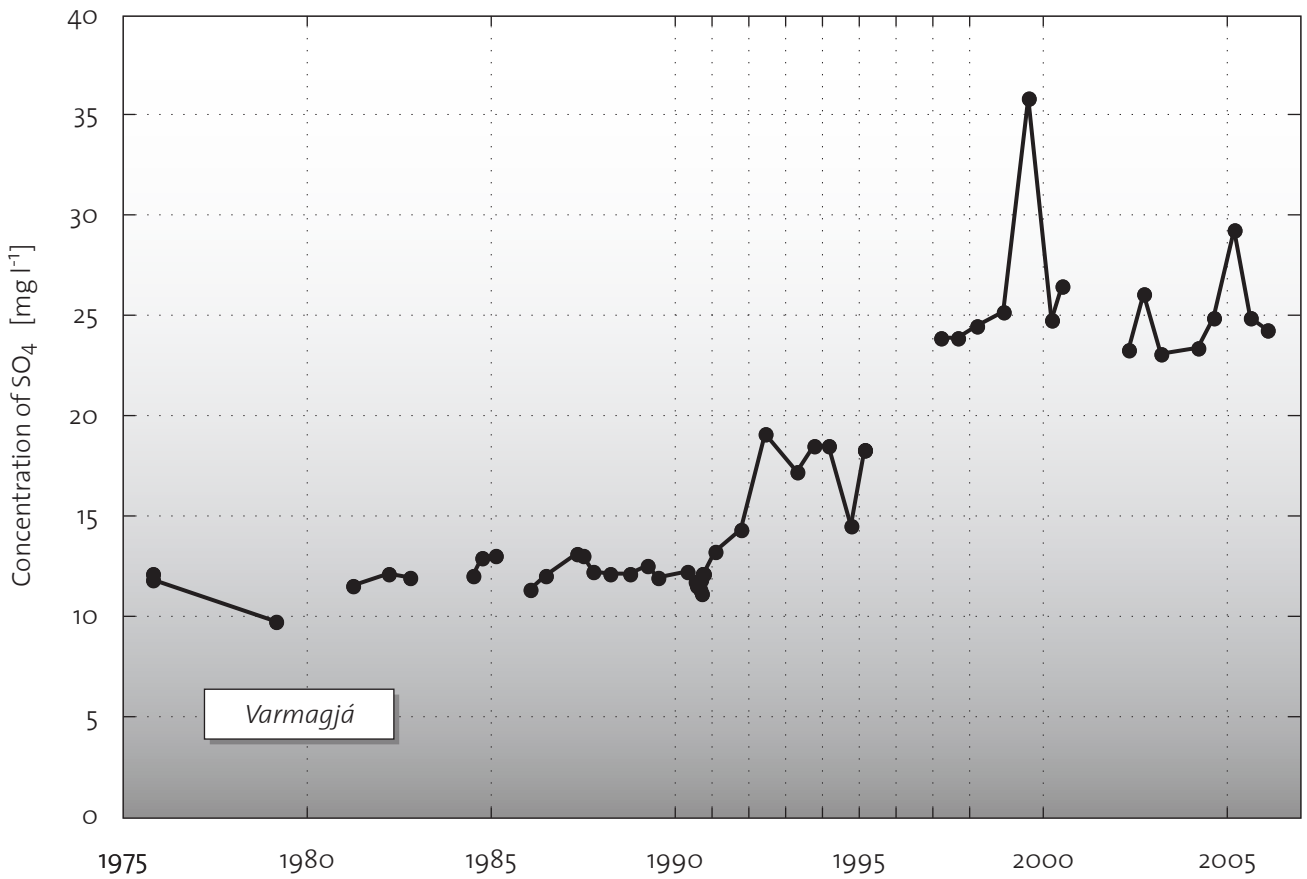
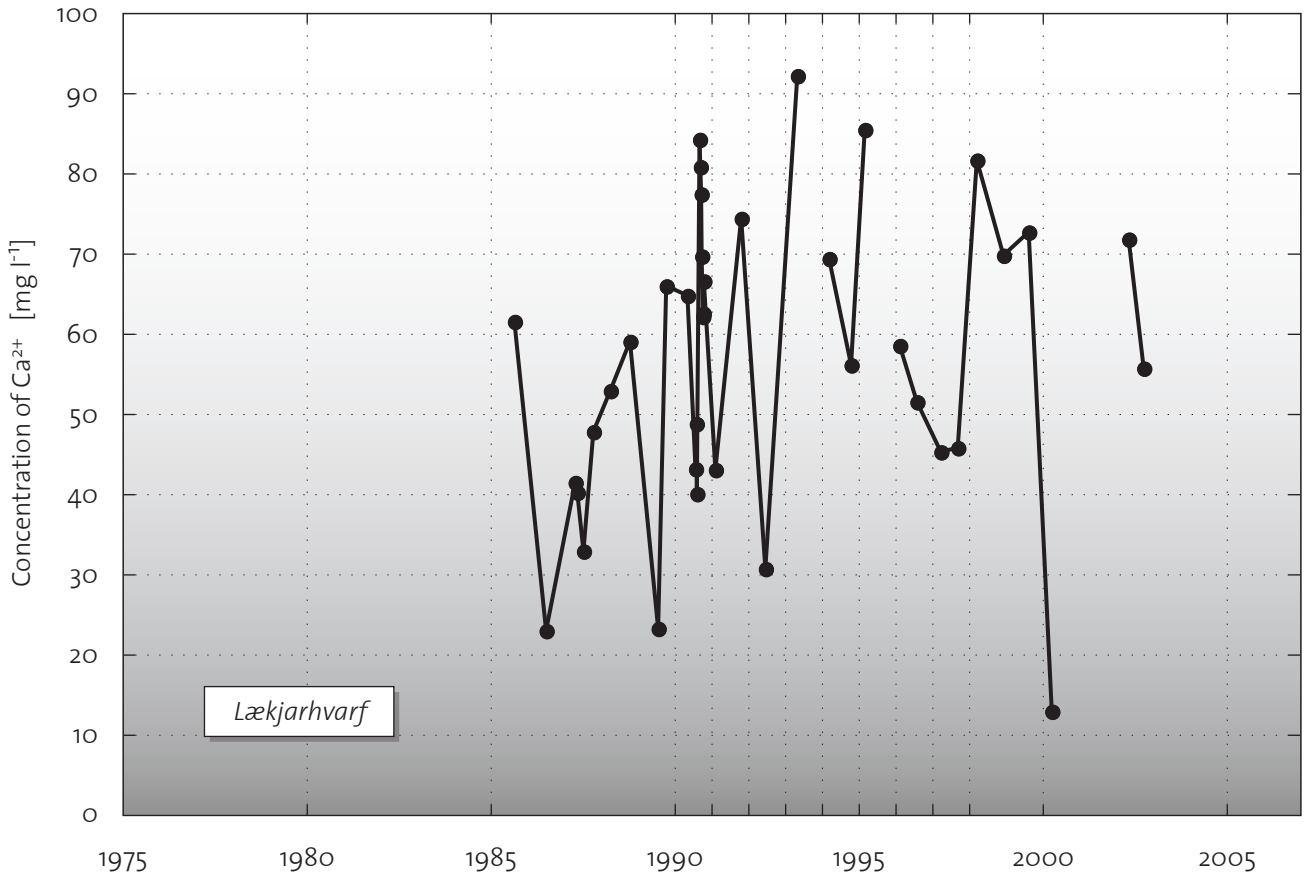
References:

Sheet 1–6: OR, 2007

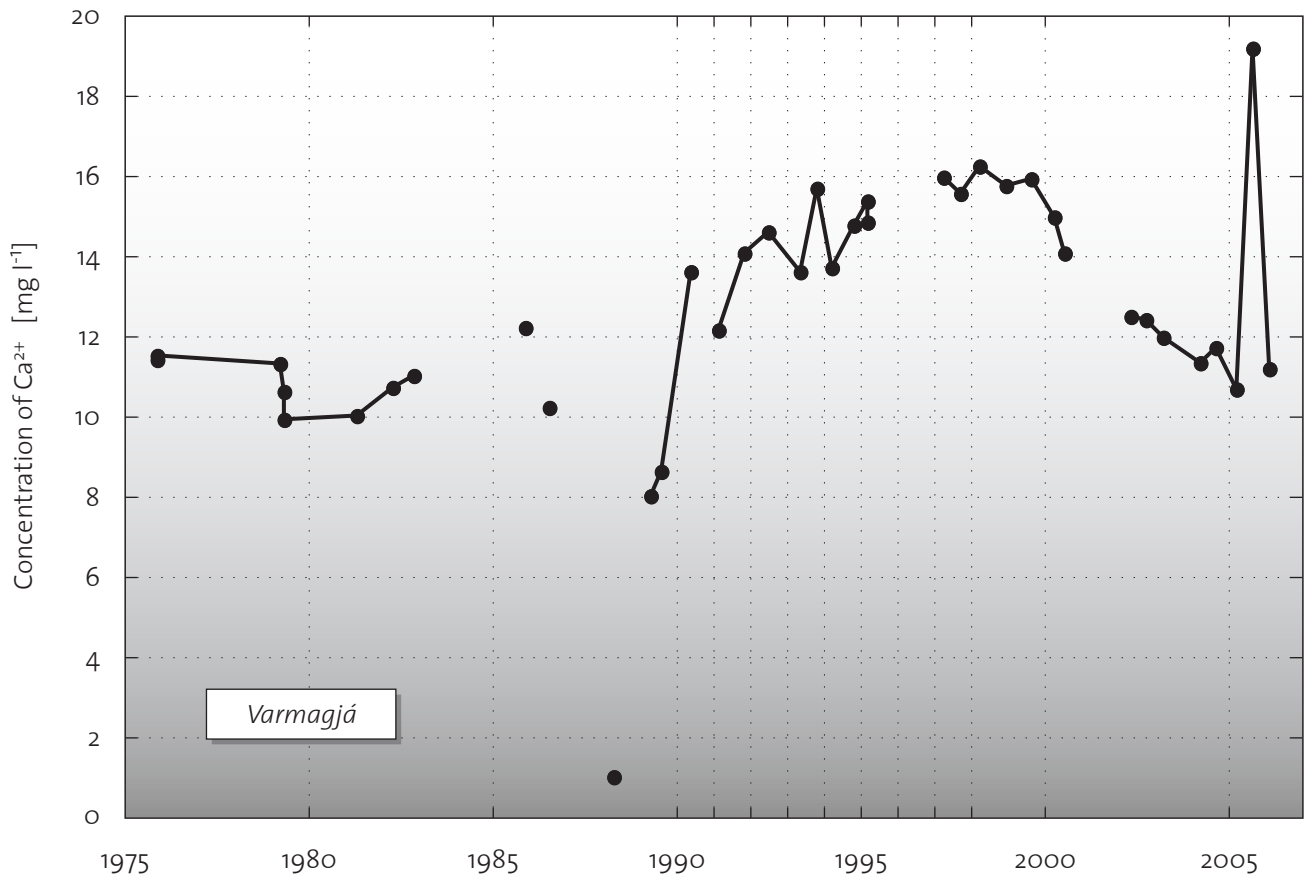
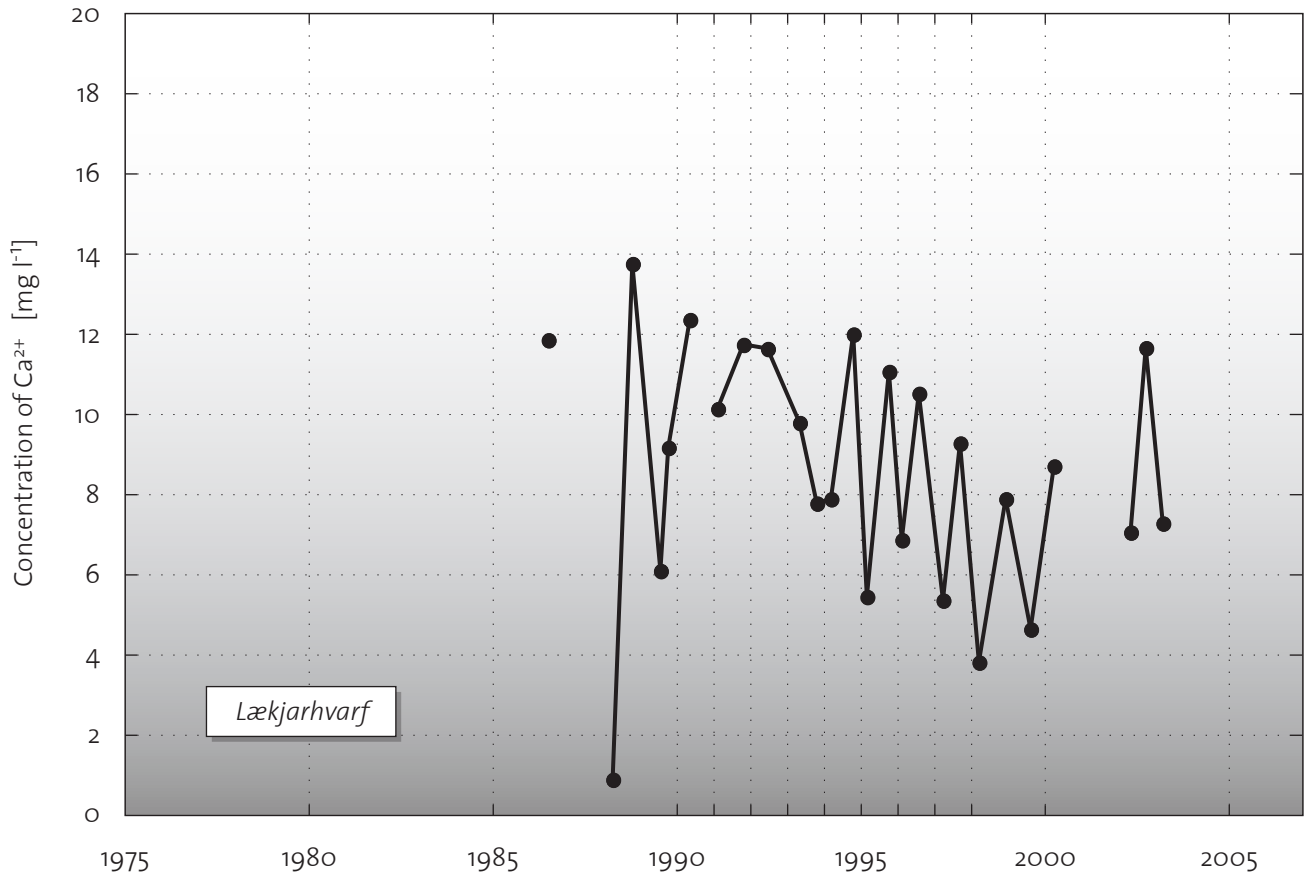
Sheet 1: CO₂ concentration



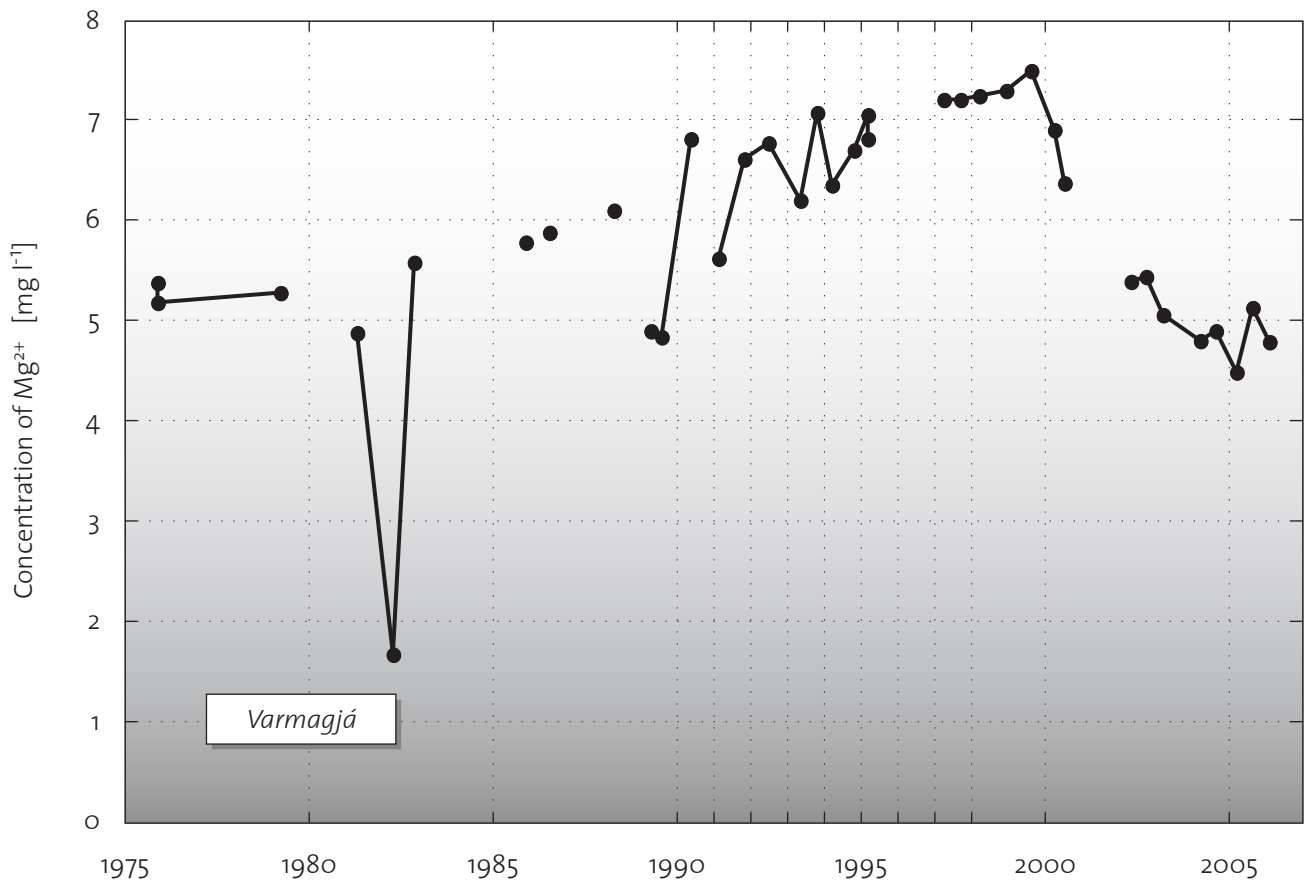
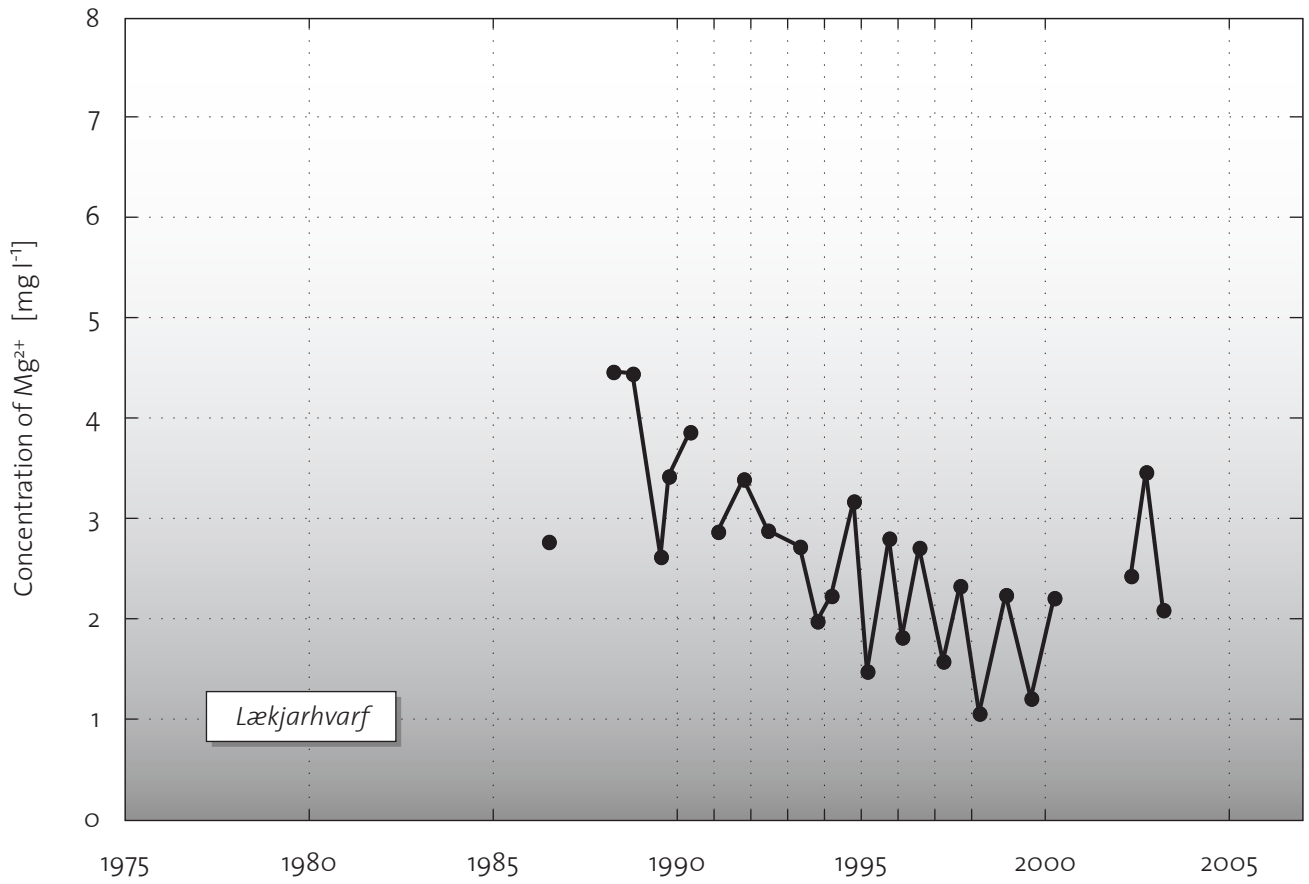
Sheet 2: SO₄ concentration



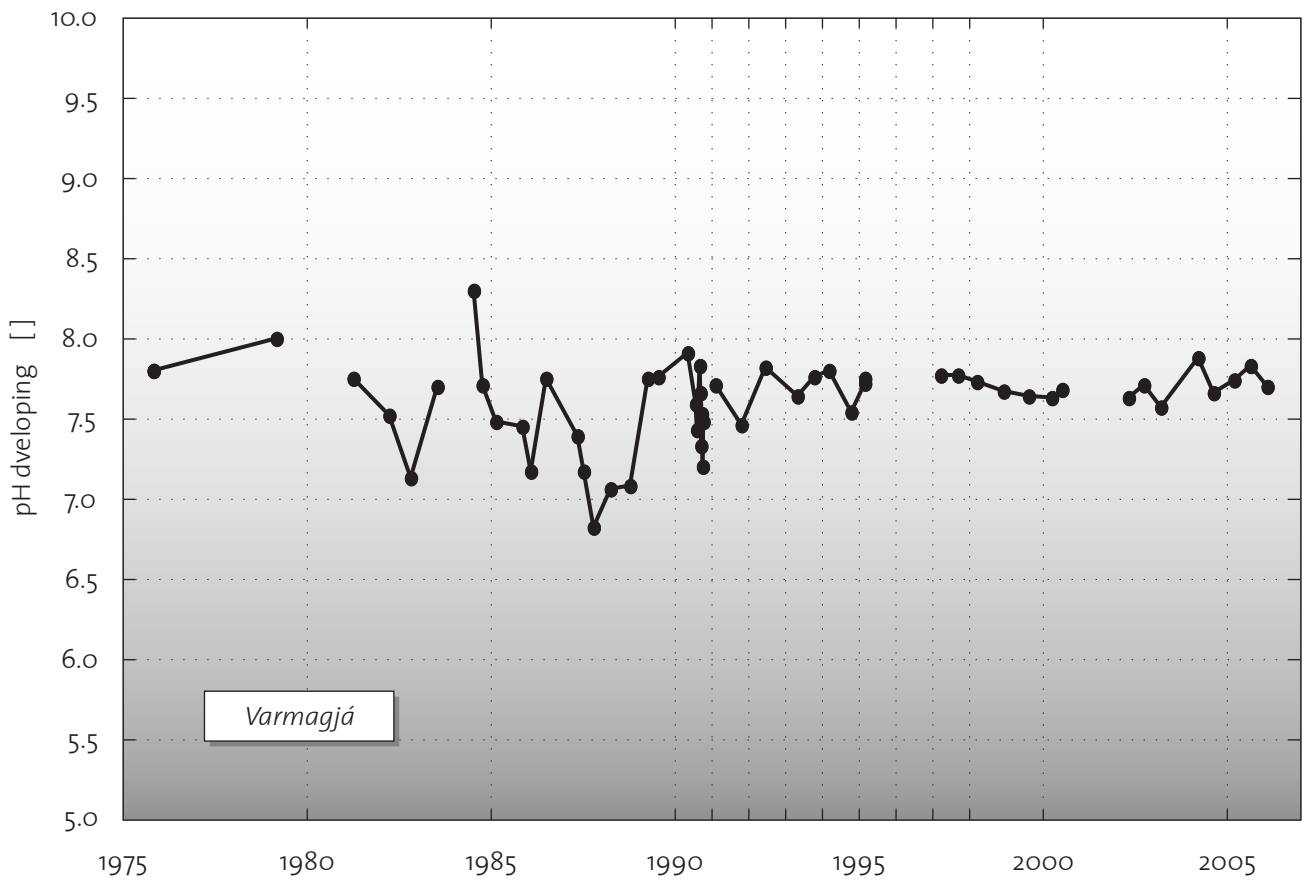
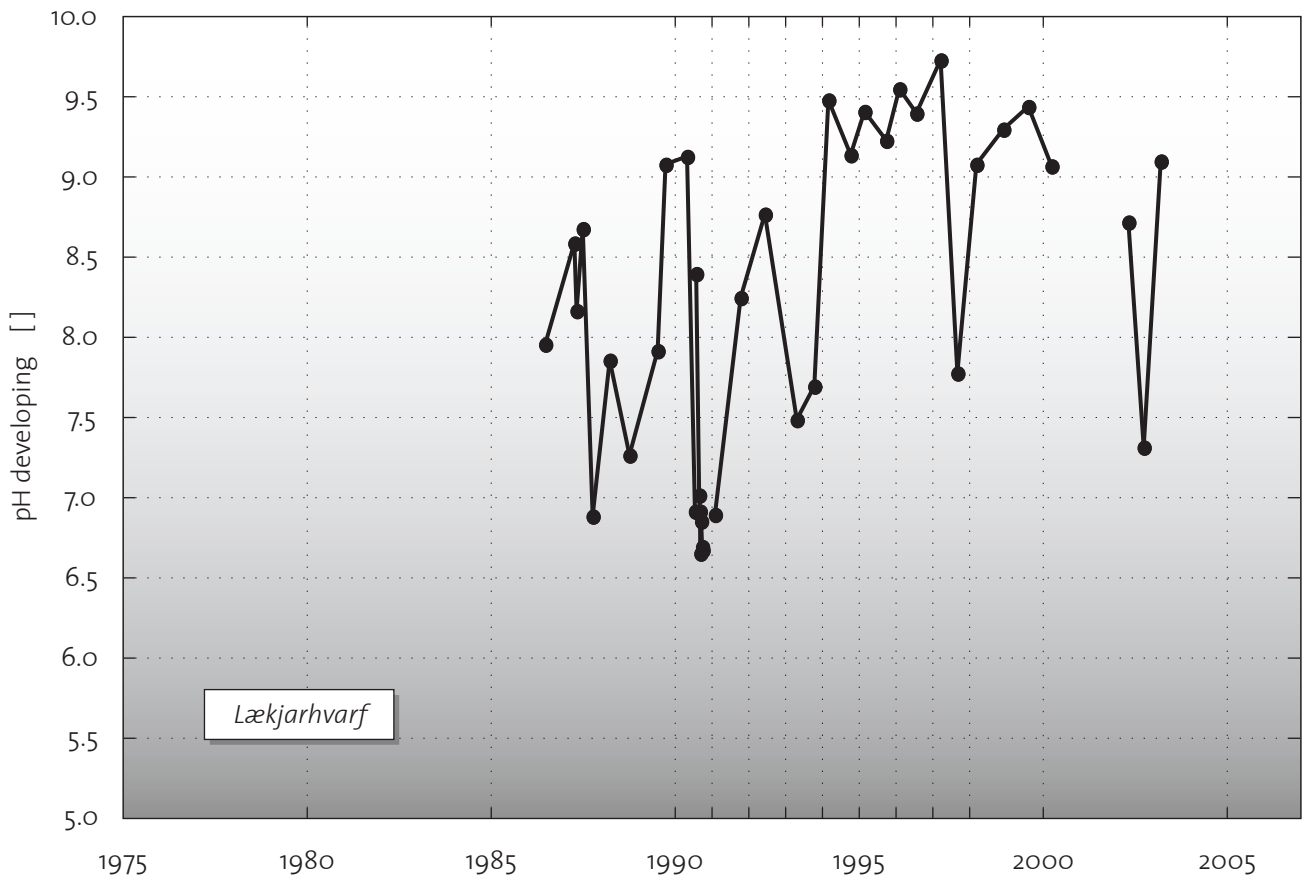
Sheet 3: Ca²⁺ concentration



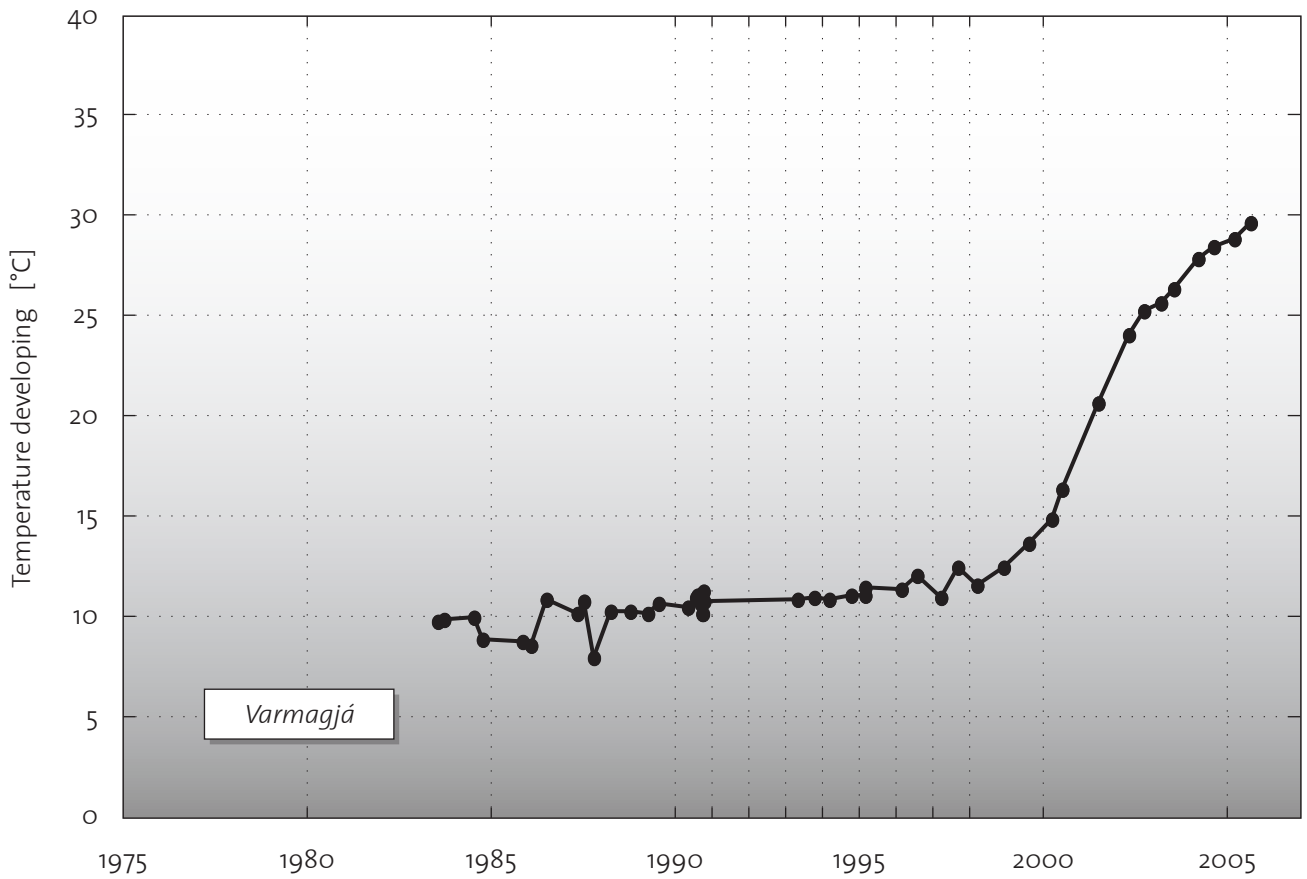
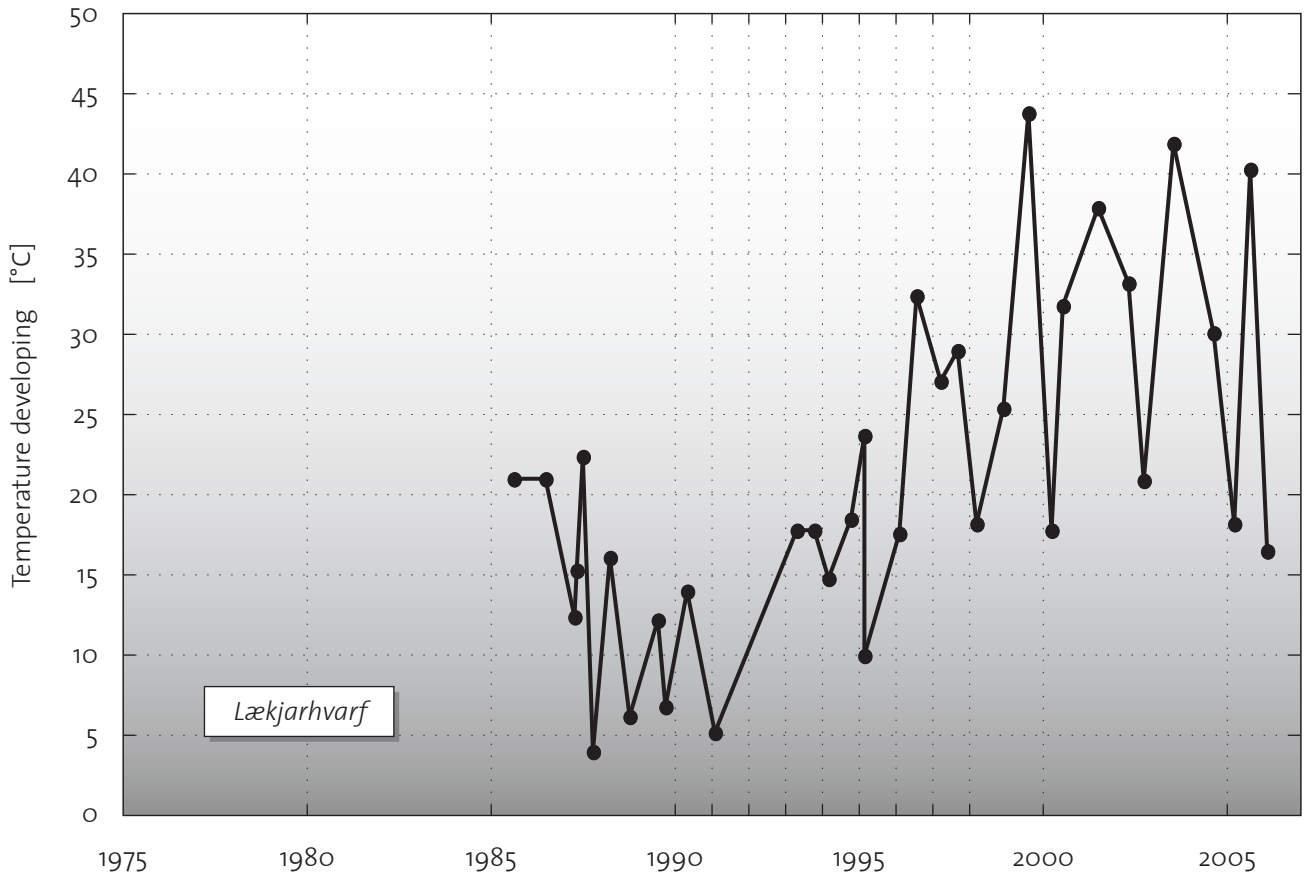
Sheet 4: Mg²⁺ concentration



Sheet 5: pH developing

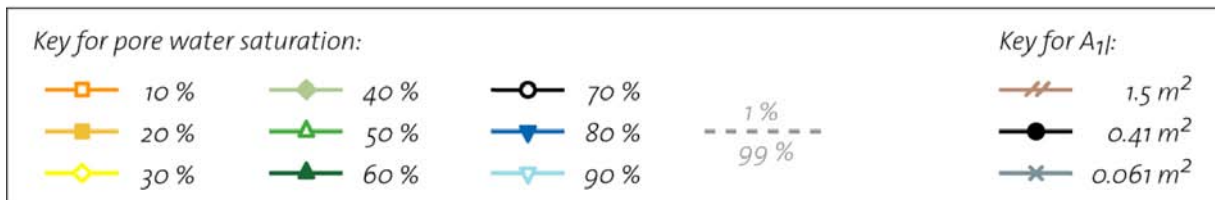
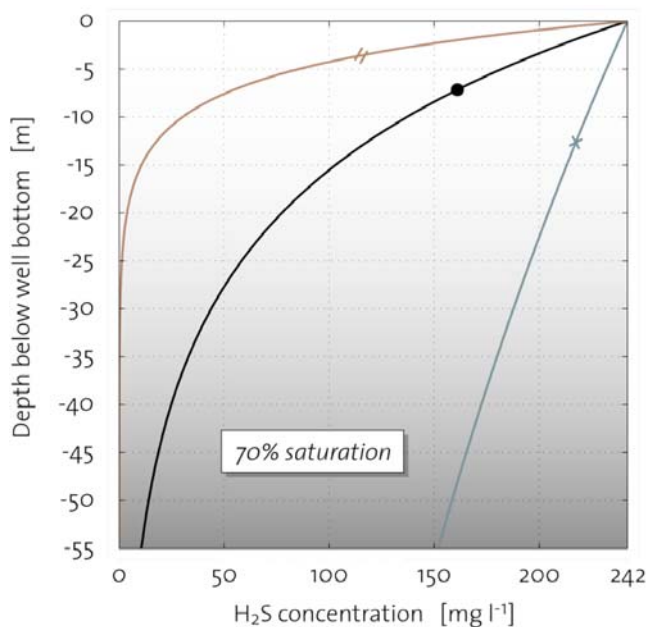
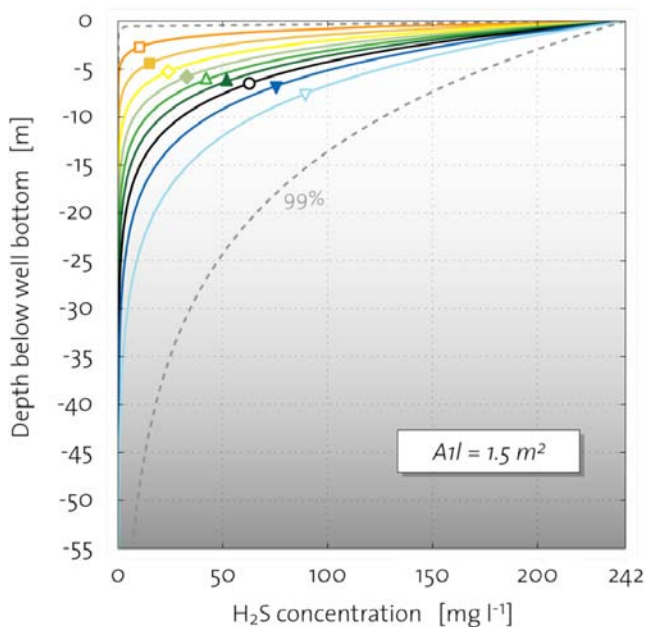
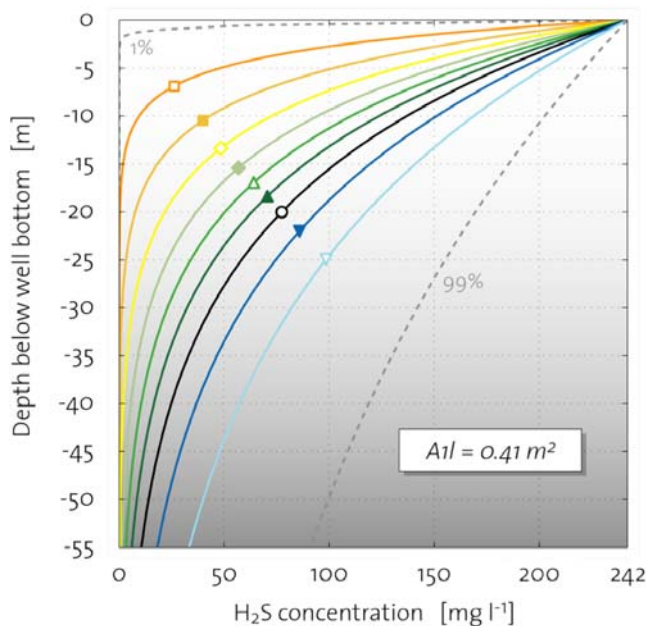
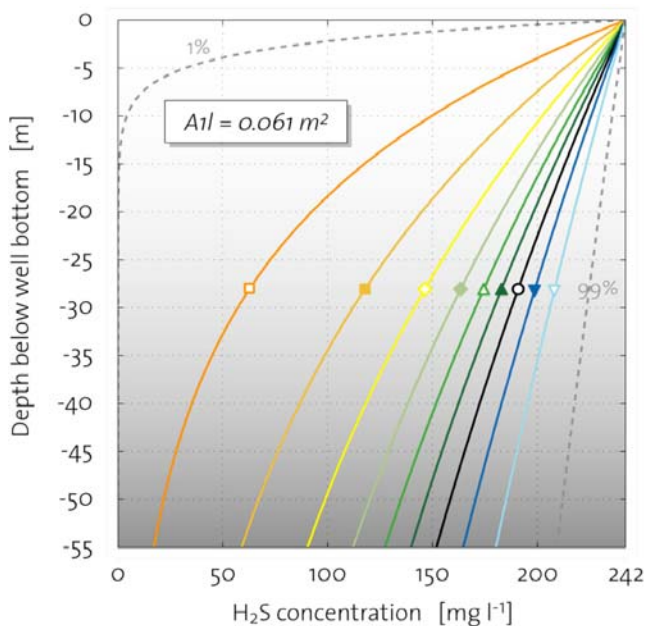


Sheet 6: Temperature developing

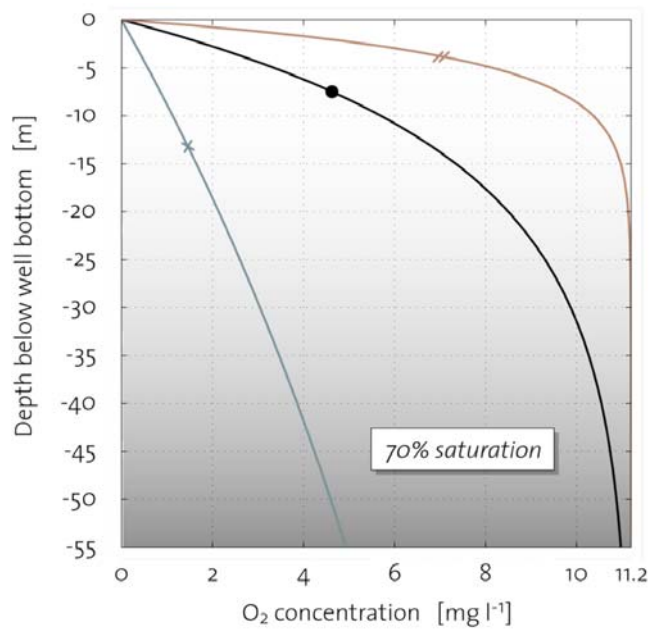
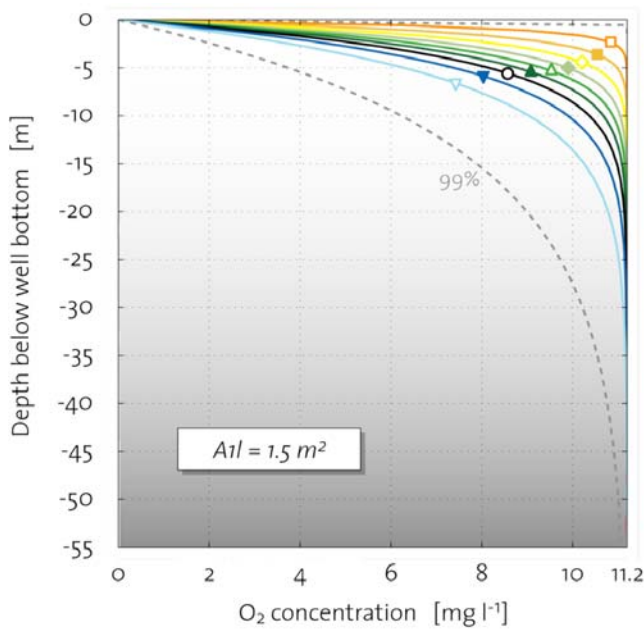
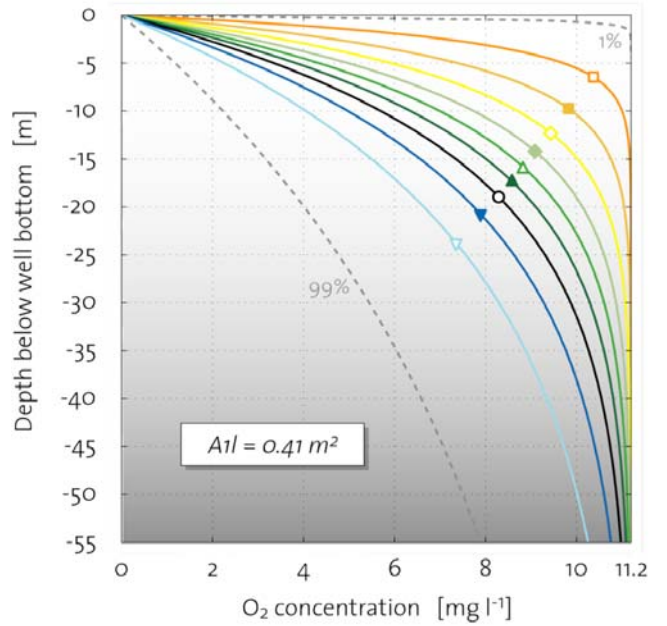
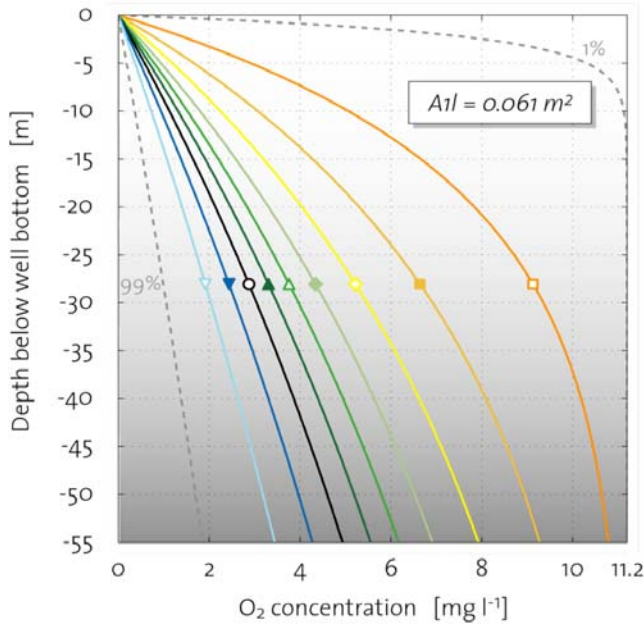


Appendix 9: Additional plots of the seepage phase modeling

Developing of the H₂S concentration during seepage phase



Developing of the O₂ concentration during seepage phase



Key for pore water saturation:				Key for A _{1l} :	

Sheet 3: Developing of the Mg²⁺ concentration during seepage phase

